

Czech Technical University in Prague

Faculty of Electrical Engineering

Doctoral Thesis

June 2019

Catalina Burtscher

Czech Technical University in Prague
Faculty of Electrical Engineering
Department of Telecommunication Engineering

***DESIGN, MODELLING AND
OPTIMISATION OF PASIVE OPTICAL
COMPONENTS***

Catalina Burtscher

Prague, June 2019

Ph.D. Programme: Electrical Engineering and Information Technology

Branch of study: Telecommunication Engineering

Supervisor: *Ing. Michal Lucki, PhD*

Supervisor specialist: *Dr. habil. Dana Seyringer, PhD*

Abstract

In this doctoral thesis the design, simulation and optimization of high splitting ratio $1 \times N$ Y-branch passive optical splitters ($N \geq 16$) were performed. Two main research areas are the design, simulation and optimization of high splitting ratio splitters based on: a) low index contrast and b) high-index-contrast material platforms. Low index contrast splitters have main applications in telecommunication and high index contrast splitters are mainly used for the applications in photonics integration circuits.

For the low index contrast Y-branch splitters a standard 1×32 Y-branch splitter was designed and simulated by the commercially available software tool, OptiBPM. Based on the simulation results, the optical properties of the standard Y-branch approach were analyzed. This design features high non-uniformity, insertion loss and large size of the designed structure. Deep study of the simulated results shown that the design of such optical splitters depends strongly on the used waveguide structure. Optimizing this structure, the splitting properties of the designed 1×32 Y-branch splitter were strongly improved. Based on these results the low loss, high uniformity 1×64 Y-branch splitter was designed. In this case, the length of “low loss length optimized” 1×64 Y-branch splitter was reduced to nearly one to third of its original value and additionally non-uniformity was also improved.

Beside the evaluation of the used standard Y-branch shapes, a new shape of the Y-branch splitter was optimized. Using this shape the scattering of light was strongly reduced. The problem of using this new shape was that it contains of some inaccuracies. Therefore the next task of this PhD thesis was to eliminate these shortcomings and to make this shape applicable for high splitting ratio Y-branch splitters.

For applications of the designed optical splitters in telecommunication, I investigated the influence of different optical splitters in access networks as for example GPON and XG-PON by ITU-T with triple-play services (i.e. data, voice and video). The achieved splitting parameters were incorporated in the simulations of particular passive optical network scenarios.

In case of high index contrast, a silicon nitride based 1×8 Y-branch splitter with waveguide structure and with shallow rib waveguide structure was design and optimized.

Keywords: passive optical components, Y-branch splitter, MMI splitter, FTTH, silicon nitride, optical waveguide, design, simulation, optimization, bend losses, rib waveguide, power splitter, optical splitting, integrated optics and telecommunication.

Abstrakt

Cílem disertační práce byl návrh, simulace a optimalizace pasivních optických rozbočovačů typu $1 \times N$ Y s vysokým počtem kanálů ($N \geq 16$). Dvěma hlavními oblastmi výzkumu jsou návrh, simulace a optimalizace těchto rozbočovačů podle aplikace: a) materiálu s nízkým kontrastem indexu lomu, b) materiálu s vysokým kontrastem indexu lomu. Rozbočovače s nízkým kontrastem indexu lomu nachází uplatnění v telekomunikacích; rozbočovače s vysokým kontrastem se používají hlavně pro aplikace ve fotonických integrovaných obvodech.

Pro rozbočovače typu Y s nízkým kontrastem byl navržen a simulován standardní 1×32 rozbočovač pomocí komerčně dostupného programového nástroje OptiBPM. Na základě výsledků simulace byly analyzovány optické vlastnosti standardního přístupu k návrhu těchto článků. Konstrukce typu Y se vyznačuje vysokou nerovnoměrností, vložnými ztrátami a poměrně velkými rozměry konstrukce. Hluboká studie simulovaných výsledků ukázala, že konstrukce takových optických rozbočovačů silně závisí na použité struktuře vlnovodu. Optimalizací se výrazně zlepšily dělicí vlastnosti navrženého rozbočovače s dělicím poměrem 1×32 . Na základě těchto výsledků byl navržen rozbočovač s nízkou ztrátou a konstrukcí s 1×64 kanály. Délka optimalizovaného 1×64 rozbočovače typu Y byla snížena na téměř třetinu své původní hodnoty a navíc se zlepšila rovnoměrnost výstupů.

Kromě vyhodnocení použitých standardních tvarů rozbočovačů typu Y, byl optimalizován nový tvar geometrie rozbočovače. Použitím tohoto tvaru se výrazně snížil rozptyl světla. Problémem použití tohoto nového tvaru bylo, že zahrnuje jisté nepřesnosti. Dalším úkolem této disertační práce bylo proto odstranit nedostatky řešení a aplikovat tento tvar na rozbočovače typu Y s vysokým dělicím poměrem.

Pro aplikace navržených optických rozbočovačů v telekomunikacích jsem zkoumala vliv různých optických rozbočovačů v přístupových sítích jako jsou například GPON a XG-PON od ITU-T se službami typu tripple-play (tj. přenos dat, hlasu a video). Dosažené parametry pasivních optických prvků byly začleněny do simulací vybraných pasivní optických sítí.

V případě vysokého kontrastu indexu lomu byl navržen a optimalizován rozbočovač na bázi na bázi nitridu křemičitého, s 1×8 Y kanály a se strukturou žebrového vlnovodu (shallow-rib).

Klíčová slova: pasivní optické prvky, rozbočovač typu Y, rozbočovač MMI, FTTH, nitrid křemičitý, optický vlnovod, návrh, simulace, optimalizace, ztráty ohybu, žebrový vlnovod, rozdělovač výkonu, optické dělení, integrovaná optika a telekomunikace.

Acknowledgement

Research related to low index contrast Y-branch splitters has been supported by the CTU grant under projects SGS13/201/OHK3/3T/13, SGS16/227/OHK3/3T/13 from Czech Technical University in Prague, Faculty of Electrical Engineering, Department of Telecommunication Engineering and by Research Centre for Microtechnology, Vorarlberg University of Applied Sciences, Austria. High index contrast Y-branch splitters were designed in the frame of the project 1/0929/17 of VEGA grant agency of the Ministry of Education, Science, Research and Sport of the Slovak Republic and the projects SK-AT-2017-0005, APVV-17-0662 from Slovak research and development agency of the Ministry of Education, Science, Research and Sport of the Slovak Republic and SK 15/2018 from Austrian Agency for International Cooperation in Education and Research (OeAD-GmbH), that maintained flexible environment for my research.

I would like to express my sincere gratitude to my supervisor Ing. Michal Lucki, Ph.D. for his continuous guidance, support, remarks, motivation and valuable advice, for the numerous problems and professional advancements.

My sincere thanks go to my supervisor from FH Vorarlberg, Dr. habil. Dana Seyringer, PhD. She has been a constant source of encouragement and insight during my research for the many hour of weekly discussions which always helped to push this thesis in the right direction.

Deep appreciation goes to the staff of the Department of Telecommunication Engineering from the Czech Technical University in Prague; Research Centre for Microtechnology, Vorarlberg University of Applied Sciences, Austria and to International Laser Centre in Bratislava, Slovakia.

Honesty Declaration

I hereby declare that I wrote the doctoral thesis by myself under the supervision of my thesis supervisor and I have used only the literature mentioned in the reference list. My own contribution (results, designs) are clearly distinguished from the used literature. I also declare that I agree with lending or publishing my work with the consent of the Department.

Prague, 26.6.2019

Catalina Burtscher

Contents

Czech Technical University in Prague	3
Abstract	4
Abstrakt	5
Contents	7
List of Figures	10
List of Tables	14
List of Symbols	15
List of Abbreviations	16
1 Introduction	18
1.1 Motivation.....	18
1.2 Problem Statement	18
1.3 Aims and Contributions of the Thesis	19
1.4 Structure of the Thesis	20
2 State of the Art	21
2.1 Passive Optical Networks	21
2.2 FTTH-PON Networks.....	22
2.3 Passive Optical Components for FTTH-PON Network.....	23
3 Methods and Design Principles	26
3.1 Methods.....	26
3.1.1 BPM Method.....	27
3.1.2 FDTD Method.....	28
3.2 Technological Verification of Used Photonic Tools	31
3.3 Design Principles	35
3.3.1 Optical Splitter Design.....	35
3.3.2 Splitting Parameters	39
3.3.3 S-Bend Waveguide	40
3.3.4 Used Waveguide Structures and Materials	42
3.3.5 SoS Waveguide Structure	44
3.3.6 Silicon Nitride Waveguide Structure	47
3.4 Design of Low-Index-Contrast Y-Branch Splitters	50
3.4.1 Design of 1x8 Y-Branch Splitter	50
3.4.2 Design of High Splitting Ratio Y-Branch Splitters	51

3.4.3	Length Optimization of High Splitting Ratio Y-Branch Splitters	52
3.4.4	Optimization of Optical Properties of High Splitting Ratio Y-Branch Splitter.....	56
3.4.5	Design of MMI Splitters	58
3.4.6	Optical Splitter Design for Application in Telecommunication Access Network with Triple-Play Services.....	60
3.4.7	Design and Optimization of High-Index-Contrast Y-Branch Splitters.....	63
4	Results	68
4.1	Simulation of Low Splitting Ratio SoS Based Splitters	68
4.1.1	Simulation of Standard 1x8 Y-Branch and 1x8 MMI Splitters Using OptiBPM Tool	68
4.1.2	Simulation of “Standard” 1x8 Y-Branch and 1x8 MMI Splitters Using Apollo Tool .	69
4.1.3	Comparison of Optical Properties of “Standard” 1x8 Y-Branch and 1x8 MMI Splitters	70
4.1.4	Comparison of Both Used Photonics Tools.....	71
4.1.5	Waveguide Optimization of “Standard” 1x8 Y-Branch Splitter.....	71
4.2	Simulation Results of High Splitting Ratio SoS Splitters.....	73
4.2.1	Simulation of Standard 1x16 Y-Branch Splitter	73
4.2.2	Simulation of Standard 1x16 MMI Splitter	74
4.2.3	Comparison of Optical Properties of 1x16 Y-Branch and 1x16 MMI Splitters	76
4.2.4	Waveguide Optimization of 1x16 Y-Branch and 1x16 MMI Splitters.....	76
4.2.5	Simulation of “Standard” 1x 32 Y-Branch Splitters Using OptiBPM.....	77
4.2.6	Simulation of “Length-Optimized” 1x 32 Y-Branch Splitters Using OptiBPM	78
4.2.7	Simulation of “Further length-reduced” 1x 32 Y-Branch Splitters Using OptiBPM ...	79
4.2.8	Waveguide Optimization of “Length–Optimized” 1x 32 Y-Branch Splitters Using OptiBPM.....	81
4.2.9	Comparison of the “Length–Optimized” 1x 32 Y-Branch Splitters with Different Waveguide Cross-Sections	81
4.2.10	Waveguide Optimization of the “Further Length–Reduced” 1x 32 Y-Branch Splitters Using OptiBPM Tool.....	82
4.2.11	Comparison of “Further Length–Reduced” 1x32 Y-Branch Splitters with Different Waveguide Cross-Sections	83
4.2.12	Simulation of 1x32 Y-Branch Splitters Using RSoft Tool	83
4.3	Simulation Results of “New Shape” High Splitting Ratio SoS Splitters.....	86
4.3.1	Simulation Results of “New Shape” 1x32 Y-Branch Splitter Using OptiBPM Tool...	86
4.3.2	Comparison of Optical Properties of “Standard” and “New Shape” 1x32 Y-Branch Splitter with OptiBPM Tool.....	87
4.3.3	Waveguide Optimization of “New Shape” 1x32 Y-Branch Splitter	87
4.3.4	Comparison of Optical Properties of “Standard” and “New Shape” Waveguide-Optimized 1x32 Y-Branch Splitter Applying OptiBPM Tool.....	88
4.4	Simulation Results of 1x64 Y-Branch Splitters.....	88
4.4.1	Simulation and Waveguide Optimization of “Standard” 1x 64 Y-Branch Splitters Using OptiBPM Tool.....	88
4.4.2	Simulation of “Length-Optimized” 1x 64 Y-Branch Splitters Using OptiBPM Tool..	90

4.4.3	Comparison of Optical Properties of the “Length-Optimized” 1x 64 Y-Branch Splitters	92
4.4.4	Comparison of Optical Properties of “Standard” and “Low-Loss Length-Optimized” 1x 64 Y-Branch Splitters	93
4.5	Simulation Results of Low-Loss Length-Optimized Y-Branch Splitter Implementation in PON/XG-PON	94
4.6	Simulation Results of Silicon Nitride Based 1x8 Y-Branch Splitter	96
5	Conclusions	98
	Bibliography	100
	Publications of the Author	116
	Appendix A	120
	Sworn Declaration	Error! Bookmark not defined.

List of Figures

Figure 1: Principle of the BPM (left); general problem in optical propagation (right).....	27
Figure 2: The Yee's cell used in 3D FDTD simulation.	29
Figure 3: The Yee's Grid in the Cartesian coordinate system.	29
Figure 4: Two different mask layouts consisting of AWGs and optical splitters: (left) the 2 nd technological run (2005) and (right) the 3 rd technological run (2006) [133].	32
Figure 5: Detailed view of the splitter designs from mask layout in Figure 4-right [133].	32
Figure 6: The optical characteristics of 1x32 Y-branch splitter measured in the C-Band [133].....	33
Figure 7: Detailed view of the losses together with the calculated non-uniformity [133].....	33
Figure 8: Measurement set-up at International Laser Centre in Bratislava: the measurement of AWGs [134].	34
Figure 9: Measurement of optical splitters [134].....	34
Figure 10: Geometry of 1x4 Y-branch splitter.....	35
Figure 11: Design of a conventional 1x4 MMI splitter with its characteristics parameters. ..	36
Figure 12: Principle of MMI splitter.	37
Figure 13: Comparison of Y-branch and MMI splitters [133, 135].....	38
Figure 14: Definition of insertion loss, IL , insertion loss uniformity (non-uniformity), ILu and background crosstalk, BX	40
Figure 15: S-bend waveguide geometry.	40
Figure 16: S-bend waveguide geometry.	41
Figure 17: S-bend waveguide connecting two straight waveguides.	42
Figure 18: Schematics of different geometrical structures of 2D optical waveguides (except planar waveguide).....	43
Figure 19: The cross-section of SoS waveguide structure (left); comparison of the waveguide dimensions with the standard SM fiber (right).	45
Figure 20: Design parameters of a waveguide structure in Apollo tool (left); The design of the waveguide with $(6 \times 6) \mu\text{m}^2$ core size in Apollo Photonics (right).	46
Figure 21: Optical field in the waveguide, simulated in x and y in Apollo Photonics.	46
Figure 22: Defining the waveguide structure in Optiwave tool.	47
Figure 23: Cross-section of the designed waveguide structure with all important desing parameters (left); optical field in the waveguide, simulated in x and y axis (middle and right).....	48
Figure 24: Contour map of transverse refractive index profile created in RSoft tool (left); normalized E mode profiles (middle and right).....	49
Figure 25: Dependence of N_{eff} of guided modes on waveguide width having $0.5 \mu\text{m}$ height.	49
Figure 26: Design of "standard" SoS 1x4 Y-branch splitter.....	50
Figure 27: Layout of SoS 1x8 Y-branch splitter applying OptiBPM tool.	51
Figure 28: Layout of 1x32 Y-branch splitter: "standard" structure (left); "length optimized" splitter structure (right).	52
Figure 29: Design layouts of the "further length reduced" 1x32 Y-branch splitter structures for all four options.	53

Figure 30: Layout of “standard” 1x64 Y-branch splitter (top-left); “length optimized” 1x64 Y-branch splitter using Variant 1 (top-right); “length optimized” 1x64 Y-branch splitter using Variant 2 (bottom-left) and Variant 3 (bottom-right).	55
Figure 31: Top view of all three simulated s-bend waveguides (left), field distribution of the output signals (right).	56
Figure 32: Standard branch waveguide shape (left); new branch waveguide shape (right). ..	57
Figure 33: New Y- branch waveguide shape: Top view of simulated structure (left); Field distribution of new waveguide shape (right).	57
Figure 34: Layouts of 1x4 Y-branch splitter using new shape (left) and “new-shape” 1x32 Y-branch splitter (right) designed in OptiBPM tool.	58
Figure 35: Layout of 1x8 MMI splitter applying OptiBPM tool.	59
Figure 36: Layout of 1x16 MMI splitter using OptiBPM tool.....	59
Figure 37: Wavelength ranges for GPON/XG-PON and video components.....	61
Figure 38: GPON/XG-PON simulation schemes with triple-play services employing the designed 1x64 splitters.	62
Figure 39: Structure of the standard 1x8 Y-branch splitter (left); and optimized 1x8 Y-branch splitter (right) with channel waveguide structure.	64
Figure 40: Layout of the Y1-branch together with the simulated optical power (left); Scanning of the length of the Y1-branch with regards to optical power calculated in the waveguides (right).	64
Figure 41: The scanning of the lengths of the Y2-branch (left) and Y3-branch (right).....	65
Figure 42: Layout of the silicon nitride based 1x8 Y-branch splitter with shallow rib waveguide structure.	66
Figure 43: Simulated results of coupling effect when the port pitch $W_3 = 2 \mu\text{m}$ (left) and ...	66
Figure 44: Scanning of the length of the Y3 branch (left) and Y2 branch (right).	67
Figure 45: Scanning of the length of the Y1-branch.....	67
Figure 46: Simulation results of 1x8 Y-branch and 1x8 MMI splitters applying OptiBPM tool: top view of the simulated 1x8 Y-branch (top-left) and MMI (top-right) splitter structures, field distribution at the end of 1x8 Y-branch (middle-left) and of 1x8 MMI (middle-right) splitters and non-uniformity and insertion loss of 1x8 Y-branch (bottom-left) and of 1x8 MMI (bottom-right) splitters.....	69
Figure 47: Top view the simulated 1x8 Y-branch splitter (left); multimode interference pattern of 1x8 MMI splitter (right).	70
Figure 48: Field amplitude profiles of the fundamental mode and the first mode with their distributions in the $(6 \times 6) \mu\text{m}^2$ waveguide.....	72
Figure 49: Detailed view of the splitting parameters of 1x8 Y-branch (left) and 1x8 MMI (right) splitters with the waveguide core sizes of $(5.5 \times 5.5) \mu\text{m}^2$	72
Figure 50: Field distribution at the end of the 1x16 Y-branch splitter (left). Non-uniformity and insertion loss of 1x16 Y-branch splitter with the waveguide core size of $(6 \times 6) \mu\text{m}^2$ (right).	74
Figure 51: Field distribution at the end of the “standard” 1x16 MMI splitter (left). Non-uniformity and insertion loss of MMI structure (right) with the waveguide core size of $(6 \times 6) \mu\text{m}^2$	75
Figure 52: Non-uniformity and insertion loss of 1x16 Y-branch (left) and 1x16 MMI (right) splitters with the waveguide core size of $(5.5 \times 5.5) \mu\text{m}^2$	76

Figure 53: Top view of the simulated “standard” 1x32 Y-branch splitter.....	77
Figure 54: Simulation results of the ”standard” 1x32 Y-branch splitter structure: Field distribution at the end of simulated structure together with background crosstalk, <i>BX</i> (left); Detailed view of the field distribution showing the non-uniformity, <i>ILu</i> and the insertion loss, <i>IL</i> (right).....	78
Figure 55: Simulation results of the “length-optimized” 1x32 Y-branch splitter structure: Field distribution at the end of simulated structure together with calculated background crosstalk, <i>BX</i> (left); Detailed view of the field distribution showing the non-uniformity, <i>ILu</i> and the insertion loss, <i>IL</i> (right).....	78
Figure 56: Simulation results of the “further length-reduced” 1x32 Y-branch splitter using Option 1 (top) and Option 2 (bottom) designs: Field distribution at the end of simulated structure together with calculated background crosstalk, <i>BX</i> (left); Detailed view of the field distribution showing the non-uniformity, <i>ILu</i> and the insertion loss, <i>IL</i> (right).	79
Figure 57: Simulation results of the “further length-reduced” 1x32 Y-branch splitter using Option 3 (top) and Option 4 (bottom) designs: Field distribution at the end of simulated structure together with calculated background crosstalk, <i>BX</i> (left); Detailed view of the field distribution showing the non-uniformity, <i>ILu</i> and the insertion loss, <i>IL</i> (right).	80
Figure 58: Simulation results of the “length-optimized” 1x32 Y-branch splitter structure with the waveguide core size of $(5.5 \times 5.5) \mu\text{m}^2$ (left); with the waveguide core size of $(5 \times 5) \mu\text{m}^2$ (right), namely detailed view of the field distribution showing the non-uniformity, <i>ILu</i> and the insertion loss, <i>IL</i> (right).	81
Figure 59: Simulation results of “further length-optimized” 1x32 Y-branch splitter with the waveguide core size of $(5.5 \times 5.5) \mu\text{m}^2$: Field distribution at the end of simulated structure together with background noise, <i>BX</i> (left); Detailed view of the field distribution showing the non-uniformity, <i>ILu</i> and the insertion loss, <i>IL</i> (right).	82
Figure 60: Top view of the “standard” 1x32 Y-branch splitter structure designed applying RSoft photonic tool.....	83
Figure 61: Simulation results of the “standard” 1x32 Y-branch splitter structure $(6 \times 6) \mu\text{m}^2$ (top); “length optimized” 1x32 Y-branch splitter structure with the waveguide core size of $(5.5 \times 5.5) \mu\text{m}^2$ (bottom).	84
Figure 62: Detailed view of simulated “new shape” 1x32 Y-branch splitter.	86
Figure 63: Simulation results of the “new shape” 1x32 Y-branch splitter structure with the core size of $(6 \times 6) \mu\text{m}^2$: Field distribution at the end of simulated structure together with background crosstalk, <i>BX</i> (left); Detailed view of the field distribution showing the non-uniformity, <i>ILu</i> and the insertion loss, <i>IL</i> (right).	86
Figure 64: The maximum background noise, <i>BX</i> (left), the non-uniformity, <i>ILu</i> and the insertion loss, <i>IL</i> (right) of new shape 1x32 Y-branch splitter with the waveguide core size of $(5.5 \times 5.5) \mu\text{m}^2$	87
Figure 65: Detailed view of simulated standard 1x64 Y-branch splitter.	89
Figure 66: The background crosstalk, <i>BX</i> (left), the non-uniformity, <i>ILu</i> and the insertion loss, <i>IL</i> (right) of standard 1x32 Y-branch splitter with the waveguide core size of $(6 \times 6) \mu\text{m}^2$ (top), $(5.5 \times 5.5) \mu\text{m}^2$ (bottom).	89
Figure 67: Detailed view of simulated “length-optimized” 1x64 Y-branch splitter: Variant 1 (left) and Variant 2 (right).	90

Figure 68: The achieved simulated results of “length optimized” 1x64 Y-branch splitter with a waveguide core size of $(6 \times 6) \mu\text{m}^2$ and $(5.5 \times 5.5) \mu\text{m}^2$ Variant 1.....	90
Figure 69: The achieved simulated results of “length-optimized” 1x64 Y-branch splitter with a waveguide core size of $(6 \times 6) \mu\text{m}^2$ and $(5.5 \times 5.5) \mu\text{m}^2$ Variant 2.....	91
Figure 70: Detailed view of simulated “length optimized” 1x64 Y-branch splitter: Variant 3.	92
Figure 71: The achieved simulated results of “length-optimized” 1x64 Y-branch splitter with a waveguide core size of $(6 \times 6) \mu\text{m}^2$ and $(5.5 \times 5.5) \mu\text{m}^2$ Variant 3.....	92
Figure 72: Attenuation and deviation from the mean value for each of the output ports for both: conventional (blue circle-left) and low-loss length-optimized (red triangle-right) 1x64 Y-branch splitters.....	94
Figure 73: BER (left) and Q-factor (right) values for GPON with triple-play services (blue circles-standard splitter; red triangles-optimized splitter).	95
Figure 74: BER (left) and Q-factor (right) values for XG-GPON with triple-play services (blue circles-standard splitter; red triangles-optimized splitter).....	95
Figure 75: The simulation of the optical beam propagation in the silicon nitride based 1x8 Y-branch splitter.	96
Figure 76: The optical power in each output waveguide simulated for TE (left) and TM (right) polarization.	96

List of Tables

Table 1: Essential splitting parameters.....	39
Table 2: Classification of optical waveguides.....	42
Table 3: Review of the different materials used for PLC devices.....	44
Table 4: Geometry of SoS waveguide with a core size of $(6 \times 6) \mu\text{m}^2$	45
Table 5: Summary of the high splitting ratio Y-branch splitter designs.	51
Table 6: Summary of the geometry of all four designs.....	60
Table 7: Comparison of the optical properties of 1x8 Y-branch and 1x8 MMI splitting parameters achieved from Apollo Photonics and OptiBPM tool.	70
Table 8: Comparison of the splitting parameters of 1x8 Y-branch and MMI splitters achieved from Apollo Photonics and OptiBPM tool.	71
Table 9: Comparison of splitting parameters of 1x8 Y-branch and 1x8 MMI splitters having different waveguide cross-sections.....	73
Table 10: Comparison of splitting parameters of 1x16 MMI splitter for the different widths of multimode section and different lengths of the output ports.	74
Table 11: Comparison of splitting parameters of standard 1x16 Y-branch and 1x16 MMI splitters.....	76
Table 12: Comparison of splitting parameters of “standard” 1x16 Y-branch and 1x16 MMI splitters.....	77
Table 13: Comparison of splitting parameters achieved from the simulations of Option 1, Option 2, Option 3 and Option 4 or 1x32 Y-branch splitter.....	80
Table 14: Comparison of splitting parameters of the “length-optimized” 1x32 Y-branch splitters having different waveguide core size: $(6 \times 6) \mu\text{m}^2$, $(5.5 \times 5.5) \mu\text{m}^2$ and $(5 \times 5) \mu\text{m}^2$	82
Table 15: Comparison of splitting parameters achieved from the simulations of “standard” and “further length-optimized” 1x32 Y-branch splitters with waveguide core sizes of $(6 \times 6) \mu\text{m}^2$ and $(5.5 \times 5.5) \mu\text{m}^2$	83
Table 16: Comparison of splitting parameters achieved from the simulations of “standard” and “length optimized” 1x32 Y-branch splitters with waveguide core sizes of $(6 \times 6) \mu\text{m}^2$ and $(5.5 \times 5.5) \mu\text{m}^2$	85
Table 17: Comparison of splitting parameters of “standard” and “new shape” of 1x32 Y-branch splitters.....	87
Table 18: Comparison of splitting parameters of “standard” and “new-shape” waveguide optimized 1x32 Y-branch splitters.....	88
Table 19: Comparison of splitting parameters achieved from the simulations of “Variant 1”, “Variant 2”, “Variant 3” for 1x64 Y-branch splitter having waveguide core sizes of $(6 \times 6) \mu\text{m}^2$, $(5.5 \times 5.5) \mu\text{m}^2$	93
Table 20: Comparison of splitting parameters of “standard” and “low-loss length-optimized” 1x64 Y-branch splitter having waveguide core sizes of $(6 \times 6) \mu\text{m}^2$ and $(5.5 \times 5.5) \mu\text{m}^2$	93
Table 21: Output power from Figure 74 together with calculated insertion loss, IL and non-uniformity, IL_u for both polarizations.	97

List of Symbols

a	Width of the input/output waveguides
BX	Maximum Background noise
CB	Channel Bottom
d	Thickness
D	Pitch between two neighbour output waveguides (port pitch)
DC	Cover
ε	Permittivity
ε_r	Relative permittivity
IL	Insertion loss
ILu	Insertion loss uniformity (non-uniformity)
k_0	Wave number in vacuum
L_{in}	Linear input port
L_{out}	Length of the taper
L_{MMI}	Particular length of cutting the multi-mode section
L_P	Length of the output waveguides
n_c	Refractive index of the core
n_{cl}	Refractive index of the cladding
n_{eff}	Effective refractive index
n_0	Reference refractive index
n_b	Refractive index of thermal buffer layer used in high index contrast platform
n_p	Refractive index of passivation layer
N	Number of output waveguides
μ	Permeability
μ_r	Relative permeability
W_{MMI}	Width of the multimode section
WGW	Waveguide Width
λ	Operating wavelength
λ_0	Wavelength in a vacuum
θ	Angle of incidence at the core-to-cladding interface
θ_c	Critical angle

List of Abbreviations

1D	One-Dimensional
2D	Two-Dimensional
3D	Three-Dimensional
10GEAPON	10 Gbit/s Ethernet Passive Optical Network
10GPON	10 Gbit/s Passive Optical Network
ADI	Alternating Directional Implicit
AON	Active Optical Network
AWG	Arrayed Waveguide Gratings
BPM	Beam Propagation Method
BER	Bit Error Rate
CAD	Computer-Aided Design
CMOS	Complementary Metal-Oxide-Semiconductor
CO	Central Office
CVD	Chemical Vapour Deposition
CWDM	Coarse Wavelength Division Multiplexing
DEMUX	De-multiplexer
DSL	Digital Subscriber Loop
DWDM	Dense Wavelength Division Multiplexing
EPON	Ethernet Passive Optical Network
FBT	Fused Bionic Taper
FD	Finite Difference
FD-BPM	Finite Difference Beam Propagation Method
FDM	Finite Difference Method
FDTD	Finite Difference Time Domain
FDSS	Frequency Domain Split Step
FE	Finite Element
FE-BPM	Finite Element Beam Propagation Method
FETD	Finite Element Time Domain
FEM	Finite Element Method
FFT-BPM	Fast Fourier Transform Beam Propagation Method
FTTB	Fiber-to-the-Building/ Fiber-to-the-Basement
FTTC	Fiber-to-the-Curb/ Fiber-to-the-Cabinet
FTTH	Fiber-to-the-Home
FTTN	Fiber-to-the-Node
FTTP	Fiber to the Premise
FTTx	Fiber-to-the-x
GPON	Gigabit Passive Optical Network
GPON FTTH	Gigabit Passive Optical Network Fiber-to-the-Home
HDWDM	High Dense Wavelength Division Multiplexing
HIC	High Index Contrast
IEEE	The Institute of Electrical and Electronics Engineers
ISP	Internet Service Provider
ITU	International Telecommunication Union
IPTV	Internet Protocol Television
LED	Light Emitting Diode
LPCVD	Low Pressure Chemical Vapour Deposition
MMI	Multimode Mode Interference
MUX	Multiplexer

NGPON	Next Generation PON
NT	Network Terminal
OAN	Optical Access Network
ODN	Optical Distribution Network
OLT	Optical Line Termination
ONU	Optical Network Units
ONT	Optical Network Terminal
P2MP	Point to Multipoint
P2P	Point to Point
PBS	Polarisation Beam Splitter
PDS	Passive Double Star
PECVD	Plasma Enhanced Chemical Vapour Deposition
PIC	Photonics Integrated Circuit
PML	Perfectly Matched Layer
PON	Passive Optical Network
PLC	Planar Lightwave Circuit
RIE	Reactive Ion Etching
RF	Radio Frequency
SLA	Service Level Agreement
SM	Single Mode
SOI	Silicon-on-Insulator
SoS	Silica-on-Silicon
SVFD-BPM	Semi-Vectorial Finite-Difference Beam Propagation Method
TBC	Transparent Boundary Condition
TE	Transverse Electric
TDM	Time Division Multiplexing
TDSS	Time Domain Split Step
TM	Transverse Magnetic
VHDWDM	Very High Dense Wavelength Division Multiplexing
XG-PON	10-Gigabit-capable Passive Optical Network
WDM	Wavelength Division Multiplexing

1 Introduction

1.1 Motivation

The submitted doctoral thesis summarizes the author's research work as a part of the Grant Agency of Czech projects SGS13/201/OHK3/3T/13 and SGS16/227/OHK3/3T/13, which focus on the photonic transmission media and components for optical telecommunication networks. This work was done by the author from March 2015 until December 2018. Additionally, a part of author's research work was done in collaboration with International Laser Centre in Bratislava, Slovakia in the frame of the project No. SK-AT-2017-0005 and APVV-17-0662. The focus of this project was on the design of passive optical components, namely optical splitters based on silicon nitride material platform running from January 2018 until December 2019.

Nowadays the steadily increasing data volume in communication networks is driven by a rapid proliferation of home-based and business computers, storage capacities, processing capabilities and the extensive availability of Internet. The challenge is to transfer high data volumes in short periods of time over high distances as lossless as possible. It is obvious that the more data transmitted over the same line at the same time (quasi in parallel), the higher the reachable data volume. Therefore, instead of using only one data signal per channel, currently several data signals can be combined and transmitted using only one channel. This technique is called Wavelength Division Multiplexing (WDM). In comparison to other transmissions techniques, the WDM uses optical data transmission, which provides several advantages such as long transmission distance, large information capacity, small size, low weight and immunity to electrical interference. Due to these advantages, the communication companies are moving toward optical technologies that allow larger and more flexible bandwidth [1].

1.2 Problem Statement

Splitting and combining multiple optical beams plays an important role in integrated optics [2, 3]. The task of the optical splitters in Fiber-to-the-x (FTTx) network is to split one optical signal in many identical signals bringing for example the same TV signal in different households. Of course, the more buildings can be served by one optical splitter the lower are the installation costs.

Optical power splitter is a basic device used for all optical signal processing in optical communication systems, sensing systems and many other applications. The mostly used optical splitter is based on a cascade of one-by-two waveguide branches, also called Y-branches, connected with each other. Such splitters have an advantage that they are polarization and wavelength independent, i.e. one device can be used to split optical signals in the whole operating wavelength window [4]. However, their main drawback is the high asymmetric splitting ratio of the split power over all the output waveguides [5]. Furthermore, the Y-branch splitters are rather large compared to other splitting approaches [6].

Multi-mode-interference (MMI) splitters present a different splitting approach. They feature a large splitting number and stable ratio, ensuring good uniformity over all the output signals

[7]. Furthermore, the MMI splitters are potentially much shorter in comparison to Y-branch splitters. Another advantage is their good fabrication tolerance because the splitting is performed in a large multimode section. Their main disadvantage results from the fact that the length of the multimode section is wavelength dependent, i.e. MMI splitters are designed solely for one wavelength and can only operate in a narrow wavelength band [7]. They are also polarization dependent; however, it has been shown that in the strong guidance waveguide structure this dependence is negligible [5, 7].

Since the Y-branch splitters are polarization and wavelength independent, this approach is mainly used in telecommunication applications. Therefore, in my work I concentrate especially on the design of Y-branch splitters and optimization of their optical properties.

From the technological point of view the main problem in the Y-branch splitting approach is the processing of the branching point where two waveguides start to separate [4, 5]. This generally leads to an **asymmetric splitting ratio** causing **high non-uniformity** of the split power over all the output waveguides [4]. Although it does not have a significant influence on the splitting properties of 1x2, 1x4 or 1x8 Y-branch splitters it becomes a dominant factor in the splitting of 1x16, 1x32 or 1x64 optical signals, leading to a huge rise of the variation in the splitting ratio [4]. Furthermore, such splitters are **rather large** compared to other splitting approaches [3]. Therefore, the special attention is paid mainly to the design of 1xN Y-branch optical splitters ($N \geq 16$) presenting nowadays the serious challenge for the professional designers. For this reason, the goal of my doctoral work is focused on the design of such optical splitters, particularly 1x16, 1x32 and 1x64 Y-branch splitters featuring excellent splitting properties.

In summary, there are two major tasks concerning high splitting ratio passive optical splitters as follows:

1. Influence of the waveguide structure on Y-branch splitting ratio. **I will optimize this structure to suppress the asymmetric splitting ratio.**
2. Based on the results the **size of the designed Y-branch splitters will be optimized.**

Additionally, the design, simulation and optimization of silicon nitride based Y-branch splitters will be performed. Such compact devices can easily be implemented on-chip and have already found applications in WDM systems and also in emerging applications such as optical sensors, devices for DNA diagnostics and optical spectrometers for infrared spectroscopy [5]. The aim of this work is to find the minimum physical dimensions of the designed splitters occupying minimal space on the photonics integrated circuits (PIC) chip. The optimization is done with regards to high symmetrical splitting ratio and low insertion loss, caused by bending losses coming from applied waveguides. Additionally, the determination of possible minimal distance between output waveguides without coupling between each other is studied.

1.3 Aims and Contributions of the Thesis

The goal of this thesis is the design and simulation of high splitting ratio Y-branch splitters. Additionally, the optical properties of the designed splitters will be studied and optimized.

Based on the achieved results, the size of the splitters will be optimized. To design these optical components a standard commercially available photonic software tool, OptiBPM [8], was used.

The principal contributions of this thesis are as follows:

1. Y-branch versus MMI optical splitters:
 - Design, simulation and comparison of the optical properties of MMI and Y-branch splitters (1x8, 1x16).
2. 1x32 and 1x64 Y-branch optical splitters:
 - Design and simulation of standard 1x32 and 1x64 Y-branch splitters.
 - Optimization of the optical properties of standard 1x32 and 1x64 Y-branch splitters.
 - Optimization of the length of the designed splitters.
 - Design and simulation of the low loss 1x32 and 1x64 Y-branch splitters.
3. Evaluation of the high splitting ratio Y-branch splitter designs for application in Telecommunication Access Networks with Triple-play Services.
4. Design of a new shape of the Y-branch high splitting ratio splitters (1x32 Y-branch splitters).
5. Comparison of standard and new shape 1x32 Y-branch splitters.
6. Design of the optical splitters applying different photonics design tools and their comparison:
 - OptiBPM by Optiwave (1x8, 1x16, 1x32, 1x64, Y-branch and MMI splitters).
 - Apollo by Apollo Photonics Inc [9] (1x8, 1x16 Y-branch and MMI splitters).
 - RSoft by Synopsys [10] (1x32 Y-branch splitters).
7. Design and simulation of silicon nitride based Y-branch splitters.

1.4 Structure of the Thesis

A significant part of the thesis is based on the author's articles and conference papers. Thesis contains only the basic mathematical relations in order to be as readable as possible. The thesis is organized in five chapters as follows:

- Chapter 1 – Introduction: in this chapter, the core research problems are stated and then the aim and contribution of the thesis is listed.
- Chapter 2 – State of the Art: theoretical background and general overview of the current state of the art are presented.
- Chapter 3 – Methods: design principles, simulation schemes and numerical methods are described in this chapter.
- Chapter 4 – Results and Discussion: the most important results are presented and discussed.
- Chapter 5 – Conclusions: the overview of accomplishments and scientific achievements together with future improvement research ideas is summarized in this section.

2 State of the Art

2.1 Passive Optical Networks

Passive Optical Network (PON) is a technology that provides optical fiber to the end user in both the home and business. A PON is characterized by implementing a point-to-multipoint architecture in which passive optical splitters are used to allow a single optical fiber to serve multiple endpoints (i.e. individual customers). Passive optical networks are often referred to as the "last mile" between the Internet Service Provider (ISP) and the customer [11].

Passive optical network consists of an Optical Line Terminal (OLT) at the service provider's central office, the Optical Distribution Network (ODN) and a range of Optical Network Units (ONUs) or Optical Network Terminals (ONTs) near end users. It may be optionally followed by Network Termination (NT) equipment, specified in [12, 13]. Connection between the OLTs and the ONUs consists of a network of single mode fibers and passive optical splitters, which are usually located near the user sites, and having typically splitting ratios of 1:16, 1:32 and 1:64, depending on the number of covered users. A PON implements a Point-to-Multi-Point Network Architecture (P2MP) [14] and Fiber-to-the-Premise (FTTP) [15] to provide multiple customers with data, video and voice services [16]. Compared to Point-to-Point (P2P) architectures, it reduces the amount of used fibers and central office equipment [17, 18].

A current PON generation has a form of fiber-optics access network, which uses as a primary multiplexing technique the Time Division Multiplexing (TDM) [14] and Gigabit Passive Optical Network (GPON) as a one of the most current deployed recommendations [17, 19]. The standardized and commercially available PON is defined through G.984.4 [19, 20]. However, G.984 series [11, 21] define the characteristics of GPON (G.984.1) as well as physical layer specification (G.984.2) [21] and transmission layer specification (G.984.3), ONU management and control specification (G.984.4) [22]. For example, a typical GPON standard provides a downstream data rate of 2.5 Gbit/s and an upstream data rate of 1.25 Gbit/s [23]. The downstream direction is assigned the wavelength range of 1480 nm to 1500 nm and for the upstream direction 1260 nm to 1360 nm is provided. However, the downstream RF video distribution uses a wavelength range of 1550 nm to 1560 nm [24-27].

Considering how the PON has grown exponentially in the last decade and is expected to grow in the future [12, 28], TDM PONs cannot handle bandwidth and optical power requirements. Therefore, other standards must be proposed that lead to the concept of a 10 Gigabit capable passive optical network (XG-PON) [29, 30]. The option may be the WDM PONs with the solution of separating ONU over physical wavelength to reach ONUs using optical amplification [12, 31]. This concept, based on the long-range PONs [32] combines WDM and TDM. The authors in [12] are looking at how bandwidth efficiency can be improved by developing coexistence solutions at the physical layer (migration in the same optical distribution network) in the Optical Access Network (OAN).

PON, which is based on Fiber Access Systems technology (covering a range of only tens of kilometers (0-20 km)), has been widely used in Asia, Europe and the US (G-PON is mainly used by European and US suppliers, while Asian suppliers prefer EPON/GePON) to support

higher bandwidth demands by ONUs in the future. However, it is necessary to upgrade the existing PON architecture to the Next-Generation PON (NGPON) concept [33, 34], which includes the 10G-PON [32], 10G EPON and WDM technologies [35], bringing simplicity and cost efficiency [36, 37]. With regard to future GPON extension, many GPON enhancements are being made today, including facts such as the expansion of the GPON optical budget for exploring new opportunities [38, 39], to allow the use of a higher split ratios and longer reach including higher data rates. The Authors in [38] bring arguments by comparing two passive access networks, GPON and next-generation WDM PON [30], based on cost, capacity, and flexibility.

2.2 FTTH-PON Networks

Fiber to the Home (FTTH, where "H" applies to both home and small businesses) is a fiber-based optical network that uses GPON technology [23] as the most attractive solution for last-mile access networks [40]. FTTH [41, 42] provides an uninterrupted, high-speed Internet service from the central office to the residential premises (household) that need services. The FTTH PON solution allows the connection of up to 128 ONUs on one fiber using OLT [43] with optical splitters and data rates of up to 10 Gbps in the forward channel (i.e. ONT to ONU) and up to 2,5 Gbit/s can be achieved backward channels. Due to the maximum bandwidth available for future services such as online gaming and video streaming [40], the total number of FTTH customers is expected to grow spectacularly in the near future. FTTH Conference 2018 [44] estimates the growth of FTTH subscribers in Europe by 20%, while the author in [45] estimated contractors for the FTTH service in Japan from May 2010 to over 15 million. Due to the higher bandwidth demands in the future, an estimated bandwidth requirement of at least 1 Gbit/s by the year 2020 and more than 10 Gbit/s by the year 2030 is estimated [46, 47].

FTTH architectures [48], 100% fiber access in the access network [49], are based on the Point-to-Point network design [50] when the optical part of the access network is either active, Active Optical Network (AON) and Point-to-Multi Point network designs [51] when the optical part of the access network is passive (PON). AON or Active Ethernet Network offers Internet, TV and telephony over the common Ethernet standard, using individual fiber optics (called "home-run-fibers") for each customer, where individual fibers run from OLT to each ONU and the active part is a router to manage the signal distribution. In the PON architecture, the active part of AON is replaced by a passive optical power splitter/combiner [52], i.e. it uses only fibers and passive components. The authors in [49] present a design and implementation of an FTTH-GPON access network (based on passive P2MP) for 320-subscriber residential buildings with average bandwidth per subscriber at 62.2 Mbps downstream and 31.1 Mbps upstream, analyzing performance budget and rise time budget standard. The FTTH-PON standards use TDM with the upstream packets being time-interleaved on a time basis by the optical fiber. In addition to TDM, WDM technology is the best solution for bandwidth satisfaction over the next ten years. WDM has been successfully integrated into the FTTH architecture with two techniques, Coarse Wavelength Division Multiplexing (CWDM) and Dense Wavelength Division Multiplexing (DWDM), and the cost difference between the other two, namely AON and GPON, does not seem to differ significantly [53]. The authors in [53] analyzed the cost evolution of

FTTH WDM and TDM networks in dense urban, urban, and suburban areas from a techno-economic perspective and estimated the total cost of suburban areas six times higher than in dense urban areas and four times as urban areas.

The key factors for FTTH technology are the scalable architecture, the cost, and the best ways to meet future bandwidth demands. Hence the FTTH network design and optimization [43] based on mathematical programming [42, 54-56] or other heuristic methods [57, 58] or a synthesis of both [49, 50] is an important target today with a very broad field. The authors in [43] describe and analyze the FTTH network designs with different plausible scenarios of customer behaviour, focusing on the advantages and weaknesses of very broad aspects of the engineering approach to FTTH network design. Authors in [40] proposed a cost-effective GPON-FTTH network that depends on many factors such as the number and location of optical splitters, types of fiber optic cables, and customer premises. The authors explored various design scenarios and compared the FTTH-GPON architecture at one level [56, 60, 61] with that at a multilevel level [55, 62]. The design of FTTH-PON networks with two splitter planes is at the heart of [63], where a network optimization model has been proposed which minimizes the cost of splitters and fiber optic cables. [64] presented a design and optimization model for a FTTH with a plane linking ONU to the splitter nodes assigned to a Central Office (CO), taking into account duct sharing to minimize the burden cost of trenching and ducts. In order to reduce the FTTH costs, which are central to the deployment of a new access network, the authors in [15] investigated the possibility of minimizing the planning costs of a PON deployment of long-range Greenfield [40]. This method is called Recursive Association and Relocation. It generates a variety of solutions to improve both, the ONU splitter assignment process and splitter relocation. A design model for Greenfield FTTH planning [40] is proposed in [62], with street locations and customer premises being adopted by OpenStreetMap [65].

The passive optical components such as optical splitters, optical filters, fused fiber couplers and fiber gratings play an important role in FTTH networks and are therefore used permanently in FTTH technology. Authors in [45] focused on the critical technological aspect of developing passive components in a Japanese company, opted for a system FTTH network architecture called the Passive Double Star (PDS) and improved its economic benefits, functionality, reliability and development in FTTH networks.

A typical FTTH PON network system in Japan consists of 1x4 splitters in the central office and 1x8 splitters installed close to customers in an airlock. In this way, it is possible for different users to share the cost of the devices in the fiber optic cable and at the central office, thereby reducing the overall burden on individual customers. In [66] much attention is being paid to reduce attenuation via passive optical splitters in FTTH networks using a layout design for a conventional FTTx network architecture [67].

2.3 Passive Optical Components for FTTH-PON Network

In the FTTH architecture operating in PON network, signal distribution from OLT to ONUs is handled by uniform optical splitters, a two-way passive optical components with one input port and several output ports, i.e. 1xN or 2xN, where N is the number of output ports [68]. The 1xN splitter configuration is typically used in access networks with a star configuration. The

$2 \times N$ splitter configuration is usually used in ring network architectures to provide physical network redundancy. For example, an optical power splitter 1×2 is a symmetric passive component, which equally divides power signal from a straight waveguide between two output waveguides. In this way, the optical splitters can reduce the implementation of the overall network system cost. As for other passive optical components like optical adapters, attenuators, connectors, couplers, WDM filters or MUX/DEMUX optical switches, the "passive" optical splitters do not require electrical/optical or reverse (optical/electrical) conversion for their functionality.

The simple version of a power splitter is a Y-branch. It is easy to design but it is sensitive to fabrication tolerances. Mainly, the processing of the branch point at which two waveguides begin to separate is technologically very difficult (see Section 1.2 – Problem Statement). In addition, such splitters are rather large compared to other splitting approaches, like for example MMI splitters. On the other hand, even though the dimensions of the MMI splitters are not critical, however these passive components can be designed for a particular wavelength, only. Anyway, both splitters are symmetrical, that is, 50% of the input power is carried by each output waveguide. The asymmetric power splitters may also be designed for specific purposes, for example to compensate the attenuation of ODNs. The authors in [69] propose a novel 1×24 splitter with three branching structures and 21 Y-branching elements and utilize these as a successful technique to improve the uniformity. The authors in [69] focused on the splitter design, namely on the branching angles of cascaded splitter (Y-branch splitter). They showed that there are many factors, which have to be taken into account in the design of the splitter elements and that the power loss is higher for wider angles. If two branches are separated by tilted straight waveguides, the tilt angle must be small, typically several degrees. However, the key parameter of the optical splitter remains the splitting ratio. The both mentioned power splitters are very important elements for photonic and opto-electronic integrated circuits due to their simple structure, their large optical bandwidth and low loss, their uniform distribution of the output power into output waveguides, the low price, the compactness and the compatibility with single-mode (SM) optical fibers [70].

In FTTH system [55], the function of the splitter is to divide the optical signal coming from one central office to multiple users, which generally has one input port and multiple output ports, typically 2-128 [71, 72]. They are the key components in FTTH networks, not only in the TDM PONs, WDM PONs [73], or in hybrid access networks (TDM-WDM-PON) [74], but in the future the optical splitters will be important passive components also in the ultra-dense WDM PONs [75, 76]. In terms of production, there are Fused Bionic Taper (FBT) Splitters or Planar Lightwave Circuit (PLC) splitters [77]. However, FTTH technology uses PLC splitters because a PLC is typically used for major advantages as very low losses, enhanced functionality and an important potential for mass production [45]. In a typical PLC, the attenuation is less than 0.1 dB/cm and the total attenuation including the coupling loss at the interface between fiber arrays and a PLC is about 1 dB or less. In general, the uniformity of the branch loss is less than 1 dB and the return loss is less than -50 dB [45]. To reach this, the authors in [45] suggested that the cores of the fibers and a PLC chip must be positioned with submicron accuracy, and they demonstrated that the fiber array depends on the geometry of optical fibers. Different PLC device technologies for the multiplexer and splitter modules become the leading technology, for example on one side Y-branches [78, 79] MMI couplers [80, 81] and star couplers [82] and

on the other side arrayed waveguide gratings (AWG) [83, 84] and matrix switches [85, 86]. There are different materials to fabricate optical waveguides and devices as LiNbO_3 [87], SiO_2 [88, 89], Silicon on Insulator (SOI) [90, 91], InP [92, 93], Polymer [94, 95], etc.

The Authors in [96] proposed different types of optical splitter structures used in PONs and analyzed their impact on energy consumption and resource sharing. They showed that the combination of Y-branch splitters with extended reach is the most beneficial. A mathematical model for PON design with a focus on splitter allocation, attenuation and split ratio is discussed in [97]. The authors in [98], [99] showed that optical splitters can directly improve PON performance efficiency.

Today, there is a great deal of interest in finding ways to increase the split ratio because it allows connecting more customers over the same transmission media. In this regard, optimized optical splitters are crucial for the high splitting ratio PONs, dense grid and long reach [100].

In this thesis I focus on the design and simulation of two different types of high splitting ratio optical splitters, namely Y-branch and MMI splitters, where Y-branch splitters create the main part of the thesis. I will show that not only processing of branching points in Y-branch splitters strongly influences splitting properties of the device but also the used waveguide structure itself. Optimizing this structure the asymmetric splitting ratio of the optical signal can be drastically suppressed. To this purpose I designed and simulated the standard 1x8, 1x16, 1x32 and 1x64 Y-branch structures with a waveguide core size of $(6 \times 6) \mu\text{m}^2$ and then the low loss optimized waveguide with core size $(5.5 \times 5.5) \mu\text{m}^2$. According to this, the low-loss length optimized structures are designed, simulated and optimized. Separately, the standard 1x64 Y-branch (waveguide core size of $(6 \times 6) \mu\text{m}^2$) and the low-loss length optimized 1x64 Y-branch splitter (waveguide with core size $(5.5 \times 5.5) \mu\text{m}^2$) were simulated and the simulations are based on GPON and XG-PON network with triple-play services [101]. The bandwidth optimization is obtained by employing CWDM and data and voice downstream components are transmitted within the wavelength range of 1480-1500 nm for GPON, 1575-1580 nm for XG-PON and 1550-1560 nm for video services, in accordance with the wavelength allocations.

3 Methods and Design Principles

This chapter describes the design and simulation methods behind photonics software tools used in this doctoral thesis and the design principles of Y-branch and MMI splitters.

3.1 Methods

In the development of PLC devices, the design and the simulation play an important role. They can be used to provide good performance and compactness of the devices and in this way the cost for product development can be reduced dramatically.

The optical properties of Y-branch and MMI splitters are numerically calculated using commercially available photonics software tools applying Beam Propagation Method (BPM) and Finite Difference Time Domain (FDTD) Methods. The used Photonics Tools are:

- OptiBPM and OptiFDTD Photonics Software Tools from Optiwave Systems Inc.
- Apollo Photonics Software Tool.
- BeamPROP™ and FullWAVE™ R-Soft Photonics Software Tool from Synopsys Inc.

There are various numerical methods for modelling waveguide structures but the main used methods are:

- Frequency-domain Mode Solvers for calculation of eigenmodes and propagation constants of straight and bent uniform waveguides, scalar, semivectorial, full vector, modal methods (Fourier modal method) [102] and discretization-based methods like Finite Difference (FD), Finite Element (FE), etc.
- Frequency-domain “beam propagation” methods (BPM) are the scattering methods to calculate optical field distribution within a waveguide structure for a given excitation field. There are various kinds of BPMs, which use approximations of the derivatives in the wave equation [103, 104], as Fast Fourier Transform (FFT-BPM) [105] using the fast Fourier transform, Finite Difference BPM (FD-BPM) using a finite-difference approximation [106] and Finite Element BPM (FE-BPM) using a finite-element approximation [107].
- Time-domain methods (FDTD) method [108] and Finite Element Time Domain (FETD) method [109]) are numerical models of optical field generated by given distribution of sources, which solve direct numerical solution of Maxwell equations [110].

Analytical Method is possible only in the case of planar (slab) optical waveguide [111] that solves a resultant transcendental equation. The Marcatili’s analytical method [111] is a semi-analytical approximation method for the analysis of buried waveguides and couplers, which gives accurate results for low-index-contrast waveguides. The authors in [112] improved Marcatili’s model in high-index-contrast (HIC) waveguides by adjusting the amplitudes of the components of the electromagnetic fields. With this improved method they derived the expressions for the effective group index and the effects of external forces on the propagation constant.

The accuracy of the numerical solution for the photonic device simulation depends on the methods and on the discretization parameters being used. [113]. The solution accuracy depends mostly on the index contrast waveguide. In case of analytical methods, the solution can be

obtained by solving the basic electromagnetic equations [114] and in opposite, numerical methods are computational models that can be used for many problems by modifying the basic model to fit the problem. But, both, analytical and numerical methods, play an important role in the modelling of optical waveguides and devices [115].

The design of optical components can be simulated successfully in 2D and 3D environment. In this thesis, Y-branch splitters were simulated in 3D only with RSoft Photonics tool and the achieved simulation results were compared with the 2D simulated results performed in Opti-BPM. Both photonics tools are based on Finite Difference Method (FDM), which is used to obtain and analyse the mode characteristics of waveguides when the eigen equation of an optical waveguide is solved. Usually BPM and FDTD are based on Maxwell's equations (see Appendix B.1) which are used to simulate optical waveguides and directional couplers and also simulate the propagation light in PLC devices.

3.1.1 BPM Method

BPM is the most used method to describe the evolution of electromagnetic wave propagation in photonics devices based on waveguide geometries, including optical waveguides. In this method the light propagation is studied in longitudinally varying waveguides such as Y-junctions, MMI couplers, tapers and bends. There are many numerical methods as Fourier transform method, the finite difference method (see Appendix D.1) and the finite element method integrated in BPM. Nevertheless, for the investigation of the light propagation in PLC devices the mostly used BPM method is based on the finite difference method.

The principle of the BPM [116] is presented in Figure 1-left. The input parameter is the field $\Phi_{in}(x, y) = \Phi_0(x, y)$ at $z = 0$ and for each propagation step the field $z + \Delta z$ is calculated and the output is $\Phi_{out}(x, y) = \Phi_D(x, y) = \Phi(x, y, D)$ at $z = D$. BPM uses equidistant discretization with respect to the z direction but in general the propagation step distance Δz can be different for each propagation step.

The general problem to be solved in case of a beam splitter is outlined in Figure 1-right, namely given an index distribution $n(x, y, z)$, which defines the optical device and a wave field at the input, at $z = 0$, $E(x, y, z = 0)$ the light distribution at the exit must be found.

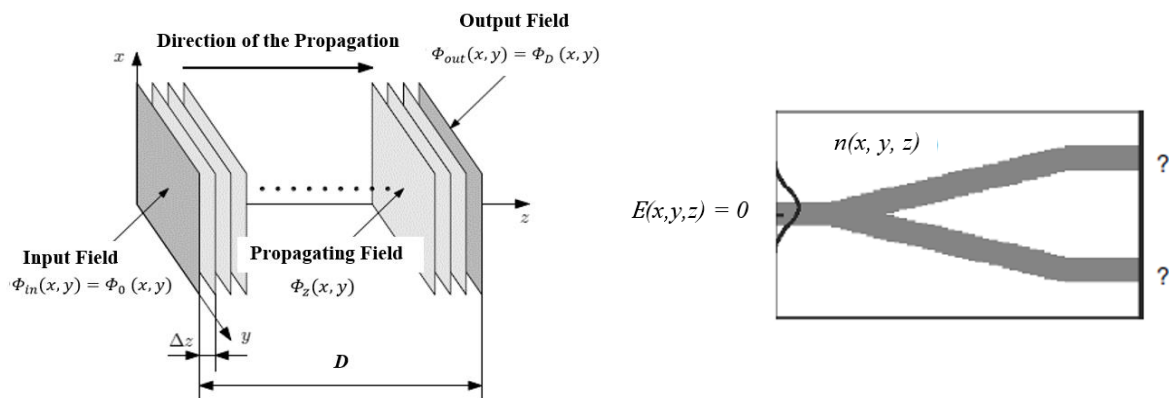


Figure 1: Principle of the BPM (left); general problem in optical propagation (right).

Based on slowly varying envelope method [117], the electrical field is $\vec{E} = E \exp(jk_0 n_0 z)$, where n_0 is a reference refractive index. Eq. A.6 (Appendix A.1) and wave equation for a homogenous waveguide can be expressed after some mathematical manipulations as:

$$\nabla^2 \vec{E} + \nabla \left(\frac{\nabla \epsilon_r}{\epsilon_r} \cdot \vec{E} \right) + k^2 \vec{E} = 0 \quad (3.1.1)$$

$$\begin{pmatrix} P_{xx} & P_{xy} \\ P_{yx} & P_{yy} \end{pmatrix} \begin{pmatrix} E_x \\ E_y \end{pmatrix} = (n_0 k_0^2 - 2jn_0 k_0 \frac{\partial}{\partial z}) \begin{pmatrix} E_x \\ E_y \end{pmatrix} \quad (3.1.2)$$

where the electrical field in Eq. 3.1.2 is the full-vectorial form of the wave equation. A common application is the semi-vectorial finite-difference beam propagation (SVFD-BPM) method taking into account the discontinuities in the normal electric field components across the internal dielectric interface. In this case the method provides efficiency and accuracy where the coupling terms P_{xy} , P_{yx} between E_x and E_y are neglected and the basic formulas are:

$$\text{Quasi-TE: } \frac{\partial}{\partial x} \left[\frac{1}{n^2} \frac{\partial (n^2 E_x)}{\partial x} \right] + \frac{\partial^2 E_x}{\partial y^2} + (n^2 k_0^2 - n_0^2 k_0^2) E_x = -2jn_0 k_0 \frac{\partial E_x}{\partial z} \quad (3.1.3-a)$$

$$\text{Quasi-TM: } \frac{\partial}{\partial y} \left[\frac{1}{n^2} \frac{\partial (n^2 E_y)}{\partial y} \right] + \frac{\partial}{\partial x} \left[\frac{\partial E_y}{\partial x} \right] + (n^2 k_0^2 - n_0^2 k_0^2) E_y = -2jn_0 k_0 \frac{\partial E_y}{\partial z} \quad (3.1.3-b)$$

Using the alternating directional implicit (ADI) method [118], each of above two equations will be split into two steps. First the equations are solved by a launch field at $z = 0$ and then they are integrated in z to obtain the field for the whole computational domain.

3.1.2 FDTD Method

Finite difference time domain method¹ is based on Maxwell's equations but a more rigorous method as BPM method, does not have any approximations or theoretical restrictions. The FDTD method was introduced by K. Yee [119] and then improved by others in the early 70s. It has the ability to model all wave effects such as propagation, scattering, diffraction, reflection and polarization through one analysis. It can also model material anisotropy, dispersion and nonlinearities [120] and can be roughly summarized as four parts:

1. Method improvement: it contain a faster simulation scheme [121], high-order FDTD schemes [122], unconditional stable schemes [123] and alternating mesh scheme [124].
2. Boundary condition: PML [125], and APML [126].

¹ Is a state of the art method for solving Maxwell's equations in complex geometries, with time and space solution by finite difference operators and offers an insight into all types of problems in electromagnetics and photonics. Additionally, it can also obtain the frequency solution by exploiting Fourier transforms, namely a full range of useful quantities can be calculated, i.e. the complex Poynting vector and the transmission/reflection of light.

3. Extending FDTD method to new material model: nonlinear material model, dispersive material model and quantum materials.
4. Extending FDTD to new advanced application areas such as bio-photonics, nanostructures and biomedical.

This leads to an algorithm², which provides reliable solutions of field distributions and is applicable for a wide range of problems of computational electrodynamics [127]. Therefore, to solve an electromagnetic problem, it is important to simply discretize both, in time and in space Maxwell's equations with central difference approximations. The Yee Algorithm divided the domain of interest (see Figure 2) into a grid of cubes (see Figure 3) and the electric field (E) at the centres of each of the faces is related to the magnetic field (H) of the pervious half time-step. In the same way, a similar grid is formed, with the cubes being a half pitch away in space and time, but this time updating the magnetic field using the electric field of the previous half time step [128].

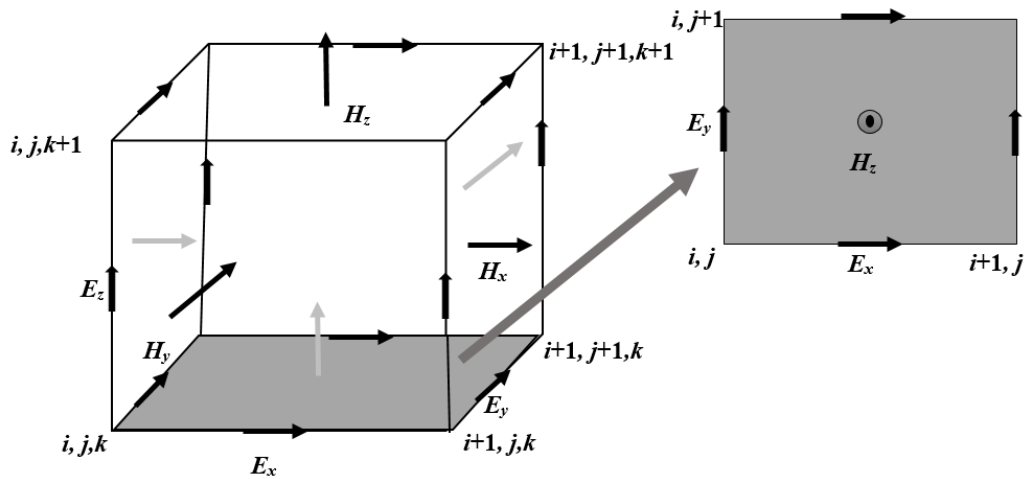


Figure 2: The Yee's cell used in 3D FDTD simulation.

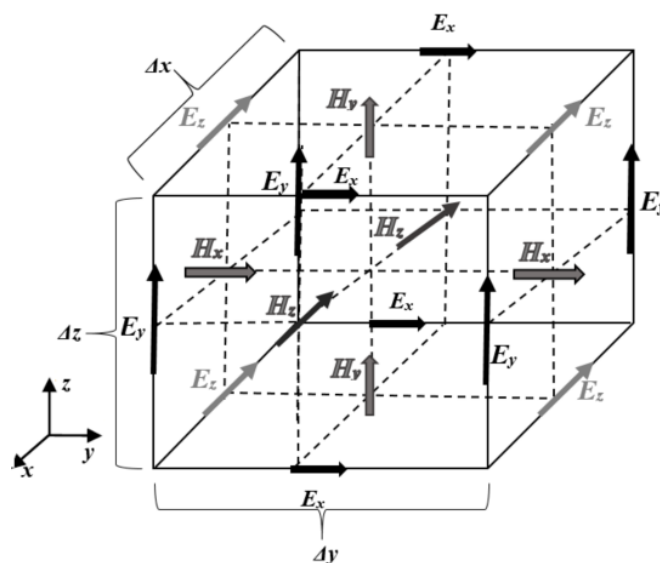


Figure 3: The Yee's Grid in the Cartesian coordinate system.

² Yee algorithm.

Therefore, the method divides the three-dimensional geometry into cells to form a grid, called Yee cell. Using two meshes alternatively, and starting from time $t = 0$, we can step forward in time, applying any excitation by setting certain values within the domain at each time step. In this way, every field component is stored on a different grid. Yee's algorithm solves for all E components at a given time-step based on previously computed and stored in memory H data. After that, the magnetic field is computed at the next time-step using E data just computed and the process is repeated until the time-stepping is concluded. However, at the each time-step the system of the electric and magnetic field components is updated based on the system of equations. The required computer memory and time is proportional to the size of computational domain, which is based on the size of photonic structure modelled.

The Eq. B.13 and B.14 (see Appendix B.1) can be rewriting for a region of space where there is no flowing currents or isolated charges as:

$$\vec{\nabla} \times \vec{E} = -\mu \frac{\partial \vec{H}}{\partial t} - \sigma^* \vec{H} \quad (3.1.4)$$

$$\vec{\nabla} \times \vec{H} = \epsilon \frac{\partial \vec{E}}{\partial t} + \sigma \vec{E} \quad (3.1.5)$$

These two curl equations can be written in Cartesian coordinates as six scalar discretized equations according to Yee's mesh [129] and then these can be solved with the FDTD method. Both, the E and H field component are put on a grid with grid points spaced Δx , Δy and Δz apart. It can be seen in Figure 3 that the field components are shifted to each other with a half of the step size. However, the time is discretized in steps of Δt and in this way the E field components are computed at time with a delay of $\Delta t/2$ compared to H field components. The discretized form of the Eq. (3.1.4) and (3.1.5) are:

$$\vec{H}^{n+\frac{1}{2}} = \left(\frac{1 - \frac{\sigma^* \Delta t}{2\mu_r}}{1 + \frac{\sigma^* \Delta t}{2\mu_r}} \right) \vec{H}^{n-\frac{1}{2}} - \left(\frac{\Delta t}{1 + \frac{\sigma^* \Delta t}{2\mu_r}} \right) \nabla \times \vec{E}^n \quad (3.1.5-a)$$

$$\vec{E}^{n+1} = \left(\frac{1 - \frac{\sigma \Delta t}{2\epsilon}}{1 + \frac{\sigma \Delta t}{2\epsilon}} \right) \vec{E}^n - \left(\frac{\Delta t}{1 + \frac{\sigma \Delta t}{2\epsilon}} \right) \nabla \times \vec{H}^{n+\frac{1}{2}} \quad (3.1.5-b)$$

The Eq. B.11 and B.12 can be iterated and solved. For an accurate simulation, the spatial grid must be small enough to resolve the smallest feature of the field to be simulated. For this, there is a limit on the time step Δt to ensure stability in the algorithm. To minimize the numerical instability is choice S , called numerical stability or Courant-Friedrichs-Lewy factor³ [130].

³ Stability factor for three dimensional geometry, which minimizes numerical instability, in this case the numerical dispersion and the numerical phase-velocity discontinuity.

When c is the speed⁴ of light in the material, Δt is the time step, Δx , Δy , Δz are the space increments in the x , y and z directions, the Courant condition⁵ [131] should be fulfilled:

$$S = c\Delta t \sqrt{\frac{1}{\Delta x^2} + \frac{1}{\Delta y^2} + \frac{1}{\Delta z^2}} < 1 \quad (3.1.6)$$

The main disadvantages of the FDTD method are relatively high memory requirements and long computational time [132]. This means, that the available memory limits the maximum size of a computational domain that can be simulated, while the long computational time restricts⁶ the use of the FDTD method for the simulations. But this limitations can be significantly reduced for example by using parallel computing. However, the PML for boundary conditions plays an important role in FDTD simulations because it prevents spurious reflections from the edge of the problem space and it is added to absorb the light emitted by the simulated structure from the boundaries of the computational region. Here can be pointed out that for this reason, the FDTD method is mostly used to simulate the small photonic structures based of high index contrast like for example the Silicon-on-Insulator (SOI) structures and not for low index photonic structures. SOI based waveguide devices used a high refractive index difference (see subsection 3.2.4) between the refractive index of the core and the cladding, this is approximately 100 times higher than that of typical low index contrast waveguides [83]. For low index contrast based waveguide structures (larger than SOI-structures) it is better to perform BPM calculation of the complete photonics structure.

3.2 Technological Verification of Used Photonic Tools

The commercial photonics software tools listed in subsection 3.1 are widely used to design passive optical components including optical splitters. As will be shown in this thesis the simulated results of the designed splitters applying these tools show similar results, confirming the correctness of the used calculation methods. However, each of these tools features some drawbacks. For example the main drawback of the Apollo Photonics tool is the fact that the exported GDSII files consist of some errors which make the file useless for the mask production. RSoft tool exports the splitter structures into GDSII format correctly however, the accuracy is much lower (10 times) than the one offered in the OptiBPM photonics tool. This has an influence mainly on the Y-branch splitter performance since this structure consists of many tiny waveguides. Therefore, the OptiBPM tool was mainly used for the splitter design.

⁴ Wave propagation speed.

⁵ A time-dependent source is placed somewhere in the structure, and the E and H fields are calculated iteratively for each time step Δt . This fields are recorded for later analysis.

⁶ The FDTD method can only simulate structures of a limited size since it requires huge amounts of physical memory to store the fields.

This software experience comes from the work done at Photeon Technologies where PhD supervisor Dana Seyringer was responsible for the development of the passive optical components (Photeon Technologies was a company which was the design supplier of passive optical components in 2000-2008 [133]).

All designs of passive optical components developed at Photeon were also technologically verified since the company had a close collaboration with various external professional foundries. Figure 4 shows as an example two mask layouts from two different technological runs. As can be seen, the mask layouts consist of optical splitters together with optical multiplexers/demultiplexers based on arrayed waveguide gratings [133].

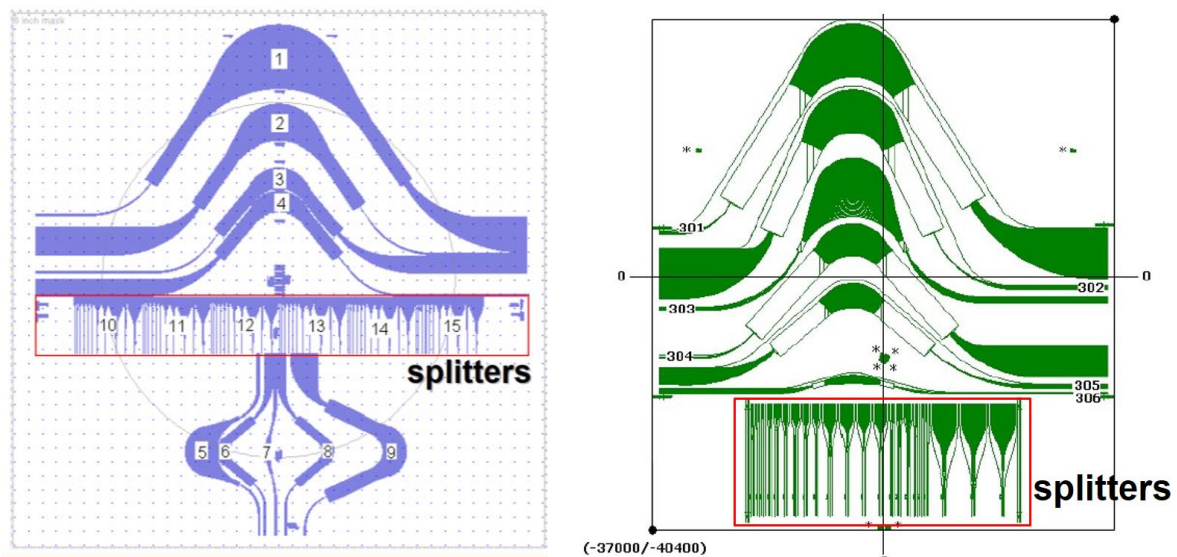


Figure 4: Two different mask layouts consisting of AWGs and optical splitters: (left) the 2nd technological run (2005) and (right) the 3rd technological run (2006) [133].

Figure 5 shows the detailed view of the splitter designs from Figure 4-right).

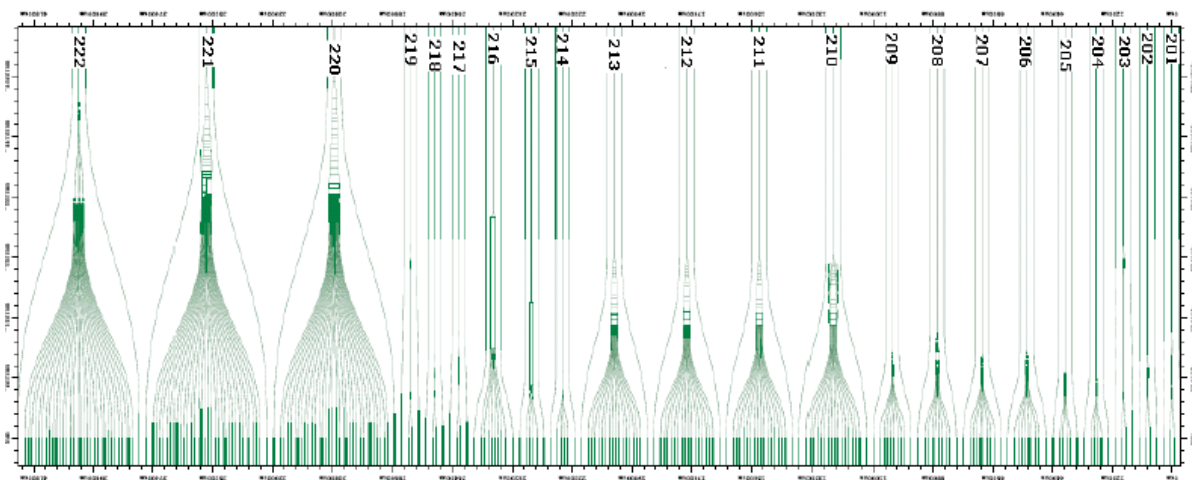


Figure 5: Detailed view of the splitter designs from mask layout in Figure 4-right [133].

The fabricated wafers were diced and the optical chips were also measured at the foundries. Figure 6 shows the splitting characteristics of 1x32 Y-branch splitter from the 3rd technological run, measured in C-Band over the whole wavelength range (1520 nm – 1570 nm).

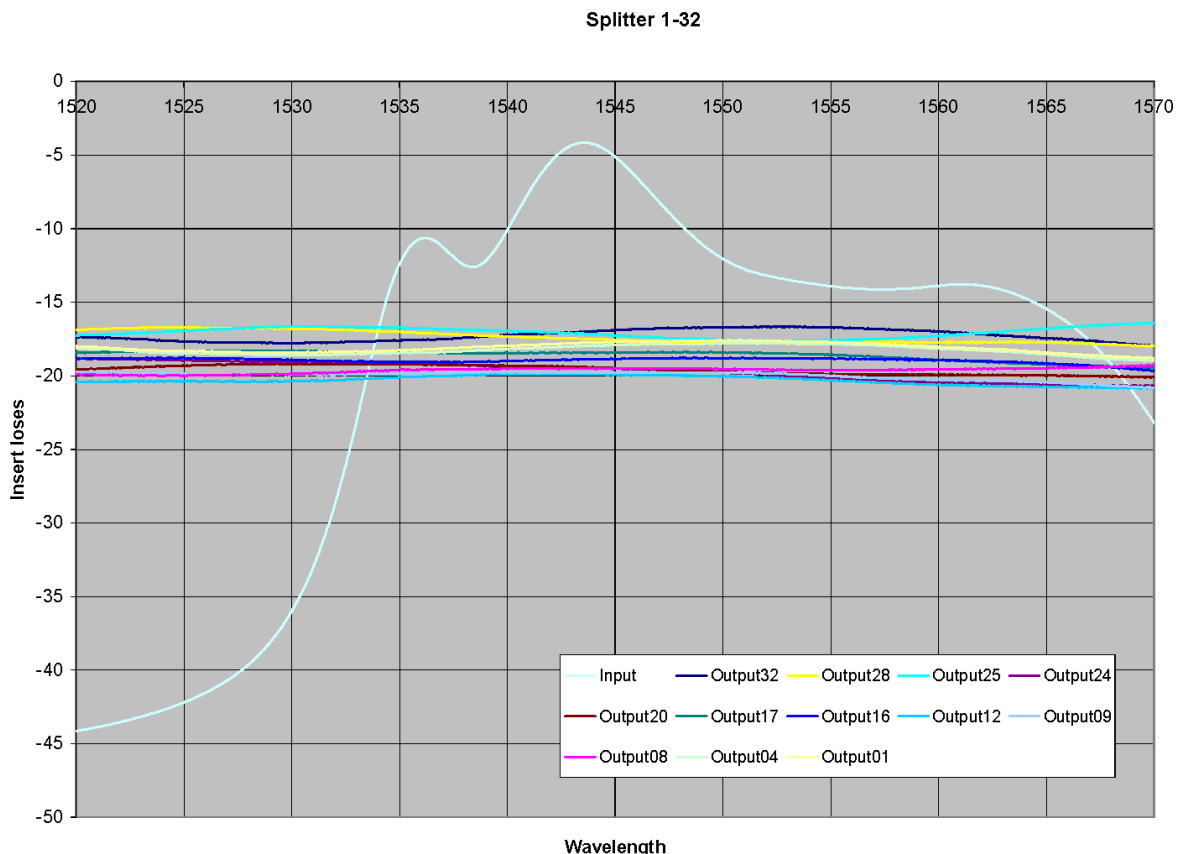


Figure 6: The optical characteristics of 1x32 Y-branch splitter measured in the C-Band [133].

As can be seen in Figure 7 the maximum measured non-uniformity ILu reached approximately 4.3 dB at $\lambda = 1570$ nm. The non-uniformity at $\lambda = 1550$ nm is $ILu = 3.35$ dB.

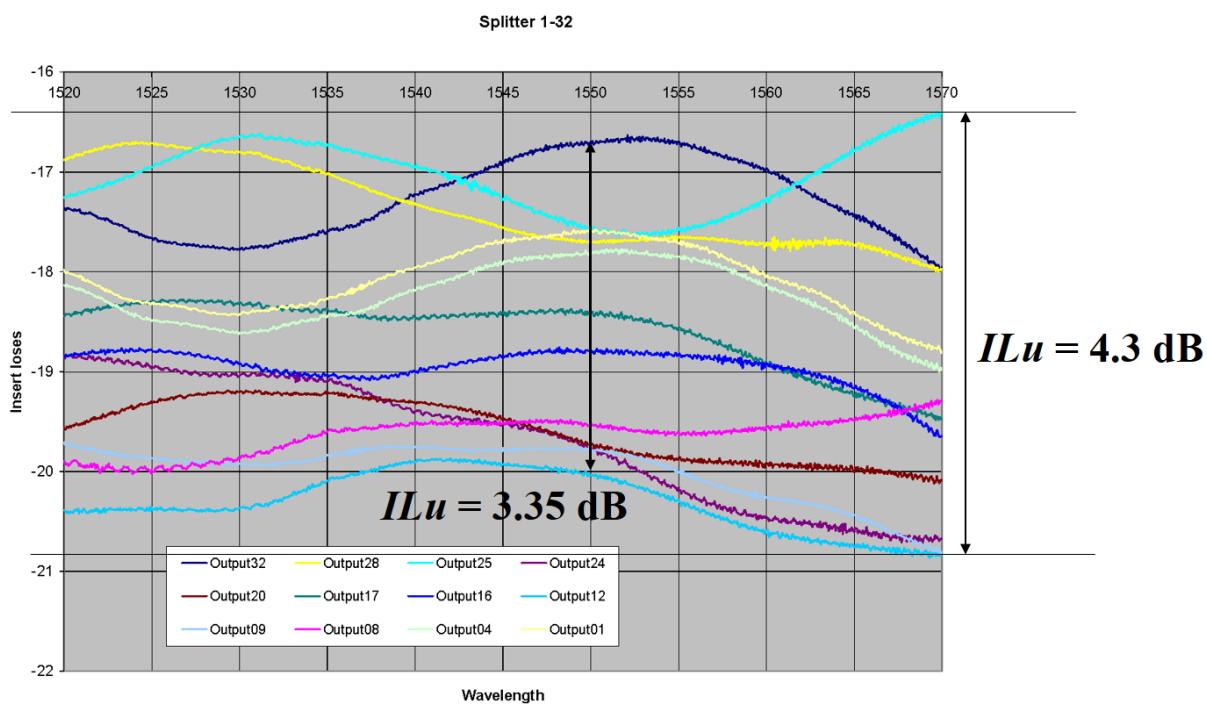


Figure 7: Detailed view of the losses together with the calculated non-uniformity [133].

Figure 8 presents the measurement set-up at International Laser Centre in Bratislava [134] who measured the fabricated optical chips in the case that the foundry did not include the chip measurement into the foundry services. Figure 9 shows the measurement of optical splitters.

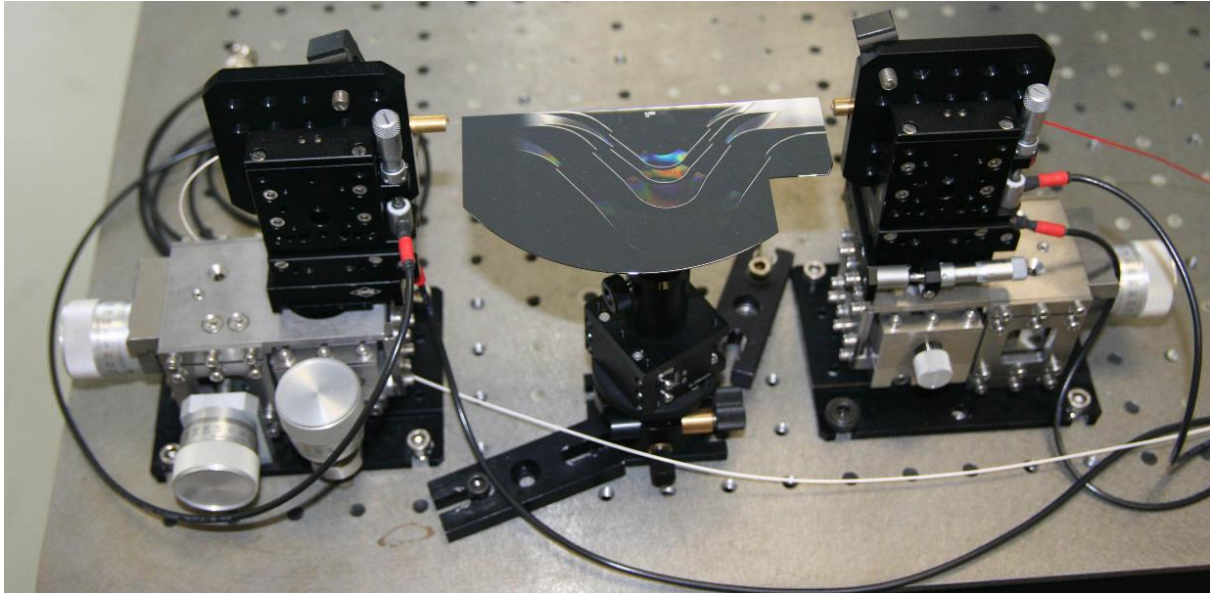


Figure 8: Measurement set-up at International Laser Centre in Bratislava: the measurement of AWGs [134].

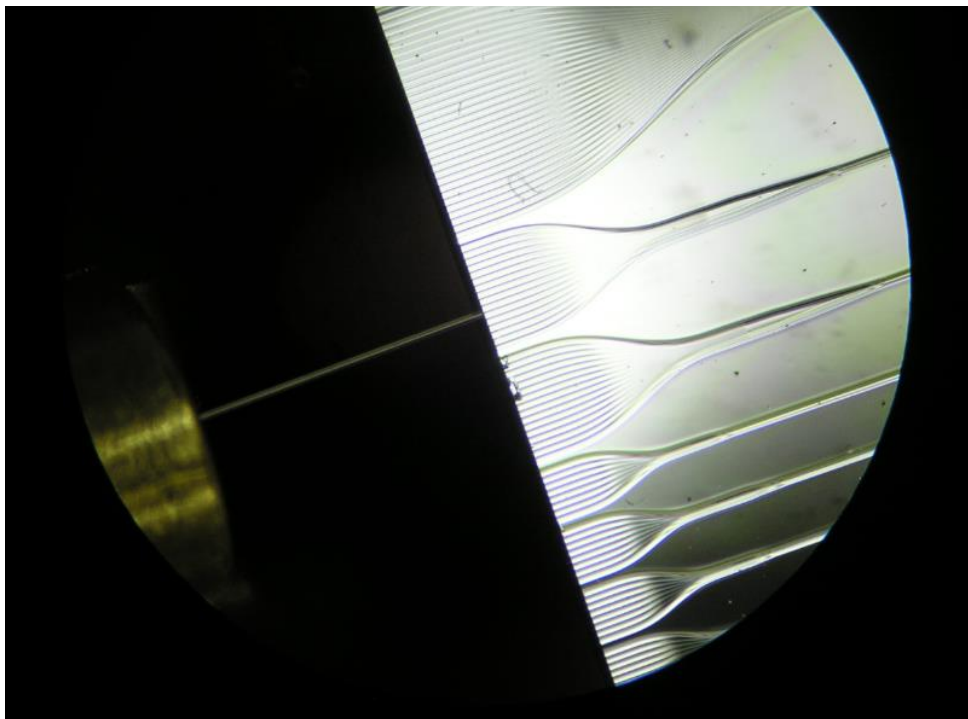


Figure 9: Measurement of optical splitters [134].

Based on this experience and also considering the fact that OptiBPM tool offers user-friendly interface with some additional useful functions we decided to use primarily this tool for the design of optical splitters presented in this work.

3.3 Design Principles

The procedure of designing optical Y-branch and MMI splitters using experimentally well verified photonics tools are discussed in this subsection.

3.3.1 Optical Splitter Design

Y-Branch Splitter

A design of conventional (standard) 1x4 Y-branch splitter with its characteristic parameters is shown in Figure 10. As can be seen from its geometry the splitter consists of a linear input port⁷, four linear outputs⁸ and three Y-branches, which are distributed into two layers. Port pitch between output branches, required for the connection with the fibers, was set to $127 \mu\text{m}$ ⁹. The length of the 2nd branch layer, L (2^{nd}) is double of the 1st branch layer, L (1^{st}).

The pitch between the waveguides in each branch layer was also doubled, i.e. in the 1st branch layer, the port pitch of output branches where fibers are connected, is W (1^{st}) = $127 \mu\text{m}$, and in the 2nd branch layer, W (2^{nd}) = $2 \times W$ (1^{st}) = $254 \mu\text{m}$.

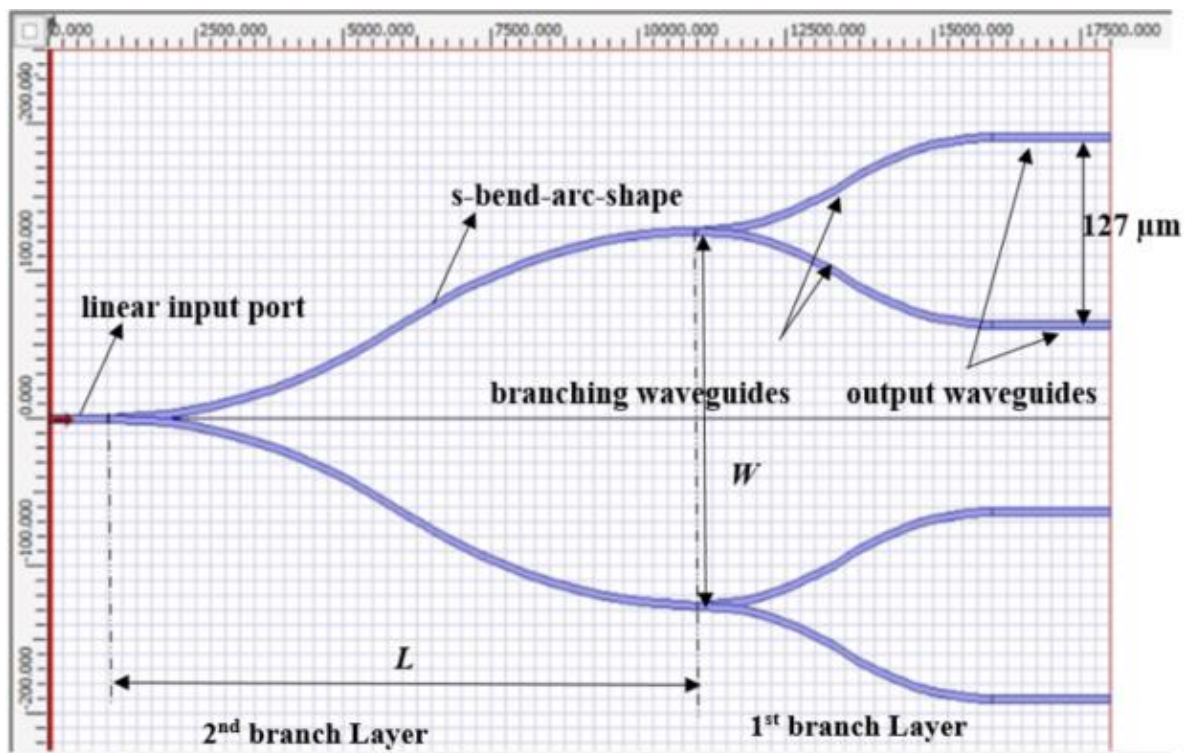


Figure 10: Geometry of 1x4 Y-branch splitter.

⁷ Set to $1000 \mu\text{m}$, since this is the minimum length required for the connection with the fibers.

⁸ Set to $2000 \mu\text{m}$.

⁹ This spacing is required for the connection with the fibers.

MMI Splitter

A design of conventional (standard) 1x8 MMI¹⁰ splitter with its characteristic parameters is shown in Figure 11. These parameters are:

- λ is the operating wavelength
- n_c is the refractive index of the core
- n_{cl} is the refractive index of the cladding
- N is the number of output waveguides
- a is the width of the input/output waveguides
- W_{MMI} is the width of the multimode section
- D is the pitch between two neighbour output waveguides (port pitch)
- L_{in} is the linear input port
- L_{out} is the length of the taper
- L_P is the length of the output waveguides.

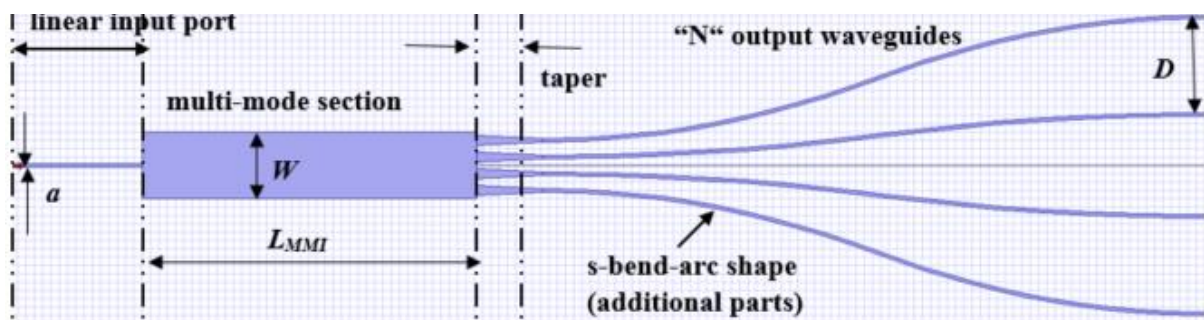


Figure 11: Design of a conventional 1x4 MMI splitter with its characteristics parameters.

The principle of MMI splitter can be seen in Figure 12. When the light enters the MMI section the high-order propagation modes of multimode section are excited. Through the interference between the excited modes, the split output signals can be formed. As shown in Figure 12 the number of output signals can be controlled by cutting the multi-mode section in a particular length L_{MMI} . From this follows that if we know the waveguide structure (n_c and n_{cl}) and the number of split output channels (N) we can choose the waveguide width (W_{MMI}) and for any wavelength λ we will get N -fold *splitting point* at a particular coupler length L_{MMI} . For example Figure 12 bottom shows 8-fold splitting. This particular coupler length can be calculated from:

$$L_{MMI} = \frac{n_c \cdot W_{MMI}^2}{N \cdot \lambda} \quad (3.3.1)$$

where n_c is the refractive index of the core, W_{MMI} is the width of the multimode section, N is the number of output signals and λ is the operating wavelength.

¹⁰ Works on the principle of self-imaging effect appearing inside the multi-mode section [7].

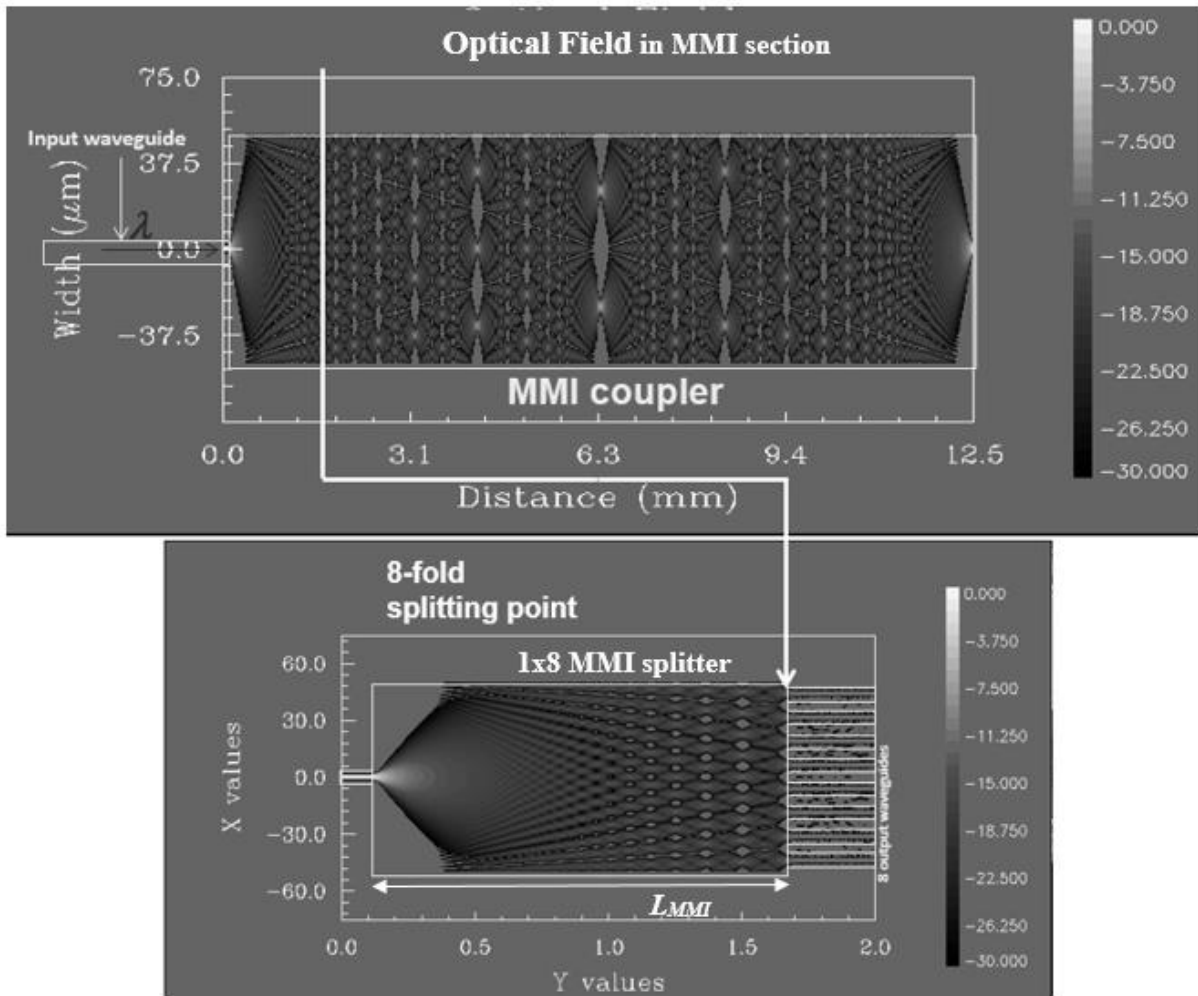
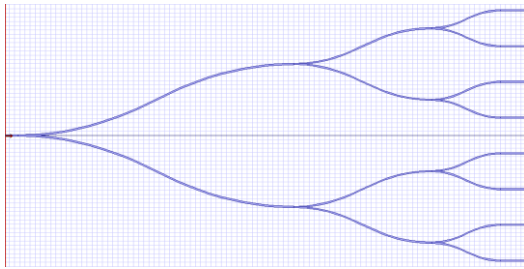


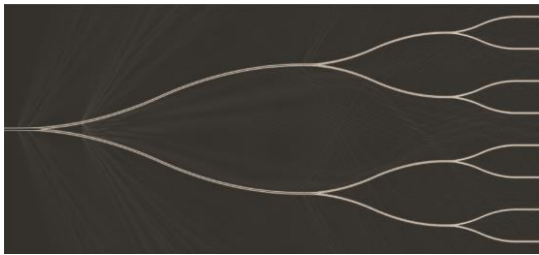
Figure 12: Principle of MMI splitter.

Figure 13 summarizes once again the advantages and the disadvantages of both, Y-branch and MMI optical splitters.

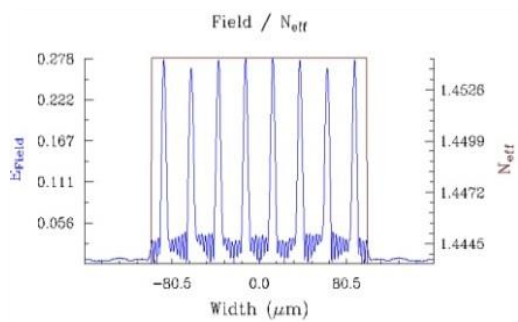
Y-branch splitter design



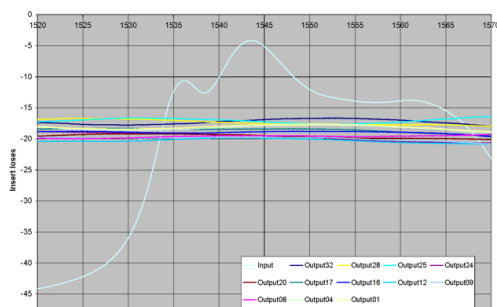
Y-branch splitter simulation



Non-uniformly split signals at the output



Wavelength independency of Y-branch splitter



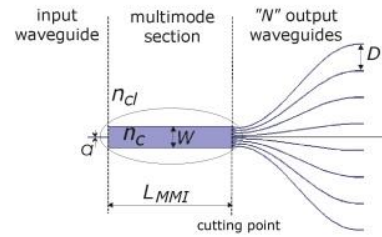
Advantages:

- wavelength independent
- polarization independent

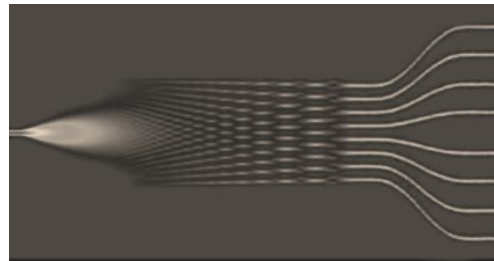
Disadvantages:

- asymmetric splitting ratio causing non-uniformity of the split power
- large size

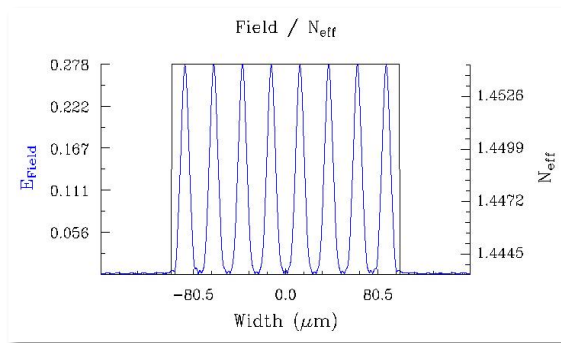
MMI splitter design



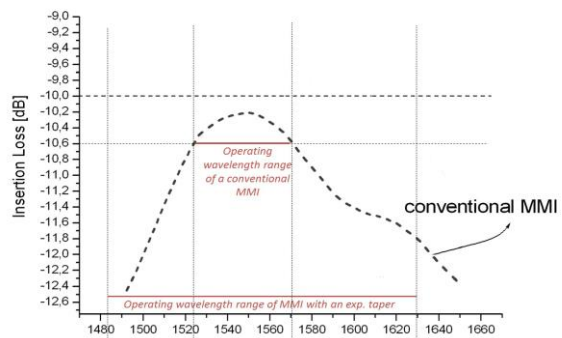
MMI splitter simulation



Uniformly split signals at the output



Wavelength dependency of MMI splitter



Advantages:

- large splitting number
- stable splitting ratio: good uniformity over all the output channels
- good fabrication tolerance

Disadvantages:

- wavelength and polarization dependent

Figure 13: Comparison of Y-branch and MMI splitters [133, 135].

3.3.2 Splitting Parameters

In the design of passive optical components for FTTH-PON networks it is necessary to consider different optical aspects as optical linear and nonlinear effects [136], optical amplification and attenuation [137], ageing of network elements [138], possible wavelength routing, etc. There are many features [70] that determine the application and function of the optical splitters, i.e. signal attenuation, direction of light transmission, number of input and output channels (ports), as well as the polarization sensitivity and single or multiple operations. The GR-1209 standard [139] defines the performance optical criteria to determine the quality of PLC splitters. These are Optical Bandpass, Optical Insertion Loss, Optical Return Loss, Uniformity, Directivity and Testing Method. For our purposes only some of these criteria are essential, which are listed in Table 1.

Table 1: Essential splitting parameters.

Splitting parameters	Abbreviation	Unit
Insertion loss	IL	dB
Insertion loss uniformity (non-uniformity)	ILu	dB
Background crosstalk	BX	dB

Insertion loss (IL), of a channel is the fraction of the power transferred from the input port to the output port. It indicates the worst value over all channels considering both polarization states which can be defined by:

$$IL = -10 \log_{10}[(\sum_{i=1}^N I_i)/I_{in}] \quad (3.3.2)$$

where I_i is the output energy from the i^{th} output waveguide and I_{in} is the energy at the input waveguide. Figure 14 shows the graphical representation of this parameter.

Insertion loss uniformity (ILu), also called the non-uniformity of the split power over all the output channels, is the difference between the highest peak and the lowest peak in the field distribution, i.e. the difference between minimum and maximum insertion loss¹¹ over all channels (Figure 14):

$$ILu = 10 \log_{10}[\min(I_i)/\max(I_i)] \quad (3.3.3)$$

Background Crosstalk (BX) is defined as the median peak transmission over all channels (Figure 14).

¹¹ There are various source for optical splitters insertion loss, which attenuate the field propagation through an splitter structure as the propagation loss in bent waveguides, the coupling loss between the fiber and the waveguide, the material and scattering losses, etc. [83].

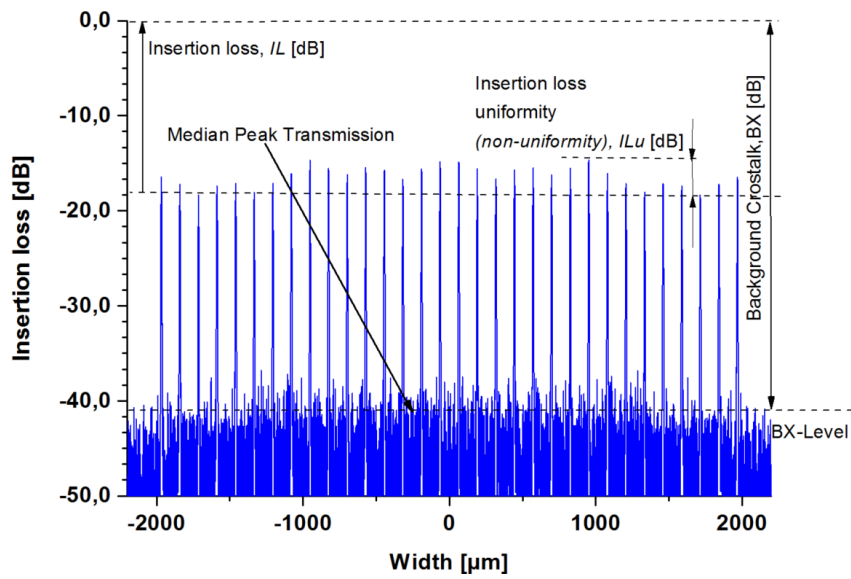


Figure 14: Definition of insertion loss, IL , insertion loss uniformity (non-uniformity), ILu and background crosstalk, BX .

3.3.3 S-Bend Waveguide

The standard bend waveguide used to design Y-branch splitter has usually a shape of one of three S-bends¹²: s-bend-sine, s-bend-cosine and s-bend-arc (double-circle) shown in Figure 15 [140, 141].

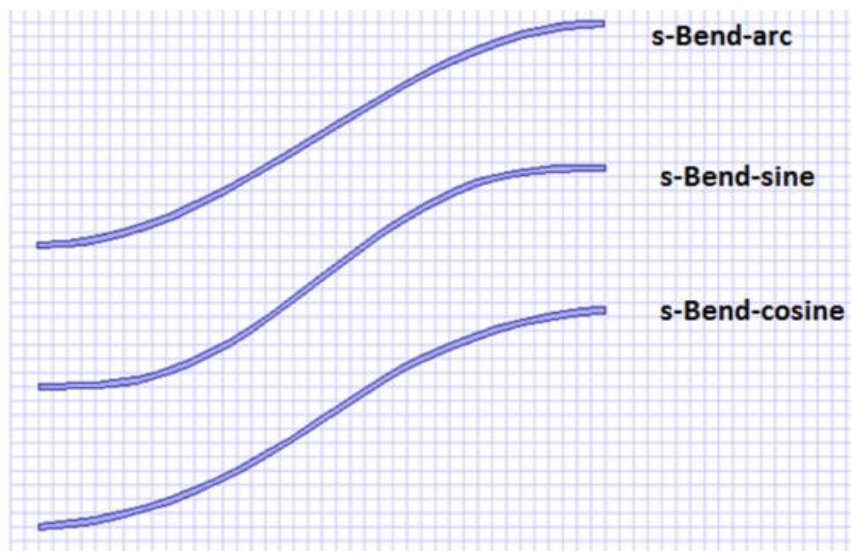


Figure 15: S-bend waveguide geometry.

The functions which describe the form of these S-bends are as follows [69]:

¹² Key elements of PICs device that perform guiding, coupling, switching, multiplexing, demultiplexing and splitting of optical signal.

$$\text{Sine:} \quad L = \sqrt{2\pi h R_{min}} \quad (3.3.1)$$

$$\text{Cosine:} \quad L = \sqrt{\frac{\pi^2}{2} h R_{min}} \quad (3.3.2)$$

$$\text{Double-circle:} \quad L = \sqrt{4h R_{min} + h^2} \quad (3.3.3)$$

where R_{min} is the minimum bend radius, h is the height of the bend and L is the length of the bend.

A condition for the bending section of directional coupler is to be slowly converging or diverging curve to minimize the radiation losses [69]. The S-bend waveguide is defined physically by two parameters, which determine the length of the device, namely the bend radius R and the offset, O ¹³ (in Figure 16):

$$L = 2\sqrt{R^2 - (R - \frac{O}{2})^2} \quad (3.3.4)$$

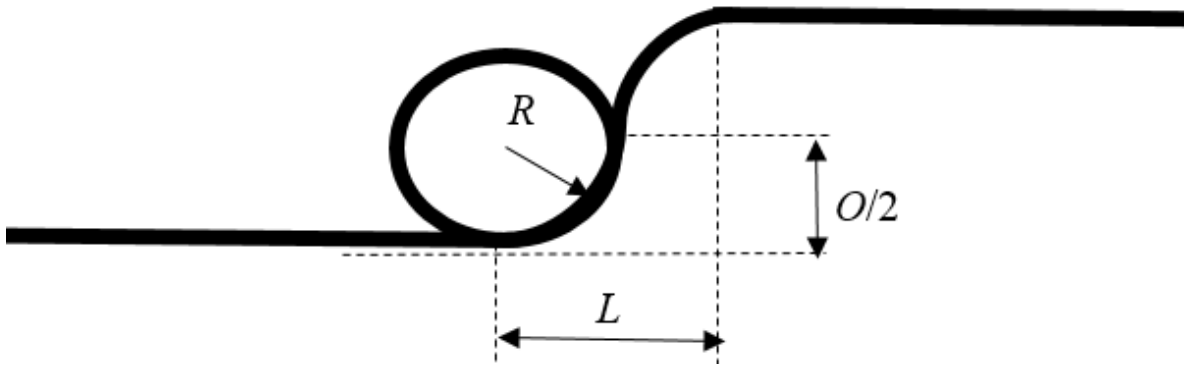


Figure 16: S-bend waveguide geometry.

The general shape of the S-bend, connecting two straight waveguides with a lateral offset and a longitudinal offset, which describes Y-branch splitter is shown in Figure 17 and the expressions for the S-bend based on sine and cosine functions are, respectively,

$$L(z) = \frac{O}{L_z} z - \frac{O}{2\pi} \sin\left(\frac{2\pi}{L} z\right) \quad (3.3.5)$$

$$L(z) = \frac{O}{2} (1 - \cos\left(\frac{\pi}{L} z\right)) \quad (3.3.6)$$

A slow convergence bending section appears in a longer effective coupling length for the device. In this way, the curvature radius R is decreasing, the optical path direction is changed

¹³ The displacement of the channel in the upper direction.

at a shorter propagation distance and the smaller device length of the bend waveguide. On opposite, the optical bending loss increases as the curvature radius R decreases [142, 143].

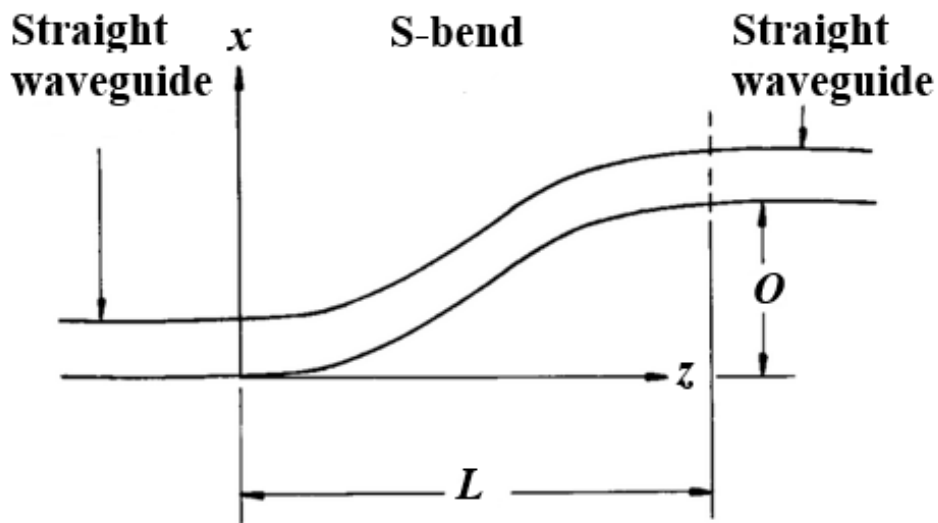


Figure 17: S-bend waveguide connecting two straight waveguides.

The influence of the shape of different predefined waveguides (s-bend-arc, s-bend-sine, s-bend-cosine) on the scattering was studied later in this thesis (see subsection 3.3.6.) by applying OptiBPM tool.

3.3.4 Used Waveguide Structures and Materials

The basic unit for photonic components is an optical waveguide¹⁴ with its basic working principle of total reflection of light. In a certain sense an optical waveguide is as the electrical wire in the electronics. In this way, an optical signal propagates always along the region with higher refractive index.

Table 2 shows a waveguide classification by looking at the number of dimensions in which the light is confined.

Table 2: Classification of optical waveguides.

Dimensions of light confinement	Classification of optical waveguides
1D	Planar waveguide
2D	Channel waveguides/Optical fibers
3D	Photonics crystals

The buried channel waveguide and different geometrical structures of commonly used 2D optical waveguides (except planar waveguide) are presented in Figure 18, where the high index layer is shown in dark grey and the low index layer in light grey.

¹⁴ An optical structure that allows the confinement of light within its boundaries by total internal reflection.

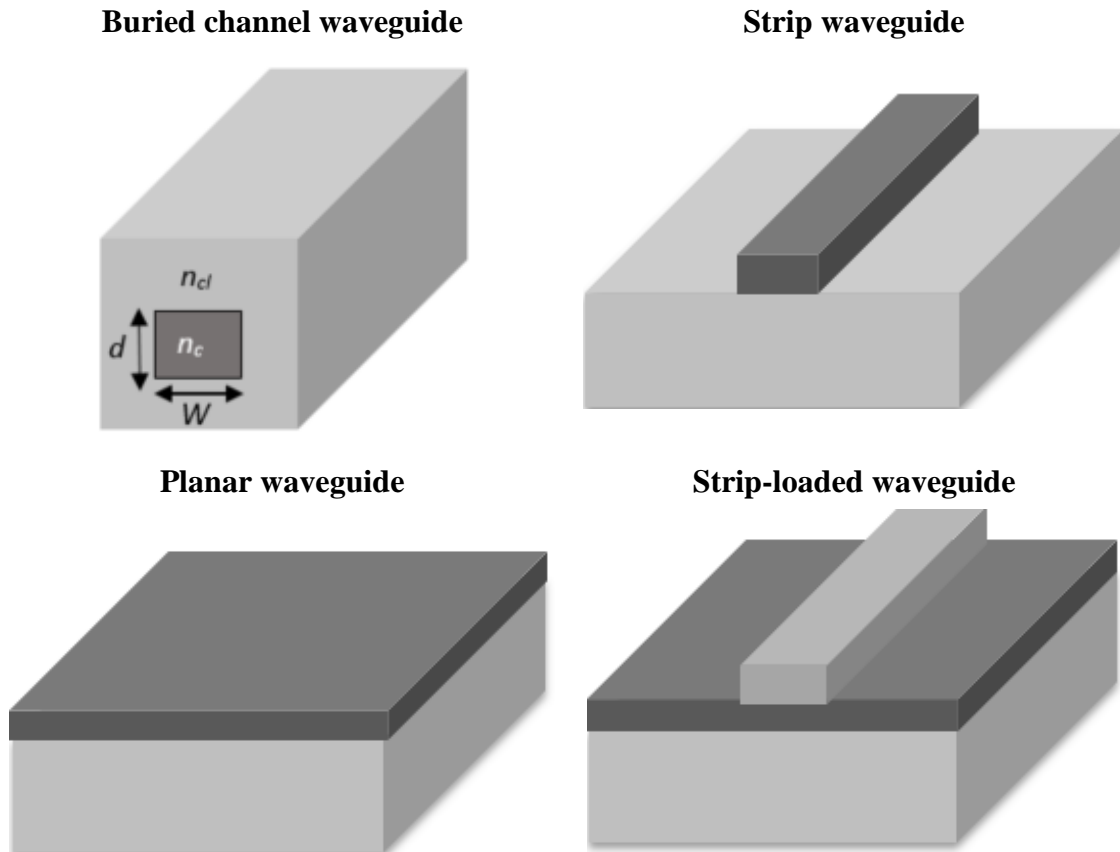


Figure 18: Schematics of different geometrical structures of 2D optical waveguides (except planar waveguide).

Depending on the applications the optical splitters can be fabricated using different material platforms as:

1. Low-index-contrast waveguide technology:
 - silica-on-silicon (SoS) buried waveguides [83].
2. High-index-contrast waveguide technology:
 - silicon-on-insulator (SOI) ridge waveguides [144 - 147]
 - SOI-nanowires [83]
 - buried InP/InGaAsP ridge waveguides [146, 148]
 - polymer waveguides [149, 150]
 - Si_3N_4 waveguides [151, 152].

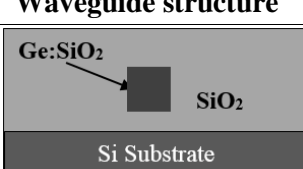
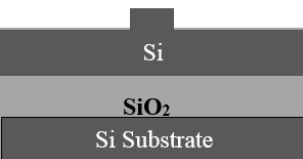
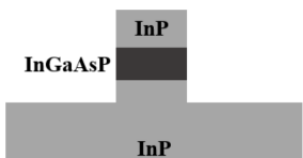
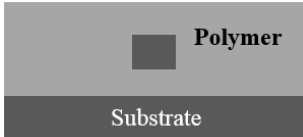
SoS: is a popular choice for passive waveguide devices used primary in telecommunication applications because of its outstanding advantages as for example the modal field matches well with that of single-mode optical fibers, making it relatively easy to couple them to fibers [83]. Another advantage of SoS-based waveguide devices is that they combine low propagation loss (<0.05 dB/cm, the reason is the little absorption and scattering) with a high fiber-coupling efficiency (low loss of order of 0.1 dB). This is the case of so called weakly guiding glass waveguide technology where the refractive index difference between cladding and core is $\Delta n = 0.75\%$ corresponding to the index contrast of the fibers.

However, the low-refractive-index contrast means a very large bending radius of the waveguides is needed. A consequence is a large size of silica-based optical splitters (several square centimetres), which limits the integration density of SiO₂-based photonic devices.

SOI: In contrast to this, the high-index-contrast waveguide technology uses a refractive index difference of $\Delta n \sim 2.055$ for Si/SiO₂ and 2.5 for Si/air, between the refractive indices of the core (Si, $n_c \sim 3.5$) and the cladding (SiO₂, $n_{cl} \sim 1.445$, or air, $n_{cl} \sim 1.0$). In percent is the refractive-index difference approximately 100 times higher than that of typical SoS waveguides, namely $\Delta n \sim 58\%$. A consequence of the fact that the waveguide size decreases proportionally to the increase of refractive index contrast is that the waveguide size for this material composition shrinks into the nanometer scale [83]. In this way it is possible to guide the light in waveguides with a far smaller bending radius (bending in order on the scale of several tens of microns), which leads to a marked reduction in the size of optical splitters by more than two orders of magnitude when compared to the optical splitters based on silica materials. Therefore, high index contrast based devices are a good candidate for high density integration on a chip.

Table 3 summarizes different materials used for waveguide manufacturing, waveguide structure, the advantages and disadvantages [151].

Table 3: Review of the different materials used for PLC devices.

Material	Waveguide structure	Advantage	Disadvantage
SiO ₂ (SoS waveguide)		Very low loss, small propagation loss and good matching to single mode (SM) fiber	Suitable only for passive functions
Si (SOI waveguide)		High refractive index contrast, high integration density, compatible with Si electronics	Indirect bandgap, unsuitable for lighting
InP		Direct bandgap, good for light emitters, high speed modulation lighting	High cost, complex technology
Polymer		Ease of fabrication, low cost, good Electro-Optic, Thermal-Optic performance	Stability, aging

3.3.5 SoS Waveguide Structure

To design optical splitters, as a first step it is necessary to design waveguide structure. The cross section of the standard SiO₂-buried rectangular waveguide structure, used in the splitter designs for telecommunication applications, is usually $(6 \times 6) \mu\text{m}^2$ to ensure the single

mode light propagation only (see Figure 19-left). The refractive-index contrast difference between the cladding and the core (waveguide) is $\Delta n \sim 0.011$ ($\sim 0.75\%$), where the refractive-index of the core $n_c \sim 1.456$ and of the cladding $n_{cl} \sim 1.445$ (taken from the standard technology of the foundry mentioned in Section 3.2). The used refractive index difference corresponds to the index contrast of the fibers, which makes it relatively easy to couple them to fibers [83], (see Figure 19-right).

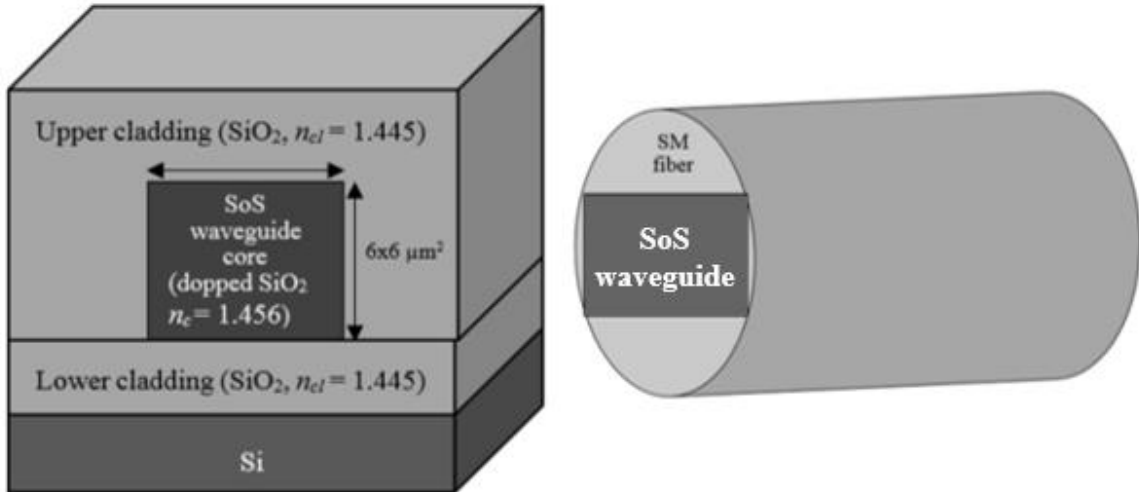


Figure 19: The cross-section of SoS waveguide structure (left); comparison of the waveguide dimensions with the standard SM fiber (right).

Design of SoS Waveguide Structure in Apollo Photonic Tool

Figure 20-left shows the structure of SoS waveguide designed in Apollo Photonics tool. The basis is the substrate, having thickness DS and width WGW with a refractive index of $n_{cl} = 1.445$. Above the *substrate* is placed a *channel* with a refractive index of $n_{cl} = 1.445$ again. Inside the *channel* is located the *core* having a refractive index of $n_c = 1.456$. The core size is defined by the width W and thickness D . Above the core is the cover with a refractive index of $n_{cl} = 1.445$ and thickness D . Some additional layers (*layer 1... layer N*) can be used to design more complex waveguide structures. Therefore, in our waveguide design the thicknesses of these layers were set to zero. According to this, the core width W and the thickness D were set to $6 \mu\text{m}$, the waveguide width WGW was set to $30 \mu\text{m}$ and the waveguide height was set to $20 \mu\text{m}$ by setting the size of the substrate DS and of the cover DC to $10 \mu\text{m}$. Figure 20 right shows the graphical representation of the channel waveguide cross-section in Apollo Photonics tool.

All geometrical parameters of the waveguide are listed in Table 4.

Table 4: Geometry of SoS waveguide with a core size of $(6 \times 6) \mu\text{m}^2$.

Name	Variable	Expression
Width	W	$6 \mu\text{m}$

Waveguide Width	WGW	$30\ \mu\text{m}$
Thickness	D	$6\ \mu\text{m}$
Channel Bottom	CB	$-3\ \mu\text{m}$
Cover	DC	$10\ \mu\text{m}$
Substrate	DS	$10\ \mu\text{m}$

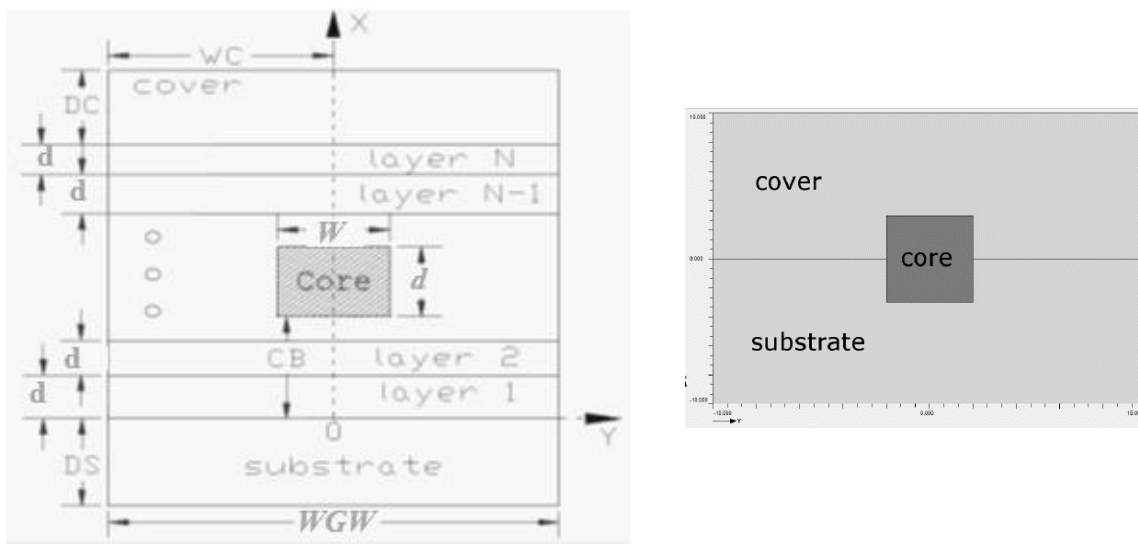


Figure 20: Design parameters of a waveguide structure in Apollo tool (left); The design of the waveguide with $(6 \times 6)\ \mu\text{m}^2$ core size in Apollo Photonics (right).

Figure 21 shows the graphical representation of the optical field simulated in the designed waveguide from Figure 20.

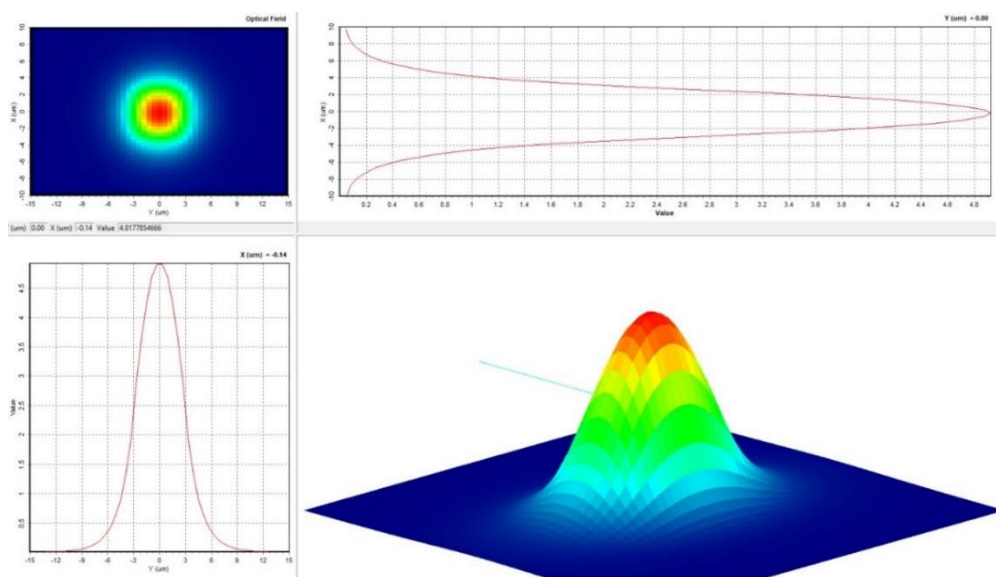


Figure 21: Optical field in the waveguide, simulated in x and y in Apollo Photonics.

Design of SoS Waveguide Structure in Optiwave Tool

Designing and simulating a waveguide structure in OptiBPM is slightly different from Apollo Photonics. In the first step two new materials were defined, namely the *cladding* with a refractive index of $n_{cl} = 1.445$ and the *core* with a refractive index of $n_c = 1.456$. After defining

the material, the waveguide was designed. The structure is the same as in Apollo Photonics tool, namely the basis of the waveguide structure forms the *Substrate* having a width of $30\ \mu\text{m}$ and a thickness of $10\ \mu\text{m}$. The material of the substrate is cladding with a refractive index of $n_{cl} = 1.445$ which was defined before. The *Channel*, that has a width of $6\ \mu\text{m}$ and a thickness of $6\ \mu\text{m}$, was located above the substrate. The material of the channel is the *core* with a refractive index of $n_c = 1.456$ and the offset was set to $6\ \mu\text{m}$ to get the same structure as in Apollo Photonics tool. The final layer forms the *Cover* with a width of $30\ \mu\text{m}$ and a thickness of $10\ \mu\text{m}$. The material is cladding, the same as of the substrate and the offset was set to $10\ \mu\text{m}$ (see Figure 22).

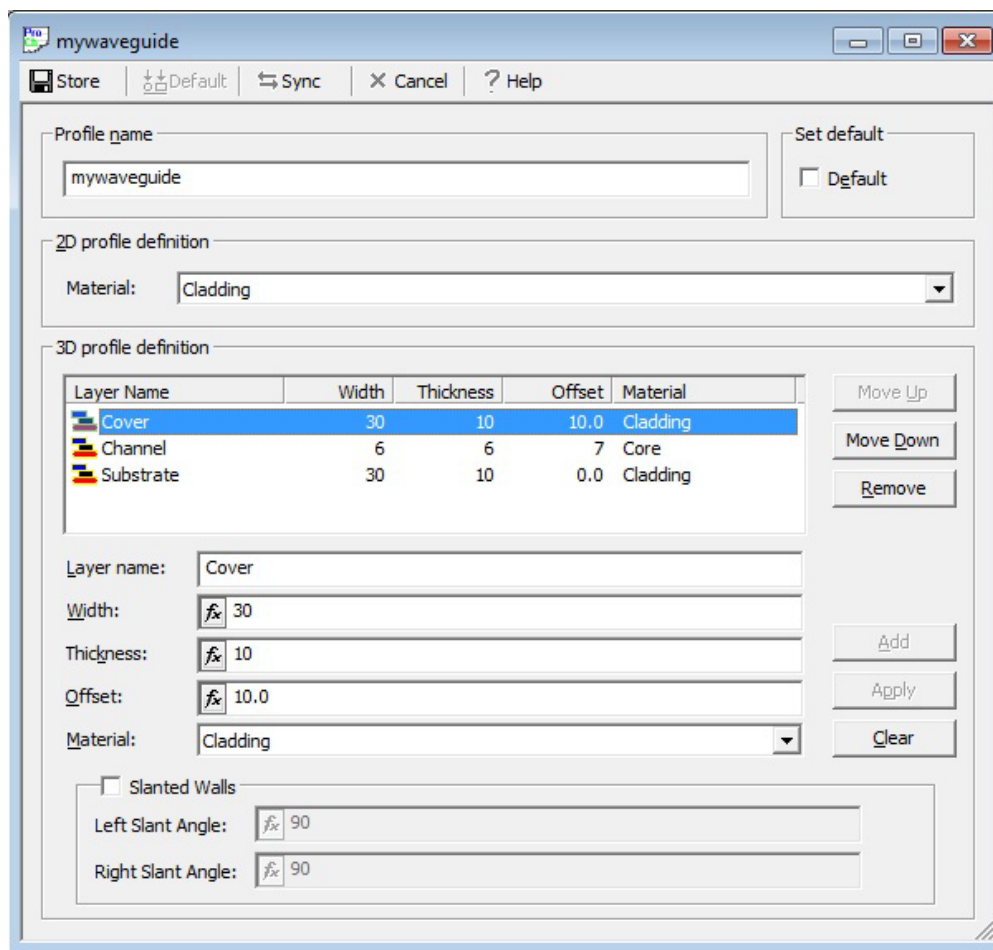


Figure 22: Defining the waveguide structure in Optiwave tool.

3.3.6 Silicon Nitride Waveguide Structure

SiN is a common material in CMOS fabs and is typically deposited by either Low Pressure Chemical Vapour Deposition (LPCVD) at high temperature ($>700\ \text{°C}$) or by Plasma Enhanced Chemical Vapour Deposition (PECVD) at low temperature ($<400\ \text{°C}$). LPCVD-based SiN, typically close to stoichiometric Si_3N_4 , is highly strained and provides excellent control over the homogeneity of material index and thickness. It has a refractive index of around 2.0 at a wavelength of $1550\ \text{nm}$. PECVD-based nitride has a composition that depends strongly on the deposition conditions and can be silicon-rich (higher refractive index) or nitrogen-rich (lower refractive index). Both types of nitride have been used for PICs. To this end the LPCVD nitride

is annealed at high temperature to drive out the hydrogen [153]. SiN is transparent throughout most of the visible range – down to at least 500 nm – it is a viable candidate to implement “silicon photonics” at wavelengths below 1.1 μm . This has led to demonstrations of spectroscopic functions, Raman spectroscopy-on-chip functions and integration with colloidal quantum dots emitting in the visible spectral range. SiN waveguides are less sensitive to a waveguide sidewall roughness in comparison to silicon photonics (SOI), while the compact footprint is largely maintained. One could say that the index contrast in silicon nitride waveguides fits nicely in the middle between the high-index and low-index-contrast waveguide material platforms.

Such compact devices can easily be implemented on-chip and have already found various applications in WDM systems and in other emerging applications, such as optical sensors [152]. SOI strip waveguides completely surrounded by a silica cladding have typical waveguide losses of 1 to 2 dB/cm, largely due to the scattering losses associated with sidewall roughness. In SiN photonic wires these losses can in principle be an order of magnitude lower. The losses can be reduced further by using shallow rib waveguides or very thin strip waveguides. Losses down to ≈ 1 dB/m have been reported for such SiN waveguides, but this is obviously at the expense of lateral and/or vertical confinement [154].

For the design of the optical splitters based on silicon nitride two different waveguide structures were used, i.e. a channel structure and a shallow rib waveguide structure.

Channel Waveguide Structure

Figure 23 shows the graphical representation of the channel waveguide cross-section (left) together with an optical field simulated in the waveguide (right). As can be seen, the waveguide has a channel structure, i.e. a core that is surrounded by a cladding. The refractive index of the core is $n_c = 1.95$ and of the cladding $n_{cl} = 1.455$. The size of the waveguide was designed to support single mode only (650×220) nm^2 .

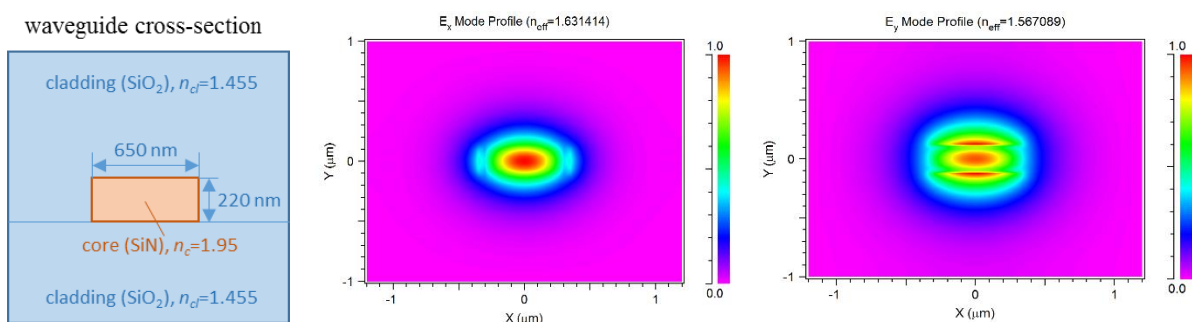


Figure 23: Cross-section of the designed waveguide structure with all important desing parameters (left); optical field in the waveguide, simulated in x and y axis (middle and right).

Shallow Rib Waveguide Structure

As can be seen in Figure 24-left, the shallow rib waveguide structure consists of a silicon substrate on which 10 μm thick thermal SiO₂ buffer layer is grown by thermal oxidation. The refractive index of this layer is $n_b = 1.456$. As a next step, a 0.5 μm thick silicon nitride active

layer, with refractive index $n_c = 1.925$, is deposited by PECVD. This layer is shallow etched down to $0.25 \mu\text{m}$ to create the rib structure of the waveguide. In the final step, a $3 \mu\text{m}$ SiO_x passivation layer with refractive index of $n_p = 1.48$ is deposited by PECVD. The width of the waveguide was tested in various simulations to reach a single mode propagation of the optical beam.

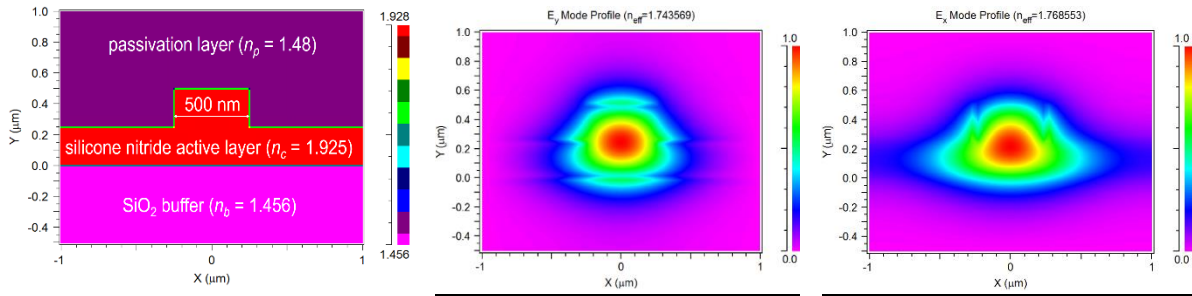


Figure 24: Contour map of transverse refractive index profile created in RSoft tool (left); normalized E mode profiles (middle and right).

Calculations of guided modes in the designed waveguide structure and their effective refractive indices (n_{eff}) were performed by finite element method (FEM in RSoft photonics tool) at 850 nm wavelength in free space. Figure 25 shows output of the calculations, i.e. the numbers and N_{eff} values of the modes guided in SiN waveguide, depending on the waveguide width. Based on these simulations we chose the width of the waveguide to be $0.5 \mu\text{m}$. Figure 24-middle and right presents normalized E_x and E_y mode profiles simulated in the final waveguide structure used later for the Y-branch splitter design (see section 3.4.6).

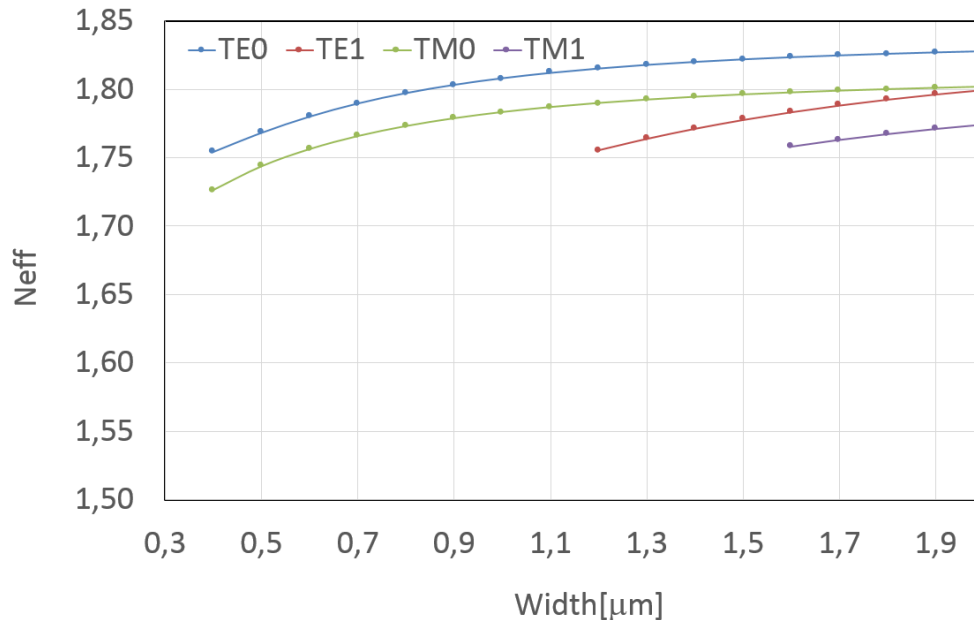


Figure 25: Dependence of N_{eff} of guided modes on waveguide width having $0.5 \mu\text{m}$ height.

3.4 Design of Low-Index-Contrast Y-Branch Splitters

Designs of SoS standard¹⁵ Y-branch splitters are based on the design of 1x4 Y-branch splitter [155] as shown in Figure 10. The branches of this splitter were designed using a predefined “s-bend-arc” shape in OptiBPM tool from Optiwave because this shape provides the lowest losses from the predefined standards shapes [156]. This splitter is composed of a three branches, a linear input port set to 1000 μm , four linear outputs and three branches, which are distributed into two layers. The width of the ports and the branches was set to 6 μm , the port pitch of the output branches, required for the connection with the fibers, was set to 127 μm . The output port's length was set to 2000 μm . The length of the 1st branch layer was tested in various simulations and set to $L(1^{st}) = 5000$ μm . If the parts were shorter (stronger bending), the losses increased, if the parts were longer (weaker bending), no improvement of the splitting parameters was achieved. The length and the width of the 2nd branch was doubled to keep the same bending of s-bend-arc parts as in the first branch. Therefore the length of the first branch was set to $L(2^{nd}) = 10000$ μm and the pitch $W(2^{nd}) = 256$ μm . Finally, the whole length of the splitter reached 18000 μm .

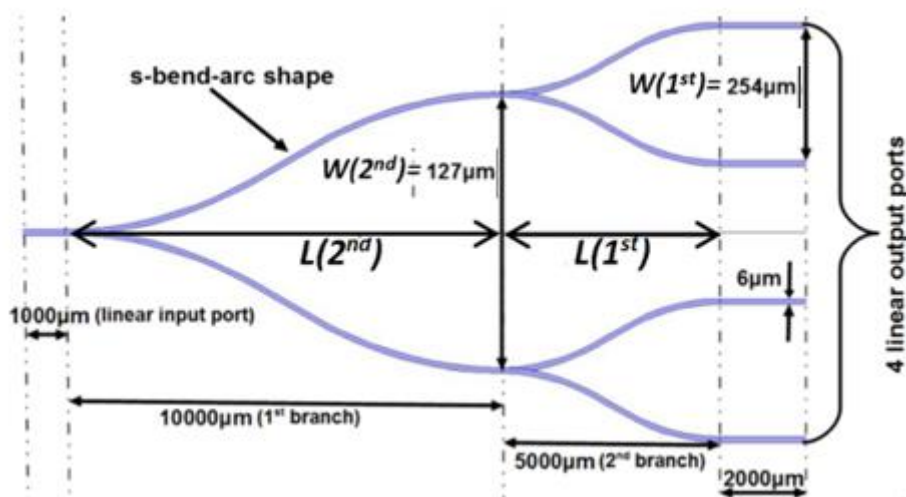


Figure 26: Design of “standard” SoS 1x4 Y-branch splitter.

3.4.1 Design of 1x8 Y-Branch Splitter

Design of 1x8 Y-branch splitter is constructed from two 1x4 Y-branch splitters connected by an additional branch (see Figure 27). To keep further the constant bending shape the 3rd branch layer was also doubled i.e. $L(3^{rd}) = 20000$ μm . The pitch between the waveguides in each branch layer was automatically doubled, i.e. in the 1st branch layer, the port pitch of output branches where fibers are connected, $W(1^{st}) = 127$ μm , in the 2nd branch layer $W(2^{nd}) = 254$ μm and in the 3th branch layer $W(3^{th}) = 508$ μm . Thereby the whole length of the 1x8 Y-branch splitter reached 38000 μm and the width of the splitter was 889 μm ($= 7 \times 127$ μm).

¹⁵ The standard shape was used, this means a waveguide having (6×6) μm^2 cross section.

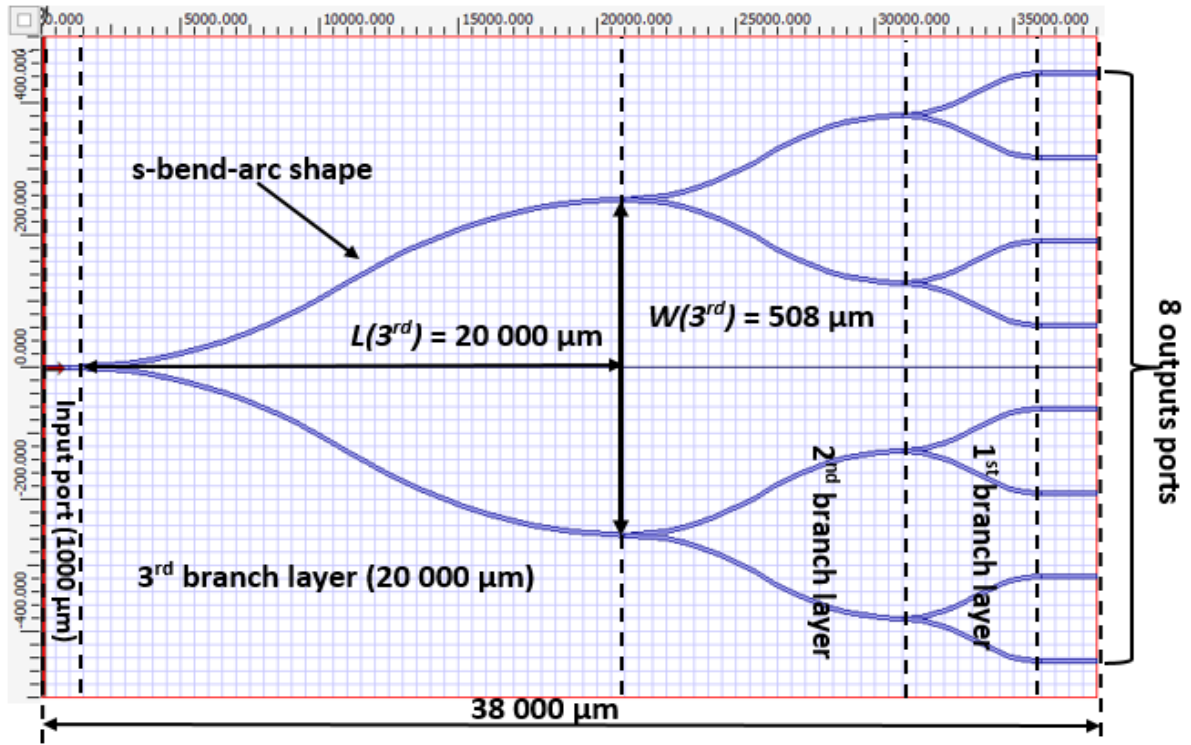


Figure 27: Layout of SoS 1x8 Y-branch splitter applying OptiBPM tool.

3.4.2 Design of High Splitting Ratio Y-Branch Splitters

The high splitting ratio Y-branch splitter designs were constructed as follows: the design of standard 1x16 Y-branch splitter was obtained from two 1x8 Y-branch splitters which were connected by another Y-branch to get 1x16 Y-branch splitter. The length of this additional branch is $L(4^{th}) = 2 \times L(3^{rd}) = 40000 \mu\text{m}$. The standard 1x32 Y-branch splitter was designed from two 1x16 Y-branch splitters by adding an additional branch having the length $L(5^{th}) = 2 \times L(4^{st}) = 80000 \mu\text{m}$. Consequently in the design of the “standard” 1x64 Y-branch splitter, two 1x32 Y-branch splitters were connected by an additional branch, namely $L(6^{th}) = 2 \times L(5^{st}) = 160000 \mu\text{m}$. The individual widths and lengths of branch layers of 1x16, 1x32 and 1x64 Y-branch splitters are given in Table 5.

Table 5: Summary of the high splitting ratio Y-branch splitter designs.

	1x16 Y-branch splitter	1x32 Y-branch splitter	1x64 Y-branch splitter
Number of layers	4	5	6
Number of Y-branches	15	31	63
Width of the splitter	1905 μm (= 127 μm x 15)	3937 μm (= 127 μm x 31)	8001 μm (= 127 μm x 63)
Length of the splitter	78000 μm	158000 μm	318000 μm

3.4.3 Length Optimization of High Splitting Ratio Y-Branch Splitters

As presented in Table 5 one of the main disadvantages of the low-index-contrast Y-branch splitters is that they are too long to keep the propagation losses in the waveguides low. Therefore, the next task of this work was to optimize the length of the “standard” high splitting ratio Y-branch splitters without destroying their optical properties.

3.4.3.1 Length Optimization of 1x32 “Standard” Y-Branch Splitter

Figure 28-left shows the design of standard 1x32 Y-branch splitter. Its size reached 158000 μm . In the length optimization of this splitter as a first step we reduced the length of the 5th and the 4th branch layers because they are too long (see Figure 28-right). To this purpose we used exactly the same splitter layout but with the length of the 5th and the 4th branch layers reduced to $L(5^{\text{th}}) = 40000 \mu\text{m}$ and $L(4^{\text{th}}) = 20000 \mu\text{m}$. After, the whole length of the splitter shrank from 158000 μm to 98000 μm . We will call such Y-branch splitter design as a “length optimized” design.

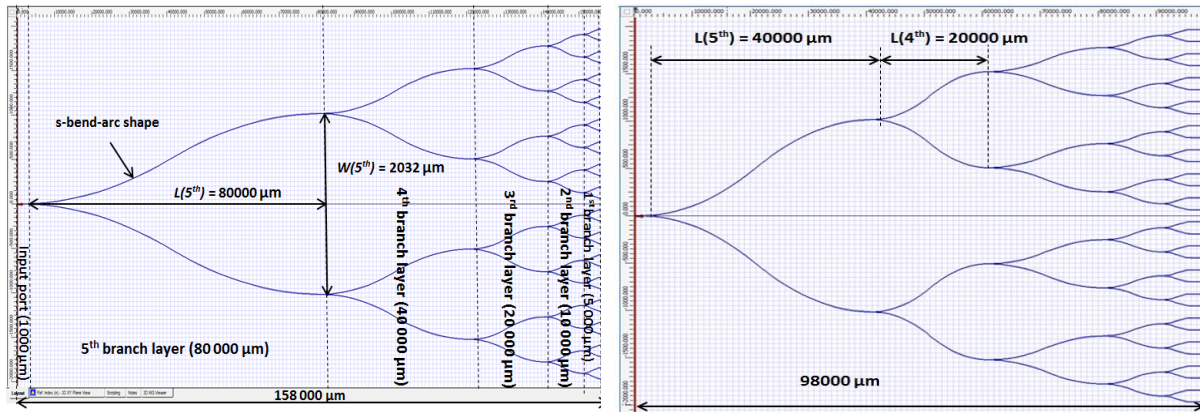


Figure 28: Layout of 1x32 Y-branch splitter: “standard” structure (left); “length optimized” splitter structure (right).

Based on the simulated results of the “length optimized” 1x32 Y-branch design (Section 4.2.6) the following further length reductions of the splitter were proposed (see Figure 29):

- The 5th branch layer length was reduced by 15% (Option 1).
- The 5th branch layer length was reduced by 20% (Option 2).
- The 5th branch layer length was reduced by 50% and between the 5th and the 4th branch layers a 500 μm linear waveguide was placed (Option 3).
- The 5th, the 4th and the 3rd branch layer lengths were reduced by 15% (Option 4).

For the clarity, these Y-branch splitters will be called as “further length reduced” 1x32 Y-branch splitters.

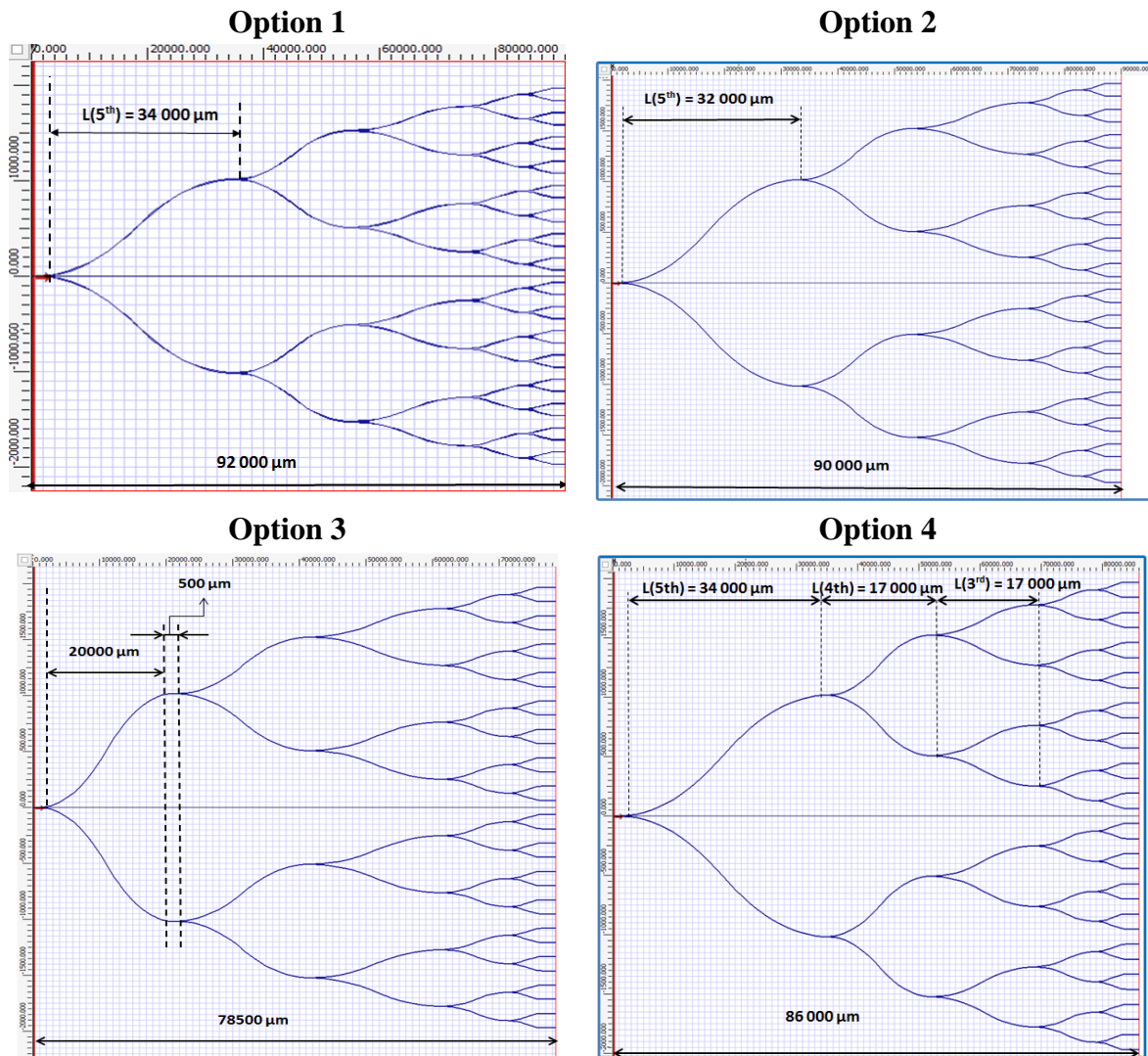


Figure 29: Design layouts of the “further length reduced” 1x32 Y-branch splitter structures for all four options.

Option 1: Reducing the 5th branch layer length by 15%: in this design the “length optimized” 1x32 Y-branch splitter layout from Figure 28-right was used but with the length of the 5th branch layer reduced further by 15% of its original value, namely $L(5^{th}) = 34000 \mu\text{m}$ (Figure 29 Option 1). After, the whole length of the splitter was reduced from 98000 μm to 92000 μm.

Option 2: Reducing the 5th branch layer length by 20%: since the further reduction of the 1x32 Y-branch splitter (Option 1) did not have a negative influence on the splitting parameters (see subsection 4.2.1), we reduced the 5th branch layer length instead of 15% by 20%, i.e. from 40000 μm to 32000 μm (see Figure 29 Option 2).

Option 3: Reducing the 5th branch layer length by 50% and adding 500 μm linear waveguide: another possibility to reduce the total length of the “length optimized” 1x32 Y-branch splitter is to reduce the length of the 5th branch to the half and to insert a 500 μm linear waveguide between the 5th and the 4th branch layers (see Figure 29 Option 3). Based on the length reducing options 1 and 2 we chose this length reduction option because the length of the 5th

branch was still too long. However, while this branch got too steep we added a linear waveguides between the 5th and the 4th branch layers. Therefore, the length of the 5th branch was halved, from 40000 μm to 20000 μm and a linear waveguide with the length 500 μm was inserted between the 5th and the 4th branch layers. The total length of the “further length reduced” splitter then reached 78500 μm .

Option 4: Reducing the 5th, the 4th and 3rd branch layer length by 15%: the same “length optimized” Y-branch splitter was used but its length was further reduced: the 5th, the 4th and the 3rd branch layer lengths were reduced by 15%, so that the length of the 5th branch, $L(5^{th}) = 34000 \mu\text{m}$, the length of the 4th branch was $L(4^{th}) = 17000 \mu\text{m}$ and the length of the 3rd branch, $L(3^{rd}) = 17000 \mu\text{m}$ (see Figure 29 Option 4). Therefore, the whole length of the splitter shrank further to 86000 μm . It is important to point out that in all optimized designs the width of the whole structure remained constant (= 31 x 127 μm).

3.4.3.2 Length Optimization of 1x64 Standard Y-Branch Splitters

Figure 30-left shows the design of standard 1x64 splitter. As can be seen the structure is too long. Based on the knowledge of the length optimization gained from 1x32 Y-branch splitter design the next task of this work was to reduce the length of the “standard” 1x64 Y-branch splitter without destroying its splitting properties, i.e. to design the shorter splitter keeping symmetrical splitting ratio. To reach this the following length reduction optimizations were proposed and simulated:

- The 6th branch of the 1x64 Y-branch structure has the standard length 160 000 μm and is combined with two identical “further length reduced 1x32 Y-branch structures (Figure 29 Option 4). This reduction is called Variant 1.
- The length of the 6th branch layer was reduced according to the length of Option 4 of the 1x32 Y-branch splitter (Figure 29), i.e. 50% and then additionally by 15% of original size. This reduction is called Variant 2.
- We took the Variant 2 but the length of the 6th branch layer is further reduced to the half, so that the lengths of the 6th and the 5th branch layers were equal, i.e. $L(6^{th}) = 34\ 000 \mu\text{m}$ and $L(5^{th}) = 34\ 000 \mu\text{m}$. This reduction is called Variant 3.

Variant 1: In this case we choose the length optimization like a combination between 1x32 Y-branch structure from the Option 4 (design of the “further length reduced” 1x32 Y-branch splitter structure, in Figure 29) and kept the 6th branch layer length of standard 1x64 Y-branch splitter constant. The design of the “length optimized” 1x64 Y-branch splitter using Variant 1 is shown in Figure 30 Variant 1. Here, the standard length of the 6th branch layer of the 1x64 Y-branch splitter was used, namely $L(6^{th}) = 160\ 000 \mu\text{m}$, but together with the “length optimized” 1x32 Y-branch splitter (Option 1). Therefore the whole length of this optimized splitter shrank from 318 000 μm to 246 000 μm . The width of the whole splitter structure remained constant.

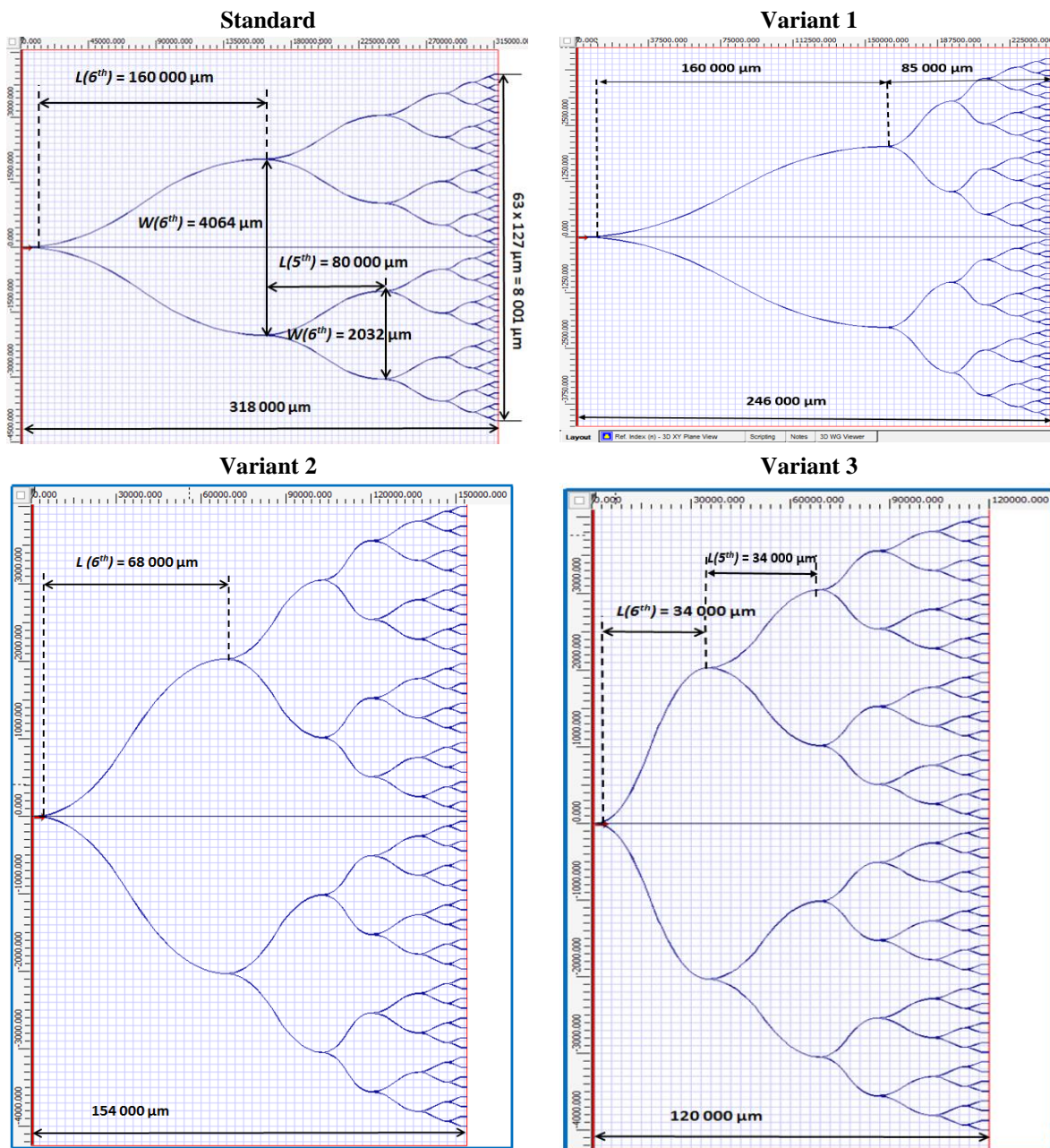


Figure 30: Layout of “standard” 1x64 Y-branch splitter (top-left); “length optimized” 1x64 Y-branch splitter using Variant 1 (top-right); “length optimized” 1x64 Y-branch splitter using Variant 2 (bottom-left) and Variant 3 (bottom-right).

Variant 2: For the length optimization by Variant 2 we reduced directly the 6th branch layer of the structure to the half and then by 15%, i.e. from 160 000 μm to the 68 000 μm and the other design parameters remained the same. The length of the standard Y-branch splitter was reduced from 318 000 μm to 154 000 μm (see Figure 30 -Variant 2).

Variant 3: Here the length of the 6th branch layer from the splitter structure from Variant 2 was reduced by 50%, so that the length of the 6th branch, $L(6^{\text{th}}) = 34000 \mu\text{m}$, the length of the 5th branch, $L(5^{\text{th}}) = 34000 \mu\text{m}$ (see Figure 30 -Variant 3). Therefore, the whole length of the splitter shrank further to 120000 μm . The width of the whole structure again remained constant.

3.4.4 Optimization of Optical Properties of High Splitting Ratio Y-Branch Splitter

As explained in the section 3.4.3 the main losses in the Y-branch splitters are caused by the scattering of the light at the curvature of the waveguides. Therefore, the influence of the shape of different predefined waveguides (s-bend-arc, s-bend-sine, s-bend-cosine, from Fig. 15) on the scattering was studied by applying OptiBPM tool (see Figure 31). Figure 31-left shows the top view of all three simulated s-bend waveguides. As can be seen the greatest scattering of light is at the curvature points.

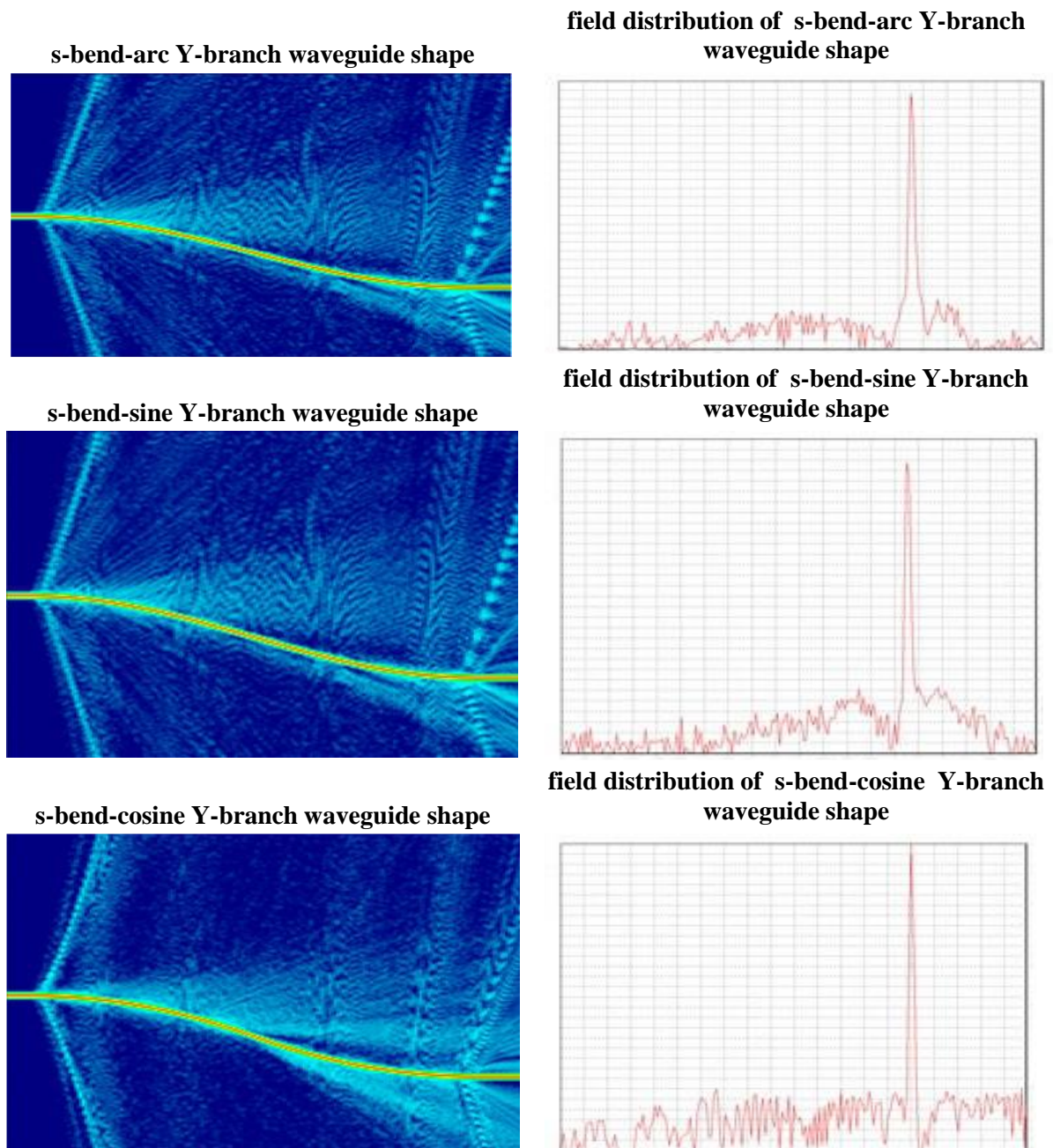


Figure 31: Top view of all three simulated s-bend waveguides (left), field distribution of the output signals (right).

Figure 31-right shows the field distributions at the output of the waveguides with some noise coming from the scattered light. Based on this study, a new design of a waveguide shape was proposed.

The structure of the new branch shape (Figure 32-right) combines two s-bend-cosine waveguides (Figure 32-left) and a linear waveguide having nearly no losses, because the light is not impeded in its “natural” motion. To obtain good light guiding through the waveguide it is important that the slope at the end of the bending equals the slope of the linear part. Only in this case the light transition from the s-bend waveguide part to the linear part is very smooth and the light is guided well and the scattering of the light is minimized (see Figure 33).

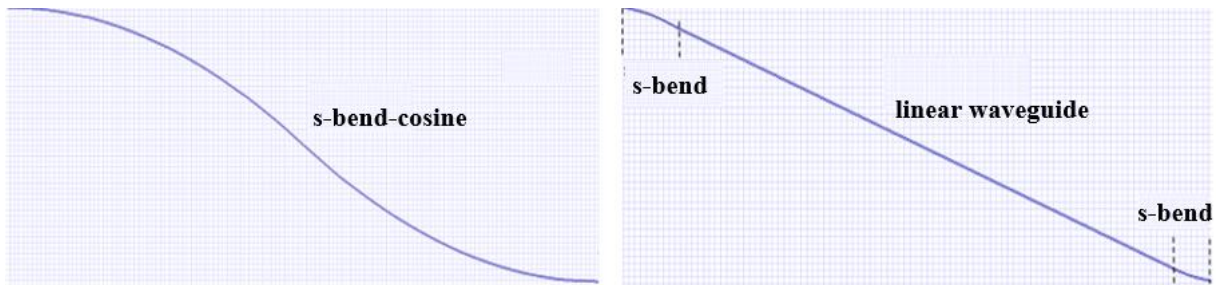


Figure 32: Standard branch waveguide shape (left); new branch waveguide shape (right).

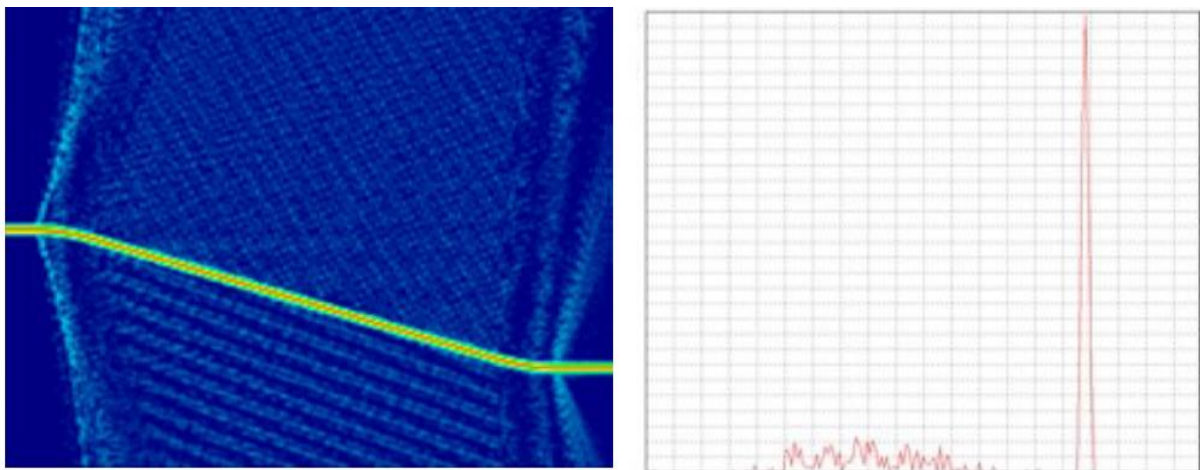


Figure 33: New Y- branch waveguide shape: Top view of simulated structure (left); Field distribution of new waveguide shape (right).

3.4.4.1 Design of “New Shape” 1x32 Y-Branch Splitter

The design of “new shape” 1x32 Y-branch structure is based on the previous splitter design, starting from “new shape” 1x4 Y-branch splitter that was tested in various simulations (see Figure 34-left). The design of 1x32 Y-branch splitter using the new shape is shown in Figure 34-right.

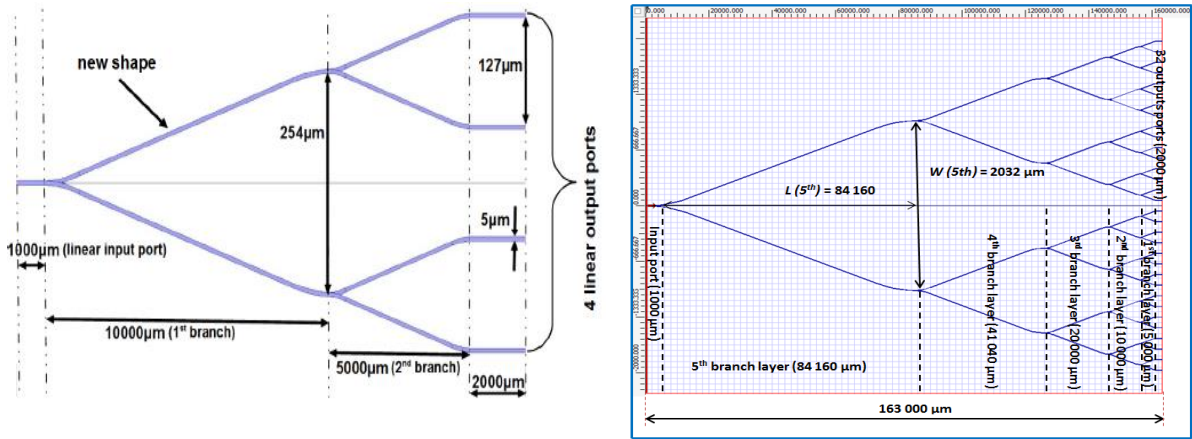


Figure 34: Layouts of 1x4 Y-branch splitter using new shape (left) and “new-shape” 1x32 Y-branch splitter (right) designed in OptiBPM tool.

The dimensions of this splitter are essentially the same as of the “standard” 1x32 Y-branch splitter design shown in Figure 28-left only the branches lengths were adjusted to comply the fact that the slope at the end of the bending is the same as the slope of the linear part to keep further constant bending shape: length of the 5th branch, $L(5^{th})$ was recalibrated to 84160 μm and the length of the 4th branch, $L(4^{th})$ to 41040 μm. The other branch dimensions are the same, namely $L(3^{rd}) = 20000$ μm, $L(2^{nd}) = 10000$ μm, $L(1^{st}) = 5000$ μm and the length of the output ports was set to 2000 μm. The length of the linear input port was set to 1000 μm. Consequently, the pitch between the waveguides in each branch layer was the same as in the “standard” 1x32 Y-branch splitter design, i.e. in the 1st branch layer $W(1^{st}) = 127$ μm, in the 2nd branch layer, $W(2^{nd}) = 254$ μm, ... , in the 5th branch layer, $W(5^{th}) = 2032$ μm. After, the whole structure reached a length of 163 000 μm and the width of the splitter was 3937 μm (= 31x127 μm). We will call this design a “new shape” design.

3.4.5 Design of MMI Splitters

A conventional MMI splitter with eight outputs was designed using OptiBPM tool and its layout together with its design parameters is presented in Figure 35. The width, W_{MMI} of the multimode section was set to 200 μm and the length, L_{MMI} was accordingly set to 4843 μm. The waveguide pitch was expanded to 127 μm port pitch, D by adding an “s-bend-arc” part to each output (similarly to Y-branch waveguides) and the length of the s-bend-arc part, L_p was set to 10000 μm. The whole length of the 1x8 MMI reached 16023 μm.

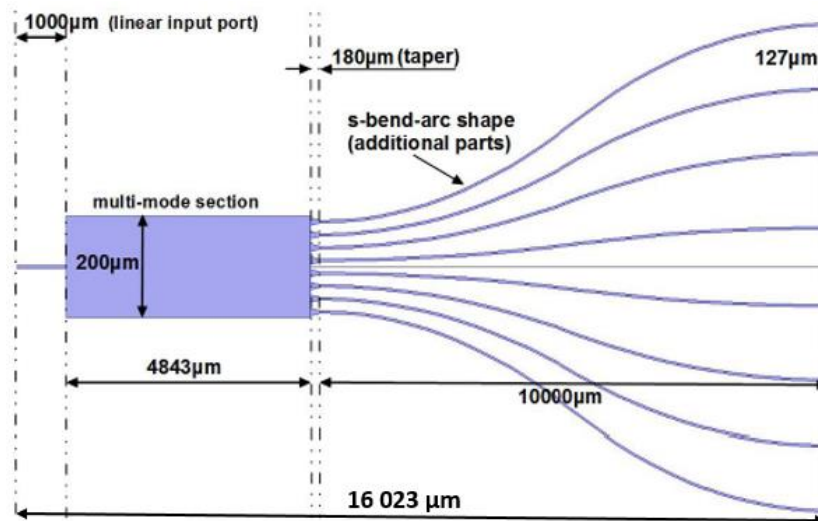


Figure 35: Layout of 1x8 MMI splitter applying OptiBPM tool.

3.4.5.1 Design of 1x16 MMI Splitters

Figure 36 shows a layout of 1x16 MMI splitter with all design parameters.

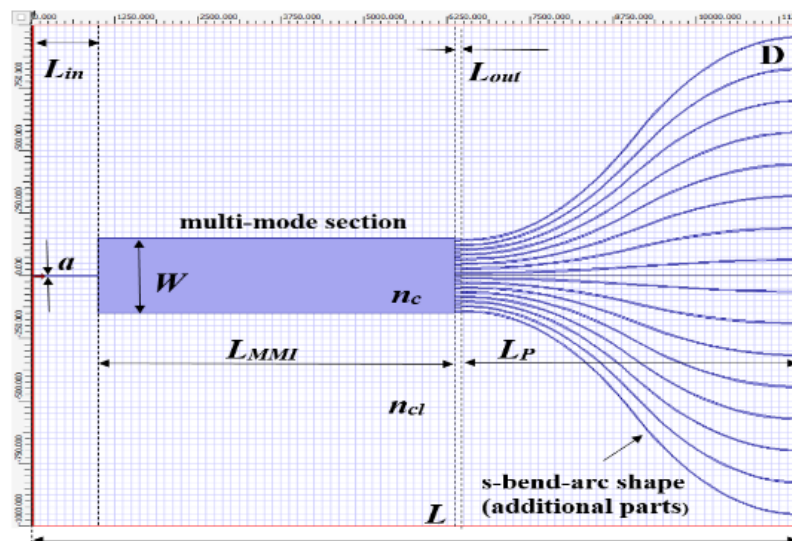


Figure 36: Layout of 1x16 MMI splitter using OptiBPM tool.

To study an influence of the design parameters on the optical properties of the MMI splitter, the width of the multimode section, W_{MMI} was varied, i.e. was set to 200 μm (Design 1 = D1), 300 μm (Design 2 = D2), 400 μm (Design 3 = D3) and 500 μm (Design 4 = D4). The length of the MMI section, L_{MMI} changed accordingly from 2458 μm to 5368 μm , to 9529 μm and to 14932 μm . The length of the output waveguides, L_P was tested for different lengths, as 5 000 μm , 7 500 μm and 10 000 μm . The length of the input port L_{in} was set to 1000 μm and the length of the tapers, L_{out} was 180 μm . The pitch of the output ports was set to 127 μm . We have used again predefined “s-bend-arc” shape for the output waveguides since these ensure the lowest losses. Table 6 summarizes all four designs.

Table 6: Summary of the geometry of all four designs.

Design	W (μm)	L_{MMI} (μm)	L_P (μm)
D1	200	2458	5 000
D1	200	2458	7 500
D1	200	2458	10 000
D2	300	5368	5 000
D2	300	5368	7 500
D2	300	5368	10 000
D3	400	9529	5 000
D3	400	9529	7 500
D3	400	9529	10 000
D4	500	14932	5 000
D4	500	14932	7 500
D4	500	14932	10 000

The 1x16 MMI splitters with different lengths L_{MMI} , different widths W_{MMI} of the MMI section and lengths, L_P of the output ports were designed and simulated and the best design of 1x16 MMI splitter was chosen.

3.4.6 Optical Splitter Design for Application in Telecommunication Access Network with Triple-Play Services

SoS based optical splitters were designed for the applications in telecommunication. Therefore, their influence in access networks as for example GPON and XG-PON by ITU-T¹⁶: with triple-play services (i.e. data, voice and video) was investigated. To this purpose, the standard and optimized splitter designs, presented in previous subsections, were used.

Based on the achieved simulation results we proposed a new extremely low-loss length optimized splitter with a smaller waveguide core size, which reduces the non-uniformity of the split power. The calculated splitting parameters were incorporated in the simulations of particular passive optical network scenarios. For this purpose “OptSim” environment using Time Domain Split Step method was employed. The length-optimized splitters from this thesis have been investigated in different PON schemes by the author R. Agalliu from the Czech Technical University in Prague, Faculty of Electrical Engineering, Department of Telecommunication Engineering, who I have cooperated during my doctoral study with. The results of these scenarios will be described in the section 4.3.

OAN mostly use the tree topology to distribute the service from the OLT on the provider’s side to the subscribers in an ONU. For the design of such networks, one has to consider different

¹⁶ International Telecommunication Union (ITU).

aspects like optical linear and nonlinear effects [157, 158], optical attenuation and amplification [8], possible wavelength routing [159], or ageing of network elements [160], among others.

The multiplexing techniques are required to efficiently utilize the available bandwidth and transmission media. One of the main multiplexing technique used in PONs is the Time Division Multiplexing, in which a certain time-slot is assigned to each of the ONUs. The recommendations, in which most of the OANs are based on, are: GPON [161] and EPON [162]. In this example we focused on GPON, because it offers higher bandwidth than EPON. We considered in the simulations also its 10 Gbps option, as recommended by the ITU-T: XG-PON [163]. The simulations were performed in OptSim environment, version 5.2 by RSoft Design [164]. We simulated the standard 1x64 Y-branch splitter with $(6 \times 6) \mu\text{m}^2$ waveguide core size and low-loss length optimized 1x64 Y-branch splitter with $(5.5 \times 5.5) \mu\text{m}^2$ waveguide core size (see section 4.3). The network design is based on GPON [162] and XG-PON [164]. We employed ITU-T recommendation [8] for the wavelength ranges, as shown in Figure 37. Allocation of the wavelengths recommended by ITU-T is selected to avoid cross-talks between GPON and XG-PON signals. A 10-nm wavelength window is allocated for the distribution of the video signals (see Figure 38).

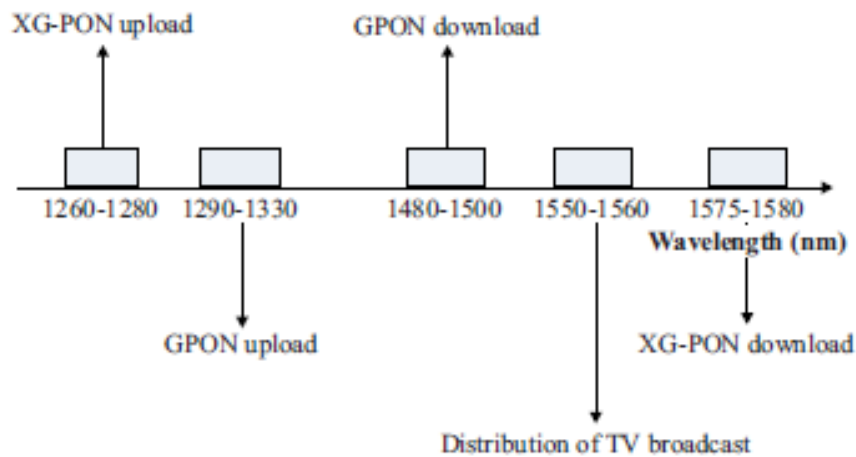


Figure 37: Wavelength ranges for GPON/XG-PON and video components.

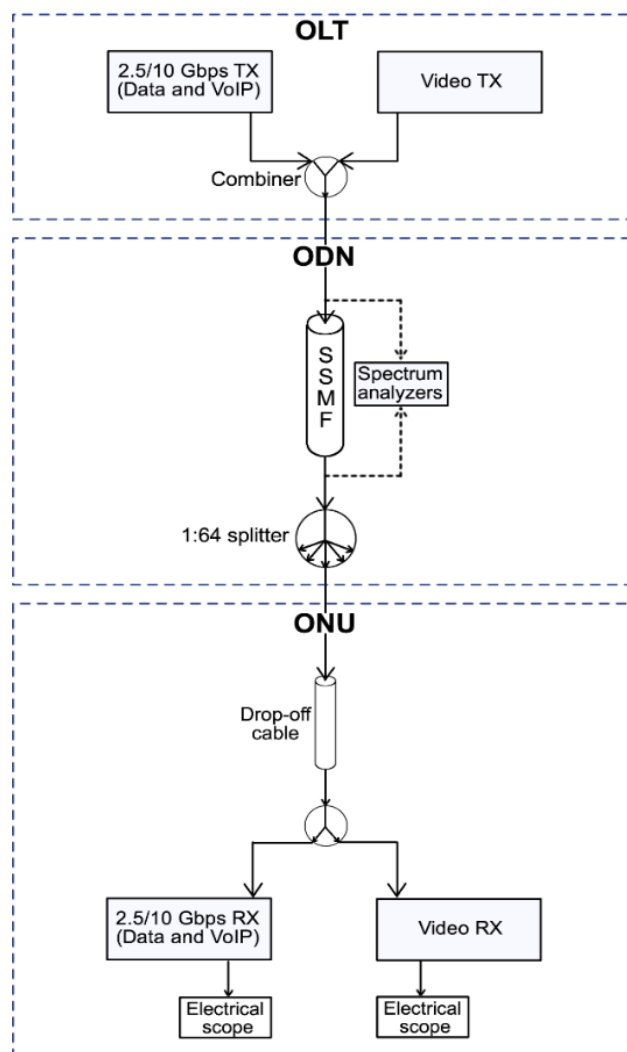


Figure 38: GPON/XG-PON simulation schemes with triple-play services employing the designed 1x64 splitters.

To this purpose we chose a “standard” Y-branch splitter with 64 outputs (from Figure 30) and the shortest length optimized 1x64 Y-branch splitter (from Figure 30). Both proposed splitter designs were deployed in a PON and compared to each other in terms of physical reach of the PON, Q-factor and Bit Error Rate (BER).

The goal of the simulations was to show the practical benefits of the proposed splitters in the optical access network, which transmits data/voice and video streams in direction to users. Simulation scheme is shown in Figure 38. We focused on the downstream traffic, which does not restrict the generality of the problem. The network consists of three parts: OLT which includes transceivers at the provider's side, ODN (the transmission path components) and ONU, including transceivers at the customer's premises.

We simulated both GPON (2.5 Gbps downstream) and XG-PON (10 Gbps downstream). Voice transmitter can be considered as a VoIP service due to its current applications and wide deployments globally. The data and VoIP transmitters generate optical Non-Return-to-Zero modulated signals, multiplexed with the video component using the Coarse WDM technique.

Wavelength selection is shown in Figure 37. The 800 Mbps video stream was generated using a 16-QAM modulation. The data/voice/video transmitter's output power was -3 dBm, which is a commonly used value for optical transmitters.

The ODN consists of a 20 km long standard SMF with the attenuation factor of 0.2 dB·km⁻¹ and the 1x64 splitter to be analyzed. The drop-off cable is several meters long. Its purpose is to consider the fiber connections at the customer promises. We used different components in OptSim environment for signal analysis, such as spectrum analyzers, power meters, among others. The investigated signal parameters are BER and Q-factor [165]. The threshold BER value is 10⁻¹², and the limit Q-factor ensuring correct transmission is 7. The Q-factor decreases as the BER increases. Essentially, Q-factor indicates the minimum required optical signal to noise ratio to achieve a certain BER value. It can be calculated as shown in (4.5.1):

$$Q[-] = \frac{\mu_1 - \mu_0}{\sigma_1 + \sigma_0} \quad (4.5.1)$$

where μ_0, μ_1 stands for the mean log.0, log.1 level values, and σ_0, σ_1 for their standard deviations. The mathematical relation between Q-factor and BER [166,167] can be expressed as:

$$\text{BER}[-] = \frac{1}{2} \operatorname{erfc} \left(\frac{Q}{\sqrt{2}} \right) \quad (4.5.2)$$

The fiber propagation equation is solved by the split-step method, which applies separately optical linear and non-linear effects. There are two main methods which differ on the way how the optical linear effects are calculated: Time Domain Split Step (TDSS) [168] and Frequency Domain Split Step (FDSS).

The simulations that we have performed in OptSim software environment are based on the TDSS technique. This method uses the convolution product in the discrete time [164], as expressed:

$$A_L[n] = A[n] * h[n] = \sum_{k=-\infty}^{\infty} A[k]h[n-k] \quad (4.5.3)$$

where A is an optical field intensity, L is the operator related to linear effects [169], such as dispersion [168] and h is an impulse response of L . TDSS method has no constraints on the shape of a signal spectrum and it has no modelling limits. On the other hand, FDSS introduces unavoidable intrinsic errors due to the circular convolution, which leads to undesirable aliasing effects and therefore to the possibility of inaccurate simulation results. Unlike the FDSS method, TDSS method exhibits higher immunity against aliasing errors and exact differential group delays, at the cost of more complex implementation and higher computational requirements [164]. However, TDSS takes advantage of the parallel computing (software pipelining), which significantly improves the TDSS computation speed.

3.4.7 Design and Optimization of High-Index-Contrast Y-Branch Splitters

Design of silicon nitride based Y-branch optical splitters was performed in the collaboration with International Laser Centre (ILC) and Slovak Technical University in Bratislava. In these

designs the technological possibilities of the technical infrastructure of the clean rooms in ILC in Bratislava are taken into account, where the fabrication of the final optical splitter designs is planned to be realized. To this purpose two 1x8 Y-branch splitters were designed.

3.4.7.1 1x8 Y-Branch Splitter with Channel Waveguide Structure

Figure 39-left presents the design of standard 1x8 Y-branch splitter. It consists of one input waveguide and one 1x2 Y-branch (Y1), connecting two 1x2 Y-branches (Y2). The output waveguides of these Y2-branches create the input waveguides for further four 1x2 Y3-branches. Eight output waveguides finalize this structure. The input/output waveguides have the length of $50\ \mu\text{m}$. Minimal distance between branches was again tested. Based on the results Y1-branch has a pitch between both branch waveguides, $W_1 = 16\ \mu\text{m}$.

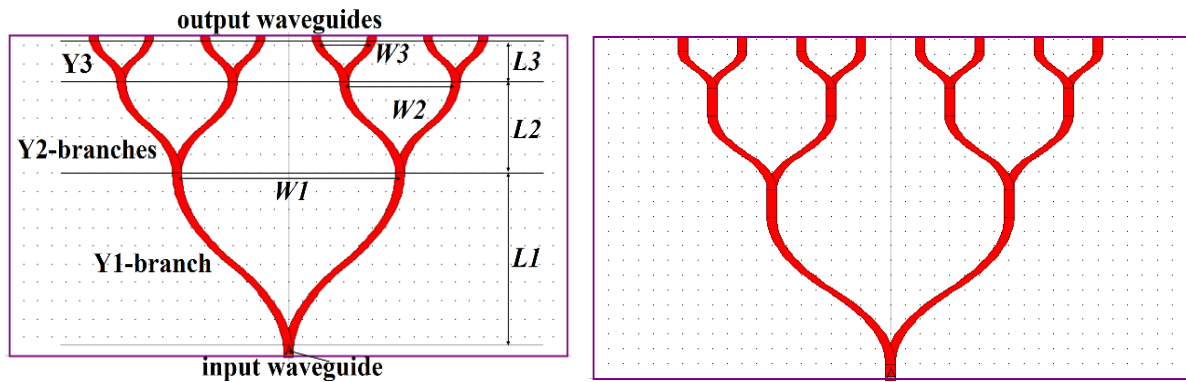


Figure 39: Structure of the standard 1x8 Y-branch splitter (left); and optimized 1x8 Y-branch splitter (right) with channel waveguide structure.

To keep the length of the splitter as short as possible, the length of the branches needs to be obtained the shortest possible, with very low losses. The layout of the Y1-branch (left) together with an output of the simulation (right) is shown in Figure 40.

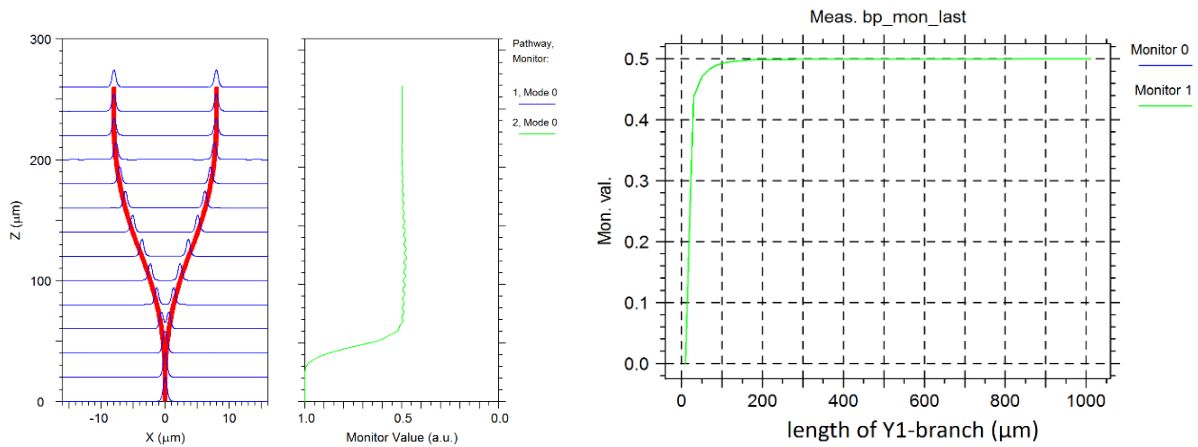


Figure 40: Layout of the Y1-branch together with the simulated optical power (left); Scanning of the length of the Y1-branch with regards to optical power calculated in the waveguides (right).

As presented, the length of the Y1-branch was scanned in a range between $10\ \mu\text{m}$ and $1000\ \mu\text{m}$. As expected, when the branch is too short, the optical power is damped. This is caused by the scattering of the light at the steep curvature of the waveguides. Extension of the Y1-branch reduces the losses and saturates approximately at $200\ \mu\text{m}$ when nearly no scattering loss appears in the waveguides. Therefore, the length of the Y1-branch was set to $L1 = 200\ \mu\text{m}$. The pitch of each next Y-branch (Y2 and Y3) was reduced to the half ($W2 = 8\ \mu\text{m}$ and $W3 = 4\ \mu\text{m}$) and the lengths of these branches were scanned again. The simulations showed that the minimum possible length of the Y2-branch reached half of the length of Y1-branch ($L2 = 100\ \mu\text{m}$) and the length of Y3 reached the half of the Y2-branch length ($L3 = 50\ \mu\text{m}$), as presented in Figure 41. This confirms constant bending shape of all designed branches. After the length optimization of the branches, the final 1x8 Y-branch splitter reached the length of $L = 450\ \mu\text{m}$.

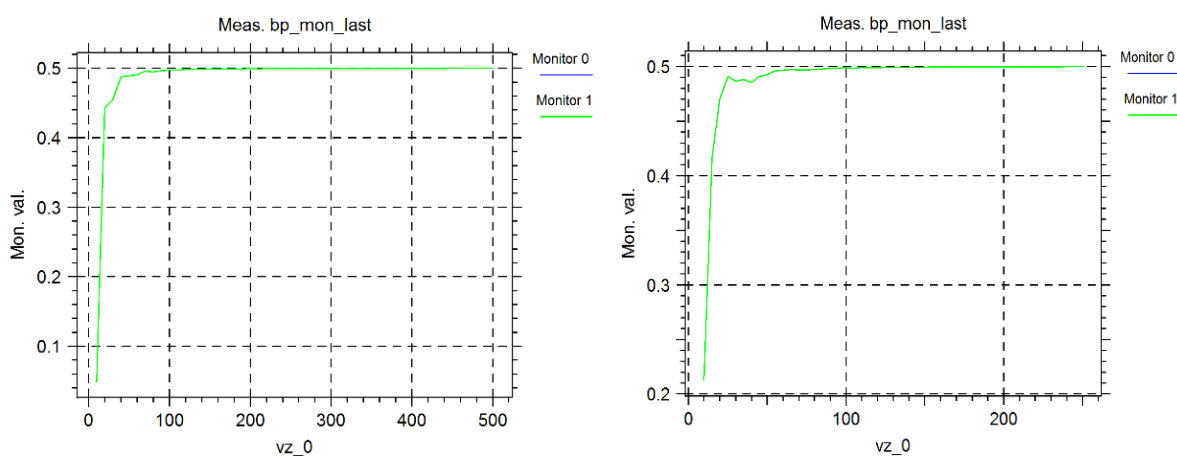


Figure 41: The scanning of the lengths of the Y2-branch (left) and Y3-branch (right).

The standard design of 1x8 Y-branch splitter was optimized as shown in Figure 39-right. Particularly, the straight waveguides were placed between Y-branches. The length of these waveguides was tested in various simulations.

3.4.7.2 1x8 Y-Branch Splitter with Shallow Rib Waveguide Structure

Figure 42 presents the design of 1x8 Y-branch splitter with shallow rib waveguide structure. It consists of one input waveguide and one 1x2 Y-branch (Y1), connecting two 1x2 Y-branches (Y2). The output waveguides of these Y2-branches create the input waveguides for further four 1x2 Y3-branches. Eight output waveguides finalize this structure. The input/output waveguides have length of $10\ \mu\text{m}$.

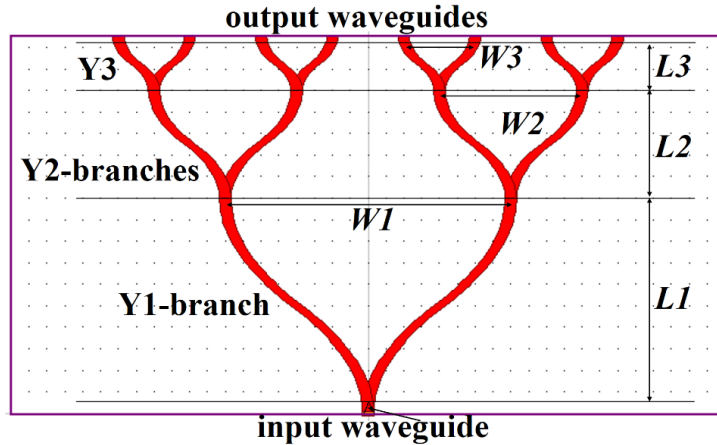


Figure 42: Layout of the silicon nitride based 1x8 Y-branch splitter with shallow rib waveguide structure.

To be able to reach the smallest size of the splitter, in the next step the minimal distance between the output waveguides (port pitch, $W3$) was tested. To this purpose two parallel waveguides were designed and the distance between these waveguides was alternated between $2\ \mu\text{m}$ (four times the width of the waveguide) and $5\ \mu\text{m}$. Simulations showed that the port pitch $3\ \mu\text{m}$ is wide enough to prevent coupling effect between the waveguides. This value was chosen as a minimum port pitch $W3$. Figure 43-left shows the simulated results of the coupling effect when the port pitch is too narrow ($W = 2\ \mu\text{m}$) and Figure 43-right the case when the coupling effect is suppressed ($W = 3\ \mu\text{m}$). The port pitch of each next Y-branch was doubled, i.e. $W2 = 6\ \mu\text{m}$ and $W1 = 12\ \mu\text{m}$.

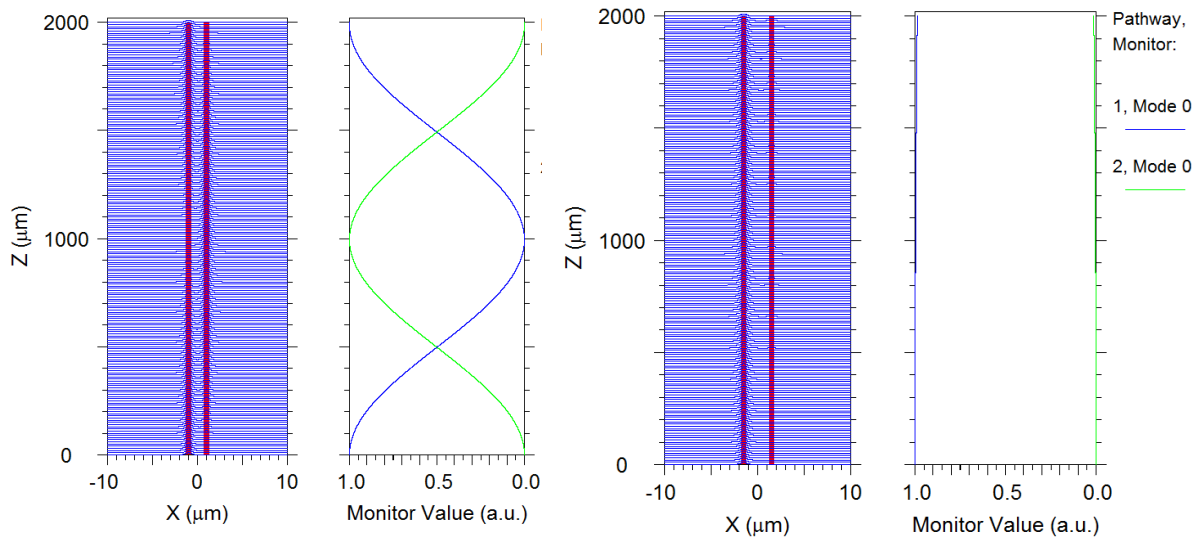


Figure 43: Simulated results of coupling effect when the port pitch $W3 = 2\ \mu\text{m}$ (left) and $W3 = 3\ \mu\text{m}$ (right).

To keep the length of the splitter as short as possible, also the length of the branches needs to be obtained the shortest possible, with very low losses. To this purpose, the length of the Y3-branch ($L3$) was scanned between $1\ \mu\text{m}$ and $120\ \mu\text{m}$. The output of the simulation is shown in Figure 44-left.

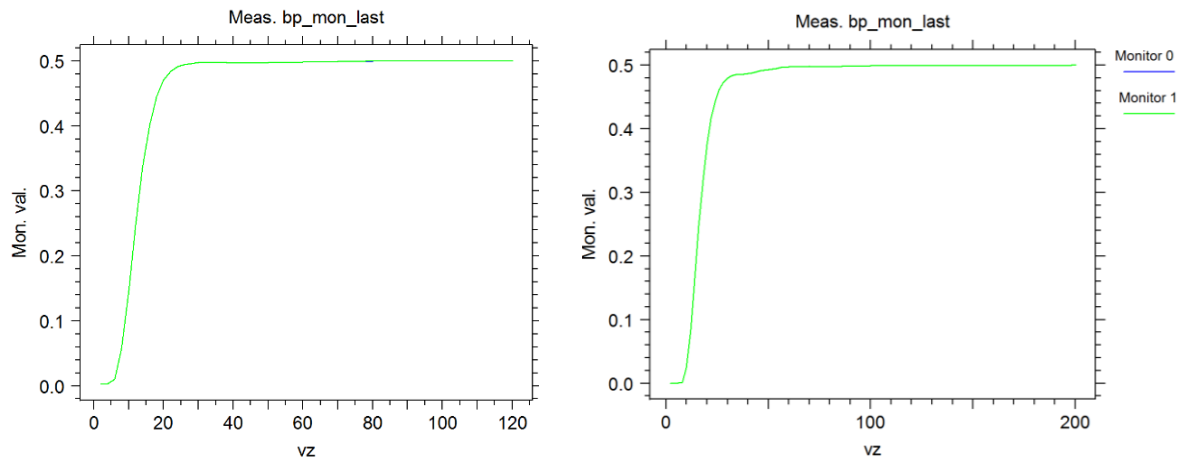


Figure 44: Scanning of the length of the Y3 branch (left) and Y2 branch (right).

As expected, when the branch is too short, the optical power is damped. This is caused by the scattering of the light at the steep curvature of the waveguides. Extension of the Y3-branch reduces the losses and saturates approximately at $40 \mu\text{m}$ when nearly no scattering loss appears in the waveguides. Therefore, the length of the Y3-branch was set to $L_3 = 40 \mu\text{m}$. The lengths of the next branches were scanned again. The simulations showed that the minimum possible length of the Y2-branch reached double value of the length of the Y3-branch ($L_2 = 80 \mu\text{m}$, see Figure 44-right) and the length of the Y1-branch reached the double value of the Y2-branch length ($L_1 = 160 \mu\text{m}$), as presented in Figure 45.

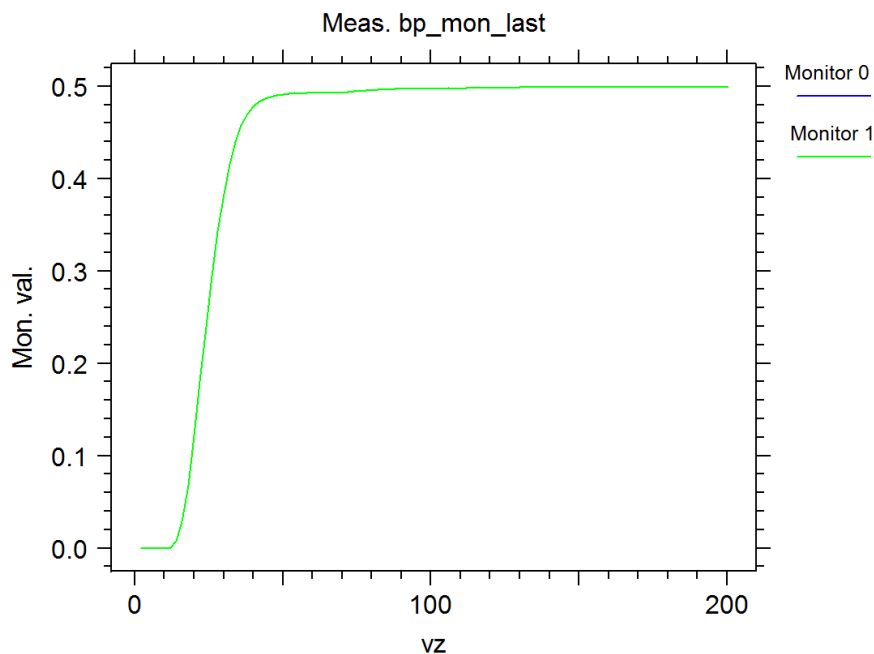


Figure 45: Scanning of the length of the Y1-branch.

4 Results

This section summarizes the simulation results of all splitter designs described in Section 3. It is important to point out that all simulations of SoS based optical splitters were performed at operating wavelength, $\lambda = 1.55 \mu\text{m}$ applying different photonics tools. OptiBPM tool from Optiwave was used for all these splitter designs. Additionally, Apollo Photonics tool was used to simulate 1x8 and 1x16 Y-branch and MMI splitter designs and Rsoft tool was used to simulate 1x32 Y-branch splitter design in 3D environment. Comparison of the simulated results of all three tools is also discussed.

The design and simulation of silicon nitride based 1x8 Y-branch splitter was performed by BeamPROPTM tool from RSoft, applying BPM.

4.1 Simulation of Low Splitting Ratio SoS Based Splitters

This subsection describes 2D simulation and optimization of low splitting ratio splitters, applying OptiBPM and Apollo Photonics tools. Particularly:

- 1x8 Y-branch splitters
- 1x8 MMI splitters

4.1.1 Simulation of Standard 1x8 Y-Branch and 1x8 MMI Splitters Using OptiBPM Tool

Figure 46 presents the top view of the simulated results of 1x8 Y-branch (see Figure 27) and MMI splitters (from Figure 35), the field distribution at the end of Y-branch and MMI structures and the non-uniformity and insertion loss parameters using OptiBPM tool. As can be seen the Y-branch approach features much lower scattering than the MMI splitter. This is confirmed by the corresponding field distribution at the end of the structures. In both approaches, all eight outputs are well separated. From the field distributions the splitting parameters (defined in Subsection 3.3.2) were calculated. The background crosstalk of Y-branch splitter, $BX = -46.81 \text{ dB}$ and that of 1x8 MMI splitter is higher, $BX = -33.53 \text{ dB}$. The uniformity of the split power over all the output channels, $ILu = 1.41 \text{ dB}$ and the insertion loss $IL = -10.01 \text{ dB}$ for Y-branch approach. For MMI splitter the non-uniformity reached value, $ILu = 0.51 \text{ dB}$. Insertion loss is comparable with Y-branch splitter, $IL = -9.91 \text{ dB}$.

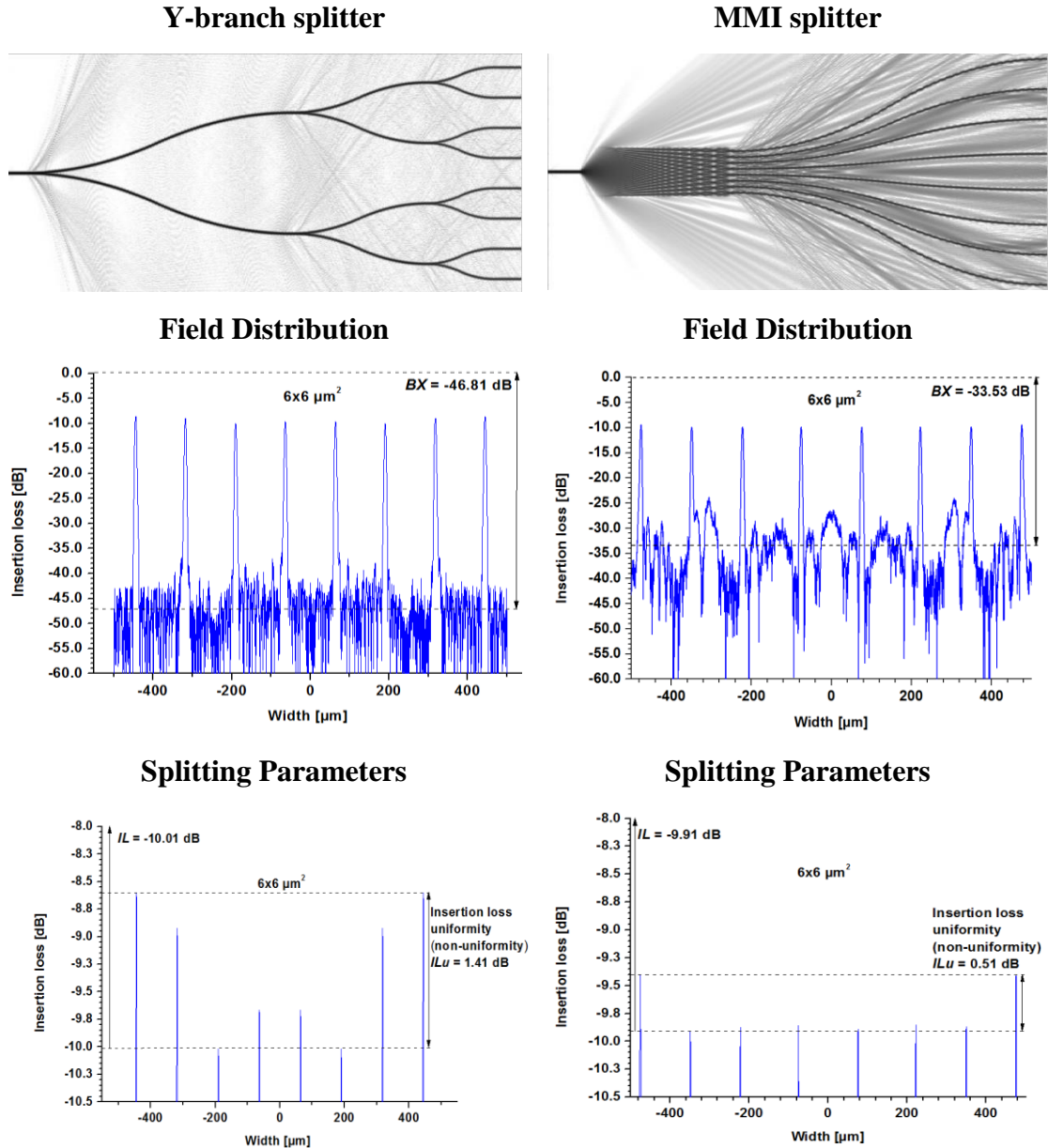


Figure 46: Simulation results of 1x8 Y-branch and 1x8 MMI splitters applying OptiBPM tool: top view of the simulated 1x8 Y-branch (top-left) and MMI (top-right) splitter structures, field distribution at the end of 1x8 Y-branch (middle-left) and of 1x8 MMI (middle-right) splitters and non-uniformity and insertion loss of 1x8 Y-branch (bottom-left) and of 1x8 MMI (bottom-right) splitters.

4.1.2 Simulation of “Standard” 1x8 Y-Branch and 1x8 MMI Splitters Using Apollo Tool

Another simulations of the same design layouts were performed using Apollo Photonics tool. To ensure the best comparability the same solver, design and simulation parameters were chosen in both software tools. Figure 47 presents the top view of simulated 1x8 Y-branch (left) and of MMI (right) structures.

The background crosstalk of 1x8 MMI splitter simulated in Apollo Photonics tool is $BX = -33.26$ dB, the non-uniformity, $ILu = 0.63$ dB and the insertion loss, $IL = -10.23$ dB. The splitting parameters of 1x8 Y-branch splitter are as follows: the background crosstalk is $BX = -46.37$ dB, the non-uniformity, $ILu = 1.58$ dB and the insertion loss, $IL = -10.21$ dB.

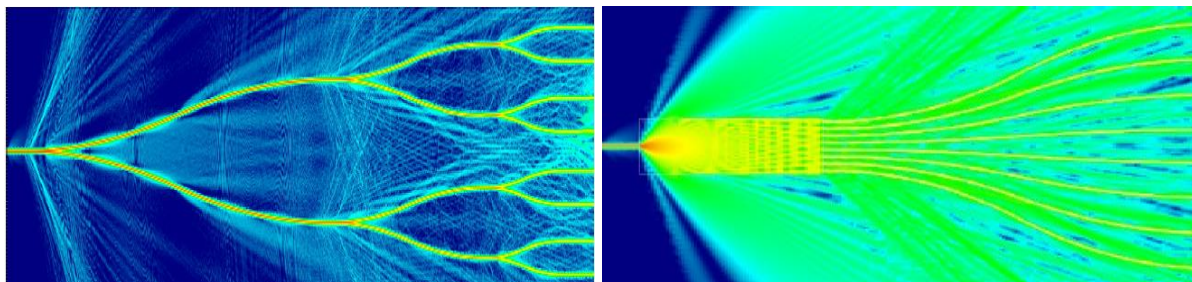


Figure 47: Top view the simulated 1x8 Y-branch splitter (left); multimode interference pattern of 1x8 MMI splitter (right).

4.1.3 Comparison of Optical Properties of “Standard” 1x8 Y-Branch and 1x8 MMI Splitters

To compare the optical properties of 1x8 Y-branch and MMI structures, we analysed the splitting parameters achieved from both photonics tools separately. As presented in Table 7 the splitting parameters of the MMI splitters are much better compared to the splitting parameters of the Y-branch splitters in both software tools. As can be seen, while the non-uniformity from Y-branch and MMI splitters simulated in Apollo differs in $\Delta = 0.95$ dB, the non-uniformity in OptiBPM differs only in $\Delta = 0.12$ dB. Insertion loss from both splitters simulated in Apollo differs in $\Delta = 0.02$ dB, while the insertion loss in OptiBPM in $\Delta = 0.1$ dB. On the other hand, the background crosstalk of MMI splitter is considerably higher than background crosstalk of Y-branch splitter in both photonics tools. As can be seen, the difference measured in Apollo $\Delta = 13.11$ dB and it is approximately the same in OptiBPM $\Delta = 13.28$ dB. The length difference between 1x8 Y-branch splitter and MMI splitter is $\Delta = 21\,977$ μm .

Table 7: Comparison of the optical properties of 1x8 Y-branch and 1x8 MMI splitting parameters achieved from Apollo Photonics and OptiBPM tool.

	Apollo			OptiBPM		
	Y	MMI	Δ	Y	MMI	Δ
Non-uniformity, IL_u	1.58 dB	0.63 dB	0.95 dB	1.41 dB	0.51 dB	0.12 dB
Insertion loss, IL	-10.21 dB	-10.23 dB	0.02 dB	-10.01 dB	-9.91 dB	0.1 dB
Background cross-talk, BX	-46.37 dB	-33.26 dB	13.11 dB	-46.81 dB	-33.53 dB	13.28 dB
Length of splitter, L	38 000 μm	16 023 μm	21 977 μm	38 000 μm	16 023 μm	21 977 μm

Conclusion: As can be seen, Table 7 confirms well the advantages and disadvantages of both approaches. Particularly, the MMI splitters have advantages over the Y-branch splitters, like their lower non-uniformity and much smaller length. In spite of the fact and considering that the Y-branch splitter is wavelength and polarisation independent and therefore preferably used in the telecommunications, the design and optimization of this splitter is a main goal of this thesis.

4.1.4 Comparison of Both Used Photonics Tools

The splitting parameters, achieved in both software tools are summarized in Table 8. As can be seen the non-uniformity from Apollo simulation differs only in $\Delta = 0.17$ dB from Optiwave simulation for Y-branch splitter and in $\Delta = 0.12$ dB for MMI splitter. Also the calculated values of the insertion loss and the background noise feature very good agreement between both software tools, namely the background crosstalk difference is $\Delta = 0.44$ dB for Y-branch splitter and $\Delta = 0.27$ dB for MMI splitter. In case of the insertion loss is the difference between Apollo and Optiwave simulation only $\Delta = 0.22$ dB for Y-branch splitters while for the MMI splitter is the difference higher, namely approximately 1.91 dB.

Table 8: Comparison of the splitting parameters of 1x8 Y-branch and MMI splitters achieved from Apollo Photonics and OptiBPM tool.

	1x8 Y-branch splitter			1x8 MMI splitter		
	Apollo Photonics	OptiBPM	Δ	Apollo Photonics	OptiBPM	Δ
Non-uniformity, ILu	1.58 dB	1.41 dB	0.17 dB	0.63 dB	0.51 dB	0.12 dB
Insertion loss, IL	-10.23 dB	-10.01 dB	0.22 dB	-10.21 dB	-9.91 dB	0.30 dB
Background Crosstalk, BX	-46.37 dB	-46.81 dB	0.44 dB	-33.26 dB	-33.53 dB	0.27 dB

Conclusion: From the parameter calculations can be concluded, that both software tools provide very comparable simulated results. Since the Apollo Photonics tool features errors in the GDSII exported files, the design, simulation and optimization of all Y-branch and MMI splitters were performed mainly in OptiBPM tool.

4.1.5 Waveguide Optimization of “Standard” 1x8 Y-Branch Splitter

From the simulations presented in section 4.1.1 is evident that the non-uniformity and insertion loss of 1x8 Y-branch splitter are not satisfying. Particularly the non-uniformity parameter ILu with over 1.41 dB is too high.

Deep analysis of the achieved simulated results showed that the main reason for such a high non-uniformity is the presence of the first mode (besides the zero (fundamental) mode) propagating in the $(6 \times 6) \mu\text{m}^2$ waveguide. Figure 48 illustrates the problem. In the fundamental mode, there is only one intensity maximum so the light beam is centred in the middle of the waveguide. The first mode features the maximum and also the minimum. Thereby the beam is damped and not guided in the center of the waveguide. When the beam propagates in the fundamental mode only, the beam is straight and centred in the middle of the waveguide and so the light is split equally at the branch. From this follows that the best splitting results can be achieved by choosing a waveguide core size supporting the fundamental mode only. The fundamental mode (0. mode) has a mode width of $4.3438 \mu\text{m}$. But if the waveguide core size is larger than $4.3438 \mu\text{m}$ (in our case $(6 \times 6) \mu\text{m}^2$) also the first mode is excited and depending on the waveguide core size

it can have weaker or stronger influence on the light propagation. Since the light is a superposition of the zero and the higher modes, it is damped and shifted. Thereby the light is split unequally at the branching points. This causes an asymmetric splitting of the optical signal [170].

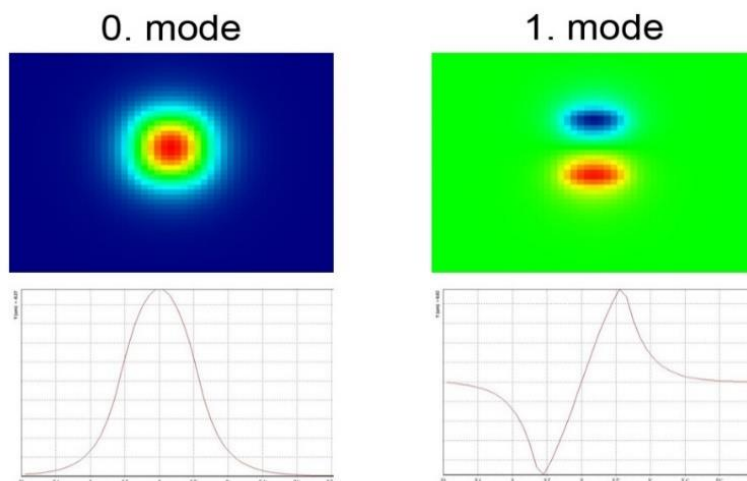


Figure 48: Field amplitude profiles of the fundamental mode and the first mode with their distributions in the $(6 \times 6) \mu\text{m}^2$ waveguide.

To show this influence we reduced the waveguide core size of both splitters in Fig. 46 from $(6 \times 6) \mu\text{m}^2$ to $(5.5 \times 5.5) \mu\text{m}^2$ while keeping the same size of the structures. The simulated results are shown in Figure 49.

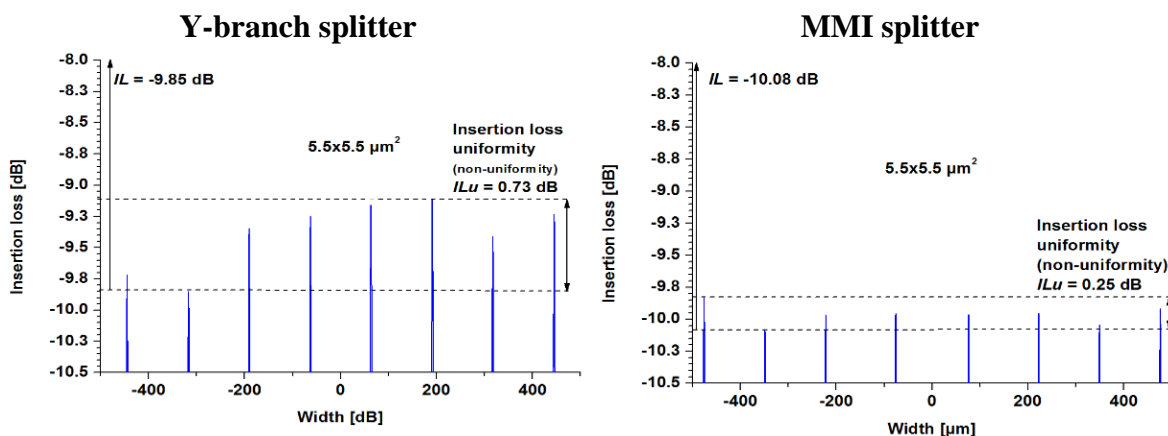


Figure 49: Detailed view of the splitting parameters of 1x8 Y-branch (left) and 1x8 MMI (right) splitters with the waveguide core sizes of $(5.5 \times 5.5) \mu\text{m}^2$.

It can be seen that the splitting parameters of MMI splitter compared to the splitting parameters of Y-branch splitter feature again better splitting properties. While the non-uniformity of MMI splitter reached $ILu = 0.25 \text{ dB}$, the non-uniformity of Y-branch splitter is still higher, $ILu = 0.73 \text{ dB}$ for the waveguide core size of $(5.5 \times 5.5) \mu\text{m}^2$.

In Table 9, the splitting parameters of the 1x8 Y-branch and 1x8 MMI splitters having different cross-sections are summarized. As can be seen, while the non-uniformity in the case of 1x8 Y-branch splitter was improved by $\Delta = 0.68$ dB, the non-uniformity of MMI splitter only by $\Delta = 0.25$ dB. The insertion loss and background crosstalk of Y-branch splitter do not feature strong improvement since the layout of the splitter was kept the same (insertion loss reduction $\Delta = 0.16$ dB, background crosstalk reduction $\Delta = 0.86$ dB). The MMI splitter shows even weaker deterioration of these two parameters, particularly the insertion loss increased from -9.91 dB to -10.08 dB ($\Delta = 0.17$ dB) and background crosstalk from -33.53 dB to -32.08 dB ($\Delta = 1.45$ dB).

Table 9: Comparison of splitting parameters of 1x8 Y-branch and 1x8 MMI splitters having different waveguide cross-sections.

Y-branch		Non-uniformity, <i>ILu</i>	Insertion loss, <i>IL</i>	Background noise, <i>BX</i>	Length of splitter, <i>L</i>
	(6x6) μm^2	1.41 dB	-10.01 dB	-46.81 dB	38 000 μm
(5.5x5.5) μm^2	0.73 dB	-9.85 dB	-47.67 dB	38 000 μm	
Δ	0.68 dB	0.16 dB	0.86 dB		
MMI	(6x6) μm^2	0.51 dB	-9.91 dB	-33.53 dB	16 023 μm
	(5.5x5.5) μm^2	0.26 dB	-10.08 dB	-32.08 dB	16 023 μm
	Δ	0.25 dB	0.17 dB	1.45 dB	

Conclusion: From the simulations is evident that keeping the same layout and decreasing the waveguide core size from (6x6) μm^2 to (5.5x5.5) μm^2 the non-uniformity particularly of the Y-branch splitter was reduced from 1.41 dB (for the waveguide core size of (6x6) μm^2) to 0.73 dB (for the waveguide core size of (5.5x5.5) μm^2) i.e. nearly to the half of its original value.

4.2 Simulation Results of High Splitting Ratio SoS Splitters

In this section we describe 2D simulation and optimization of high splitting ratio SoS splitters, applying OptiBPM photonics tool and Apollo Photonics tool. Particularly:

1. 1x16 Y-branch and MMI splitters
2. 1x32 Y-branch (“standard” and “new shape”)
3. 1x64 Y-branch splitter

4.2.1 Simulation of Standard 1x16 Y-Branch Splitter

Figure 50 presents the optical characteristics of the simulated 1x16 Y-branch splitter (subsection 3.4.2) using Optiwave tool. Figure 50-left shows the corresponding field distribution at the end of the structure. The background crosstalk of Y-branch splitter, $BX = -49.04$ dB. The

uniformity of the split power over all the output channels, $ILu = 1.77$ dB and the insertion loss, $IL = -13.09$ dB (Figure 50-right).

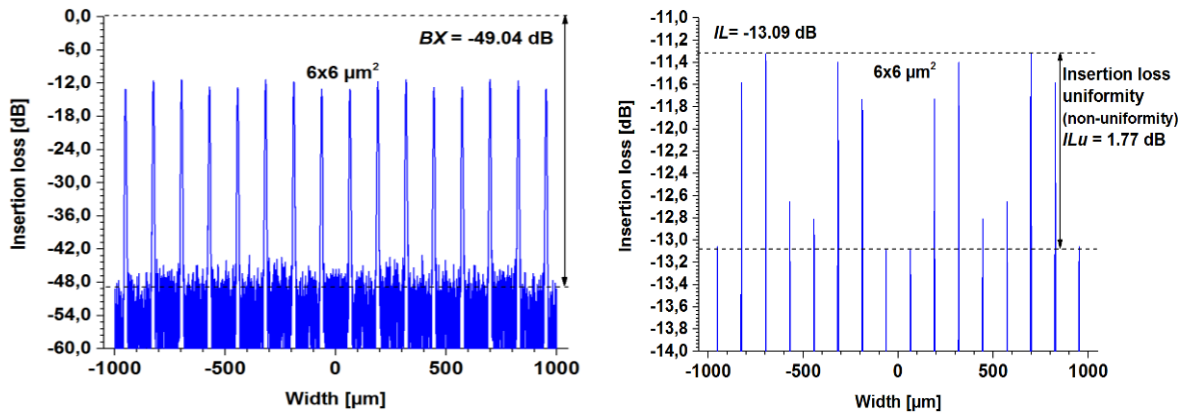


Figure 50: Field distribution at the end of the 1x16 Y-branch splitter (left). Non-uniformity and insertion loss of 1x16 Y-branch splitter with the waveguide core size of $(6 \times 6) \mu\text{m}^2$ (right).

4.2.2 Simulation of Standard 1x16 MMI Splitter

As already described in the subsection 3.4.5.1 four 1x16 MMI splitters with different widths, W_{MMI} of the MMI section and lengths, L_P of the output ports were designed and simulated to study their optical properties and to choose the best 1x16 MMI splitter design. Table 10 summarizes all splitting parameters calculated from all simulated characteristics.

Table 10: Comparison of splitting parameters of 1x16 MMI splitter for the different widths of multimode section and different lengths of the output ports.

Design	W (μm)	L_{MMI} (μm)	L_P (μm)	Non-uniformity, ILu (dB)	Insertion loss, IL (dB)	Background crosstalk, BX (dB)	Length of splitter, L_{MMI} (μm)
D1	200	2458	5 000	1.28	-12.81	-32.18	8 638
D1	200	2458	7 500	1.04	-12.83	-36.85	11 138
D1	200	2458	10 000	0.95	-12.80	-37.72	13 638
D2	300	5368	5 000	0.51	-12.54	-36.8	11 548
D2	300	5368	7 500	0.39	-12.56	-37.71	14 048
D2	300	5368	10 000	0.26	-12.44	-41.35	16 548
D3	400	9529	5 000	0.92	-12.93	-32.76	15 709
D3	400	9529	7 500	0.61	-13.27	-33.21	18 209
D3	400	9529	10 000	0.57	-12.89	-35.06	20 709
D4	500	14932	5 000	1.72	-14.89	-30.17	21 112
D4	500	14932	7 500	1.91	-14.44	-33.63	23 612
D4	500	14932	10 000	0.83	-13.85	-37.69	26 612

Considering the Splitting Parameters

For the non-uniformity ILu , insertion loss IL and background crosstalk BX as expected, the best results were obtained when applying the longest output ports, $L_p = 10\,000\ \mu\text{m}$ in all designs. Namely, in the design D1 ($L_p=10000\ \mu\text{m}$) the background crosstalk, $BX = -37.72\ \text{dB}$, non-uniformity, $ILu = 0.95\ \text{dB}$ and insertion loss, $IL = -12.80\ \text{dB}$. In the design D2 ($L_p=10000\ \mu\text{m}$) the background crosstalk, $BX = -41.35\ \text{dB}$, non-uniformity, $ILu = 0.26\ \text{dB}$ and insertion loss, $IL = -12.44\ \text{dB}$. In the design D3 ($L_p=10000\ \mu\text{m}$) the background crosstalk $BX = -35.06\ \text{dB}$, the non-uniformity $ILu = 0.57\ \text{dB}$ and the insertion loss $IL = -12.89\ \text{dB}$. In the case of design D4 ($L_p=10000\ \mu\text{m}$) the background crosstalk $BX = -37.69\ \text{dB}$, the non-uniformity $ILu = 0.83\ \text{dB}$ and the insertion loss $IL = -13.85\ \text{dB}$. Comparing all these four designs can be concluded that the best splitting characteristics were obtained for the design D2 ($L_p=10000\ \mu\text{m}$) with the width of the MMI section, $W_{MMI} = 300\ \mu\text{m}$.

Considering the Length of MMI Splitter

The simulation results showed that the optimal width of the MMI coupler for which we were able to get the best performance of the MMI splitter, i.e. low non-uniformity, low insertion loss and low background noise, was obtained in design D2. **Therefore, taking into account also the size of the splitter, we proposed the design D2 with the shortest $L_p = 5000\ \mu\text{m}$ as “standard” 1x16 MMI splitter design for the next simulations.** Figure 51 presents the top view and the simulated characteristics of this structure, namely the background crosstalk, $BX = -36.8\ \text{dB}$ (Figure 51-left), the uniformity of the split power over all the output channels, $ILu = 0.51\ \text{dB}$ and the insertion loss $IL = -12.548\ \text{dB}$ (Figure 51- right).

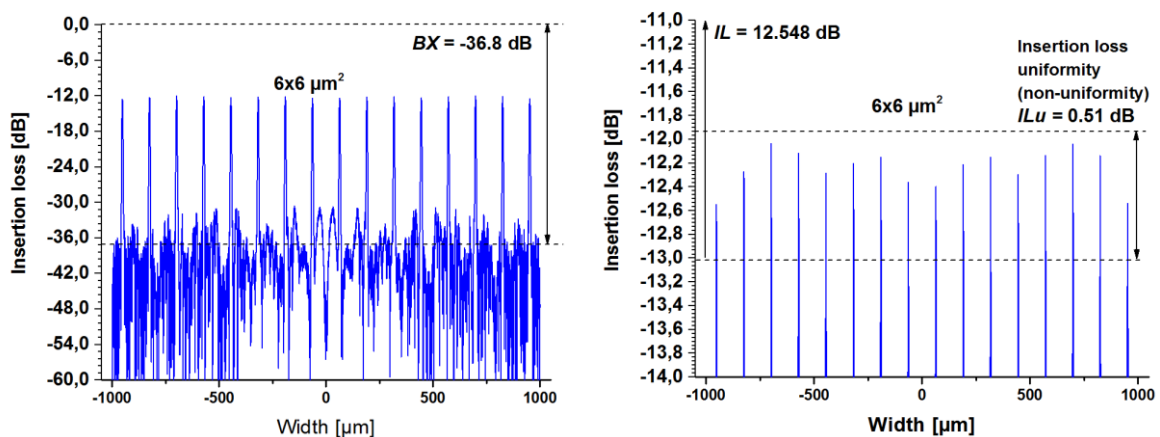


Figure 51: Field distribution at the end of the “standard” 1x16 MMI splitter (left). Non-uniformity and insertion loss of MMI structure (right) with the waveguide core size of $(6 \times 6)\ \mu\text{m}^2$.

Conclusion: From the simulation results is obvious that the width, W_{MMI} of the multimode interference coupler together with the lengths of the output ports are the important design parameters.

4.2.3 Comparison of Optical Properties of 1x16 Y-Branch and 1x16 MMI Splitters

The simulations referred in subsection 4.1 confirmed that MMI splitters have some advantages over the Y-branch splitters. The main advantage is their low non-uniformity and small size. The simulated results presented in the Table 11 confirm that for standard waveguide core size of $(6 \times 6) \mu\text{m}^2$ the non-uniformity, $ILu = 0.51$ dB is in case of MMI splitter much lower than the non-uniformity, $ILu = 1.77$ dB for Y-branch splitter, about $\Delta = 1.26$ dB. The MMI splitter is approximately seven times shorter than the Y-branch splitter, namely $11\,548 \mu\text{m}$ in contrast to $78\,000 \mu\text{m}$. Furthermore, the insertion loss, $IL = -12.548$ dB for MMI approach is slightly lower than insertion loss, $IL = -13.09$ dB for Y-branch splitter, in $\Delta = 0.54$ dB. On the other hand, the background crosstalk of MMI splitter, $BX = -36.8$ dB is considerably higher than background crosstalk of Y-branch splitter, $BX = -49.04$ dB, in $\Delta = 12.24$ dB.

Table 11: Comparison of splitting parameters of standard 1x16 Y-branch and 1x16 MMI splitters.

	Non-uniformity, ILu	Insertion loss, IL	Background crosstalk, BX	Length of splitter, L
Y-branch	1.77 dB	-13.09 dB	-49.04 dB	78 000 μm
MMI	0.51 dB	-12.548 dB	-36.8 dB	11 548 μm
Δ	1.26 dB	0.54 dB	12.24 dB	66 452 μm

4.2.4 Waveguide Optimization of 1x16 Y-Branch and 1x16 MMI Splitters

The study of the achieved simulation results summarized in Table 11 showed again that in the standard $(6 \times 6) \mu\text{m}^2$ waveguide not only propagation of the single mode is supported but also the presence of the first mode is already so strong that it causes additional asymmetric splitting of the optical signal at the branching points in Y-branch splitters. Therefore, we reduced the waveguide core size from $(6 \times 6) \mu\text{m}^2$ to $(5.5 \times 5.5) \mu\text{m}^2$ in both splitters keeping the same size of the structures. The simulated results, namely the non-uniformity, ILu and insertion loss, IL of 1x16 Y-branch and 1x16 MMI splitters are shown in Figure 52. As can be seen in Figure 52-right, the splitting parameters of the MMI splitter are only slightly improved since the splitting appears in the large coupler.

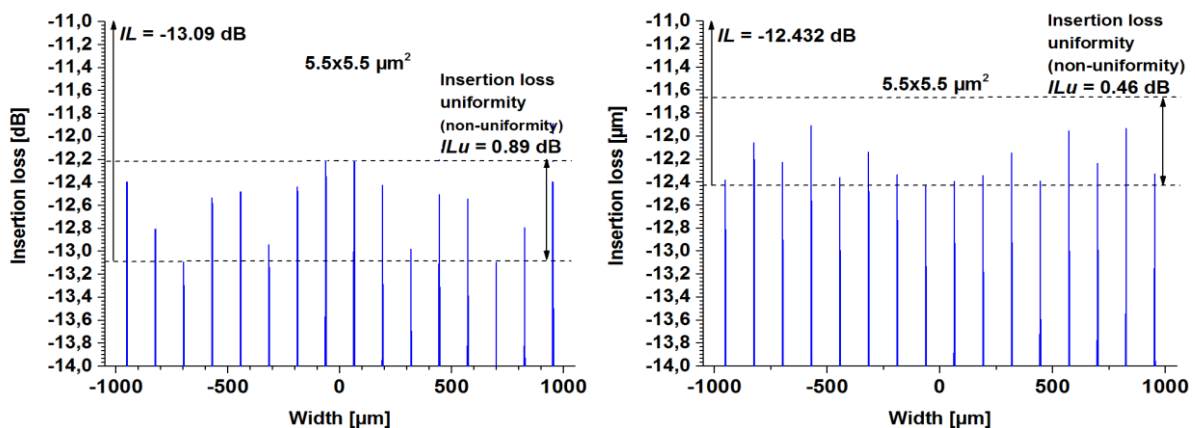


Figure 52: Non-uniformity and insertion loss of 1x16 Y-branch (left) and 1x16 MMI (right) splitters with the waveguide core size of $(5.5 \times 5.5) \mu\text{m}^2$.

On the other hand, Y-branch splitter, consisting of many waveguides, features strong improvement of its optical properties (see Figure 52-left).

Table 12 shows that for waveguide core size $(5.5 \times 5.5) \mu\text{m}^2$ the non-uniformity of Y-branch splitter is strongly reduced from $ILu = 1.77$ dB for $(6 \times 6) \mu\text{m}^2$ to $ILu = 0.89$ dB, that is less than one half of its original value. In this way, again decreasing the waveguide core it was possible to suppress presence of the first mode and to reduce strongly the non-uniformity parameter in Y-branch splitters.

Table 12: Comparison of splitting parameters of “standard” 1x16 Y-branch and 1x16 MMI splitters.

		Non-uniformity, ILu	Insertion loss, IL	Background crosstalk, BX	Length of splitter, L
Y-branch	$(6 \times 6) \mu\text{m}^2$	1.77 dB	13.09 dB	-49.04 dB	78 000 μm
	$(5.5 \times 5.5) \mu\text{m}^2$	0.89 dB	13.09 dB	-49.18 dB	78 000 μm
	Δ	0.88 dB	0 dB	0.14 dB	
MMI	$(6 \times 6) \mu\text{m}^2$	0.51 dB	12.548 dB	-36.80 dB	11 548 μm
	$(5.5 \times 5.5) \mu\text{m}^2$	0.46 dB	12.432 dB	-36.84 dB	11 548 μm
	Δ	0.05 dB	0.116 dB	0.04 dB	

4.2.5 Simulation of “Standard” 1x 32 Y-Branch Splitters Using OptiBPM

The design of “standard” 1x32 Y-branch splitter (from Figure 28-left) with waveguide core size of $(6 \times 6) \mu\text{m}^2$ was simulated in OptiBPM tool. Figure 53 shows the top view of the simulated structure. As can be seen 32 output signals are well separated, the light is guided well in the waveguides but at the branching points there is a lot of scattered light. This scattered light causes losses in the Y-branch splitter and also high background noise. Figure 54-left presents the corresponding field distribution at the end of the splitter structure. The maximum background crosstalk, BX is better than -39.36 dB. The uniformity of the split power over all the output waveguides, $ILu = 4.21$ dB and the insertion loss (worst peak) $IL = -18.54$ dB as illustrated in Figure 54-right.

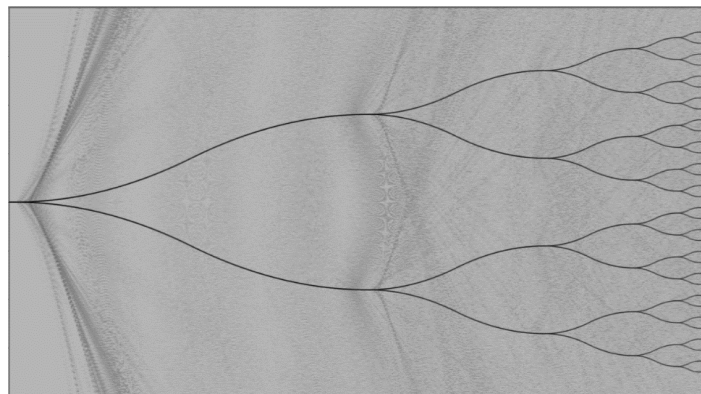


Figure 53: Top view of the simulated “standard” 1x32 Y-branch splitter.

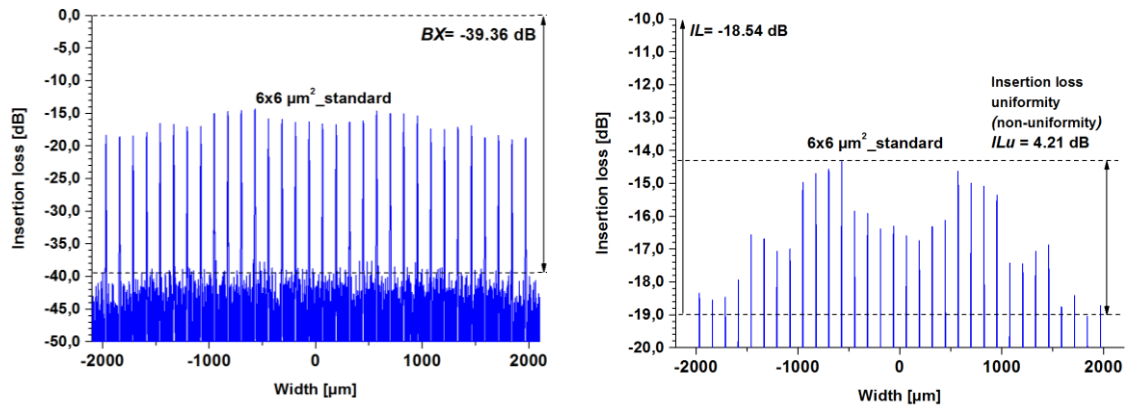


Figure 54: Simulation results of the "standard" 1x32 Y-branch splitter structure: Field distribution at the end of simulated structure together with background crosstalk, BX (left); Detailed view of the field distribution showing the non-uniformity, ILu and the insertion loss, IL (right).

Conclusion: From the simulation is clear that increasing the number of output waveguides leads to a strong degradation of splitting parameters as well as to a huge increase in the length.

4.2.6 Simulation of "Length-Optimized" 1x 32 Y-Branch Splitters Using OptiBPM

As described in subsection 3.4.3.1 the length of 1x32 Y-branch splitter, described above, was optimized (in Figure 28-right). This design with waveguide core size of $(6 \times 6) \mu\text{m}^2$ was simulated by OptiBPM tool. Figure 55 shows the achieved simulation results. Figure 55-left presents the field distribution at the end of the splitter structure. As shown the maximum background noise, BX reached again about -40.0 dB. The non-uniformity, ILu slightly decreased from 4.21 dB to 4.12 dB and the insertion loss remained at the similar value, $IL = -18.34$ dB (see Figure 55-right).

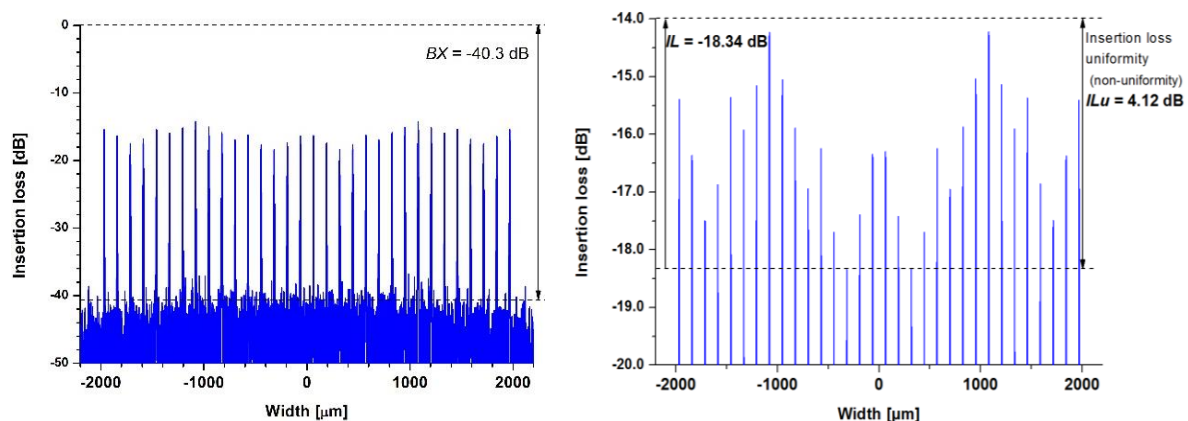


Figure 55: Simulation results of the "length-optimized" 1x32 Y-branch splitter structure: Field distribution at the end of simulated structure together with calculated background crosstalk, BX (left); Detailed view of the field distribution showing the non-uniformity, ILu and the insertion loss, IL (right).

4.2.7 Simulation of “Further length-reduced” 1x32 Y-Branch Splitters Using OptiBPM

The “further length-reduced” 1x32 Y-branch splitter: Option 1, Option 2, Option 3 and Option 4 described in subsection 3.4.3.1 were simulated and the simulation results for Option 1 and Option 2 are presented in Figure 56. Column left presents the field distribution at the end of the splitter structure and the column right presents the detailed view of the field distribution of both, Option 1 and Option 2 structures. As shown in case of Option 1, the maximum background noise, $BX = -42.1$ dB, the non-uniformity, ILu is 1.87 dB and the insertion loss remained at nearly the same value, $IL = -17.15$ dB (see Figure 56 top). As can be seen in case of Option 2 by reducing the length of the 5th branch by 20% the maximum background noise, $BX = -41.64$ dB, the non-uniformity, ILu features 1.6 dB and the insertion loss, $IL = -17.06$ dB (see Figure 56 bottom).

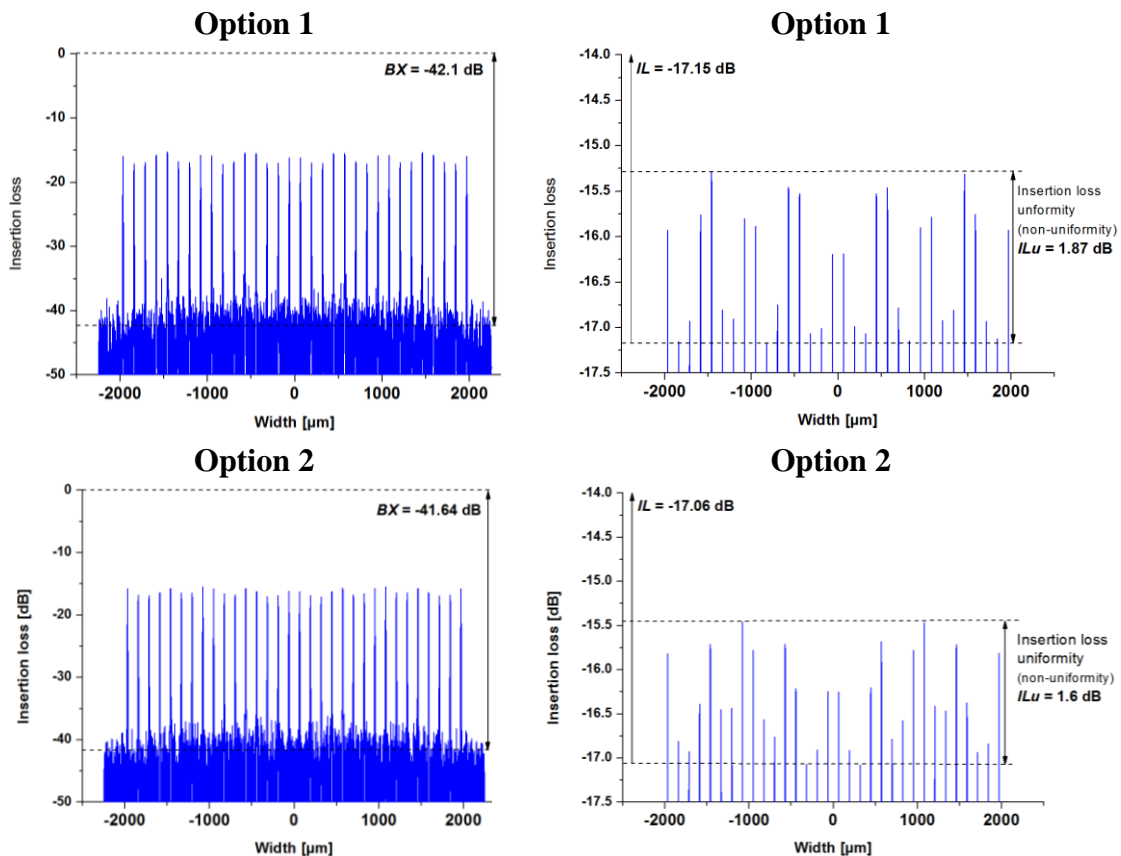


Figure 56: Simulation results of the “further length-reduced” 1x32 Y-branch splitter using Option 1 (top) and Option 2 (bottom) designs: Field distribution at the end of simulated structure together with calculated background crosstalk, BX (left); Detailed view of the field distribution showing the non-uniformity, ILu and the insertion loss, IL (right).

The simulation results of the modified splitters Option 3 and Option 4 are presented in the Figure 57. For the Option 3 the maximum background noise, $BX = -42.48$ dB, the non-uniformity, $ILu = 2.8$ dB and the insertion loss, IL is -17.51 dB (see Figure 57 top). From this we can conclude that this 50% reduction of the 5th branch was too strong (see Figure 29 and subsection 3.4.3.1). For the Option 4, the non-uniformity, $ILu = 1.96$ dB, the insertion loss, $IL = -17.35$ dB and the maximum background, $BX = -40.78$ dB.

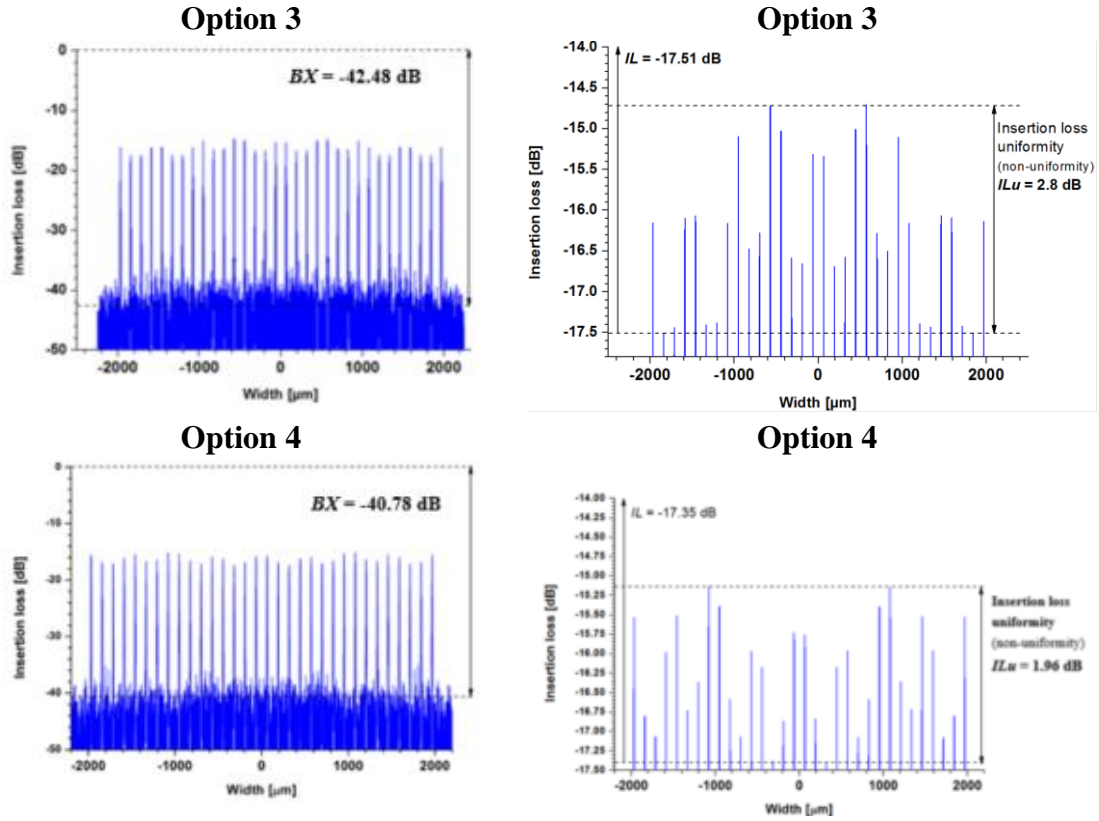


Figure 57: Simulation results of the “further length-reduced” 1x32 Y-branch splitter using Option 3 (top) and Option 4 (bottom) designs: Field distribution at the end of simulated structure together with calculated background crosstalk, BX (left); Detailed view of the field distribution showing the non-uniformity, ILu and the insertion loss, IL (right).

Table 13 shows a summary of all four further length reduction options of the “length-optimized” 1x32 Y-branch splitter.

Table 13: Comparison of splitting parameters achieved from the simulations of Option 1, Option 2, Option 3 and Option 4 or 1x32 Y-branch splitter.

	Option 1 (6x6) μm^2	Option 2 (6x6) μm^2	Option 3 (6x6) μm^2	Option 4 (6x6) μm^2
Non-uniformity, ILu	1.87 dB	1.6 dB	2.8 dB	1.96 dB
Insertion loss, IL	-17.15 dB	-17.06 dB	-17.51 dB	-17.35 dB
Max. background noise, BX	-42.1 dB	-41.64 dB	-42.48 dB	-40.78 dB
Chip size	92 000 μm	90 000 μm	78 500 μm	86 000 μm

Conclusion: As can be seen from Table 13 the worst splitting parameters were obtained for the Option 3, particularly parameter ILu . The other 3 options show similar results. Particularly, the splitting parameters insertion loss and background noise do not vary very much from each other.

4.2.8 Waveguide Optimization of “Length–Optimized” 1x 32 Y-Branch Splitters Using OptiBPM

The simulation results of “standard” and “length-optimized” 1x32 Y-branch splitters showed that the non-uniformity and insertion loss were not satisfying. Particularly the non-uniformity parameter ILu with over 4 dB is too high. The main reason for such a high non-uniformity is again the presence of the first mode (besides the zero mode) propagating in the $(6 \times 6) \mu\text{m}^2$ waveguide. Based on this knowledge the same “length-optimized” design of 1x32 Y-branch splitter with waveguide core size of $(5.5 \times 5.5) \mu\text{m}^2$ was simulated. The results of this simulation are shown in Figure 56.

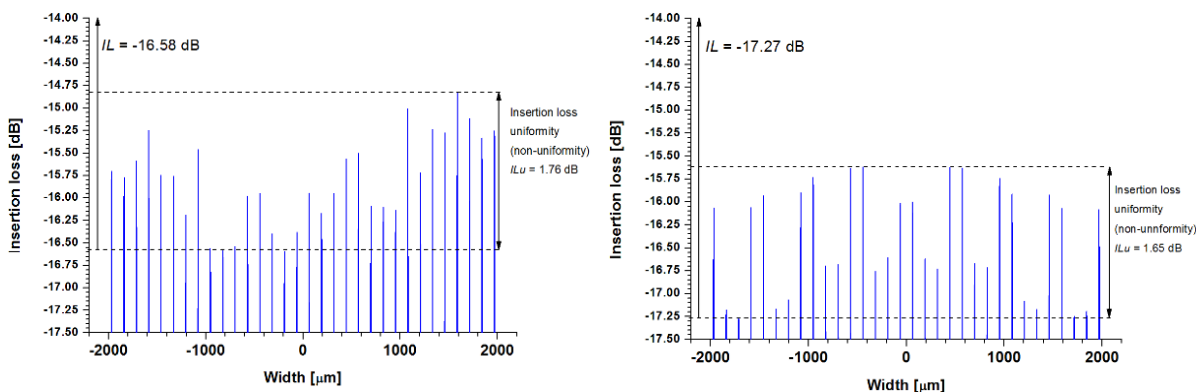


Figure 58: Simulation results of the “length-optimized” 1x32 Y-branch splitter structure with the waveguide core size of $(5.5 \times 5.5) \mu\text{m}^2$ (left); with the waveguide core size of $(5 \times 5) \mu\text{m}^2$ (right), namely detailed view of the field distribution showing the non-uniformity, ILu and the insertion loss, IL (right).

Compared to the simulation results illustrated in the Figure 55 the strong improvement of the splitting parameters was again reached: the non-uniformity, $ILu = 1.76$ dB and the insertion loss, $IL = -16.58$ dB. The maximum background crosstalk, $BX = -40.25$ dB remained constant. Therefore, another simulation of the “length-optimized” 1x32 Y-branch splitter with waveguide core size of $(5 \times 5) \mu\text{m}^2$ was performed (Figure 56-right). The simulation results feature further weak improvement of the splitting parameters compared to the case when the waveguide core size of $(5.5 \times 5.5) \mu\text{m}^2$ was used: the non-uniformity, $ILu = 1.65$ dB and the insertion loss, $IL = -17.27$ dB. The background crosstalk, $BX = -40.72$ dB did not change significantly.

4.2.9 Comparison of the “Length–Optimized” 1x 32 Y-Branch Splitters with Different Waveguide Cross-Sections

The presented simulations showed again that the waveguide core size has a high impact on the Y-branch splitting parameters (see Table 13).

The “length-optimized” 1x32 Y-branch splitter having a $(6 \times 6) \mu\text{m}^2$ core size features a high non-uniformity, ILu of 4.12 dB and also high insertion loss, $IL = -18.34$ dB. Decreasing the waveguide core size to $(5.5 \times 5.5) \mu\text{m}^2$ a strong improvement of ILu was achieved ($ILu = 1.76$ dB). Additionally, insertion loss, IL was reduced by more than 2 dB ($IL = -16.58$ dB). The “length-optimized” Y-branch splitter with a waveguide core size of $(5 \times 5) \mu\text{m}^2$ reached the non-

uniformity even of $ILu = 1.65$ dB. Similarly, the insertion loss, IL is improved by more than 1 dB compared to the length optimized Y-branch splitter with $(6 \times 6) \mu\text{m}^2$ waveguide core size, while the background crosstalk, BX is rarely influenced.

Table 14: Comparison of splitting parameters of the “length-optimized” 1x32 Y-branch splitters having different waveguide core size: $(6 \times 6) \mu\text{m}^2$, $(5.5 \times 5.5) \mu\text{m}^2$ and $(5 \times 5) \mu\text{m}^2$.

“LENGTH-OPTIMIZED” 1X32 Y-BRANCH SPLITTER					
Waveguide core size	$(6 \times 6) \mu\text{m}^2$	$(5.5 \times 5.5) \mu\text{m}^2$	Δ	$(5 \times 5) \mu\text{m}^2$	Δ
Non-uniformity, ILu	4.12 dB	1.76 dB	2.36 dB	1.65 dB	2.47 dB
Insertion loss, IL	-18.34 dB	-16.58 dB	1.76 dB	-17.27 dB	1.07 dB
Background crosstalk, BX	-40.3 dB	-40.25 dB	0.05 dB	-40.72 dB	0.42 dB

Conclusion: From this can be concluded that keeping the same Y-branch layout and decreasing the waveguide core size the splitting properties of the Y-branch splitter can be strongly improved. Mainly, the insertion loss was reduced by nearly 2 dB and the non-uniformity, ILu was reduced nearly to one third of its original value.

4.2.10 Waveguide Optimization of the “Further Length–Reduced” 1x 32 Y-Branch Splitters Using OptiBPM Tool

Finally, “further length-reduced” design (Option 4 from Figure 29) was simulated with a core size of $(5.5 \times 5.5) \mu\text{m}^2$ first and the results are shown in Figure 59. As can be seen the non-uniformity, ILu was further reduced to less than one third of the non-uniformity of the standard Y-branch splitter ($ILu = 3.68$ dB), namely $ILu = 1.12$ dB. The insertion loss was also further reduced to $IL = -16.17$ dB and the maximum background crosstalk, $BX = -40.5$ dB remained constant.

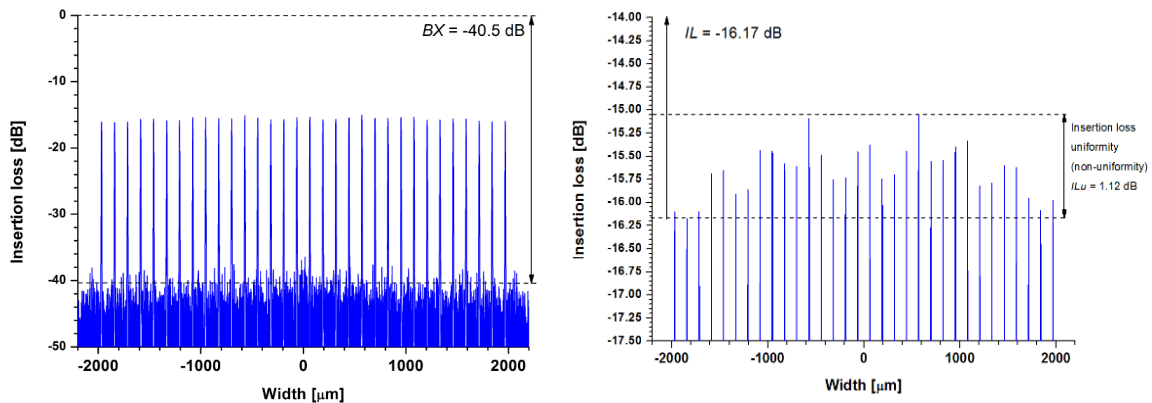


Figure 59: Simulation results of “further length-optimized” 1x32 Y-branch splitter with the waveguide core size of $(5.5 \times 5.5) \mu\text{m}^2$: Field distribution at the end of simulated structure together with background noise, BX (left); Detailed view of the field distribution showing the non-uniformity, ILu and the insertion loss, IL (right).

4.2.11 Comparison of “Further Length–Reduced” 1x32 Y-Branch Splitters with Different Waveguide Cross-Sections

Table 15 summarizes all important achieved simulated results. Compared to a “standard” Y-branch splitter the “further length-optimized” splitter (Option 4) with $(5.5 \times 5.5) \mu\text{m}^2$ waveguide core size achieved much better values of the non-uniformity (ILu was reduced from 4.21 dB to 1.12 dB), the insertion loss, IL was reduced from -18.54 dB to -16.17 dB while the background crosstalk, BX was rarely influenced.

Table 15: Comparison of splitting parameters achieved from the simulations of “standard” and “further length-optimized” 1x32 Y-branch splitters with waveguide core sizes of $(6 \times 6) \mu\text{m}^2$ and $(5.5 \times 5.5) \mu\text{m}^2$.

1X32 Y-BRANCH SPLITTER					
Waveguide core size	Standard (6x6) μm^2 (Figure 54)	Further length-reduced (5.5x5.5) μm^2	Δ	Further length-reduced (6x6) μm^2	Δ
Non-uniformity, ILu	4.21 dB	1.12 dB	3.09 dB	1.96 dB	2.25 dB
Insertion loss, IL	-18.54 dB	-16.7 dB	1.84 dB	-17.35 dB	1.19 dB
Background crosstalk, BX	-39.36 dB	-40.5 dB	1.14 dB	-40.78 dB	1.36 dB
Chip size	158000 μm	86000 μm	72000 μm	86000 μm	72000 μm

Conclusion: The “further length-reduced” 1x32 Y-branch splitter with $(5.5 \times 5.5) \mu\text{m}^2$ waveguide core size reached the best splitting parameters. This final design will be called “further length-optimized design”.

4.2.12 Simulation of 1x32 Y-Branch Splitters Using RSoft Tool

1x32 Y-branch splitters both, the “standard” and “further length-optimized” were also designed and optimized using RSoft photonic tool from Synopsys Inc. [171], [172]. This task was realized by Anton Kuzma from International Laser Centre in Bratislava, who I have cooperated with. The top view of the “standard” structure is presented in Figure 60.

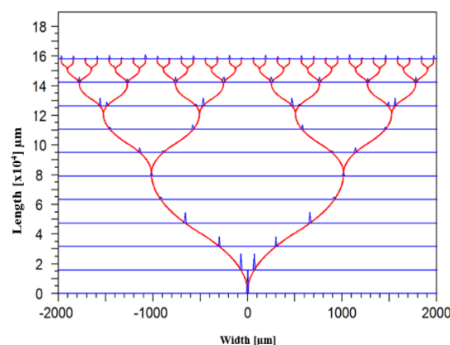


Figure 60: Top view of the “standard” 1x32 Y-branch splitter structure designed applying RSoft photonic tool.

The optical properties of the “standard” 1x32 Y-branch splitter, simulated with RSoft in 3D environment, are displayed in Figure 61-top. The non-uniformity, $ILu = 2.15$ dB and the insertion loss, $IL = -16.44$ dB.

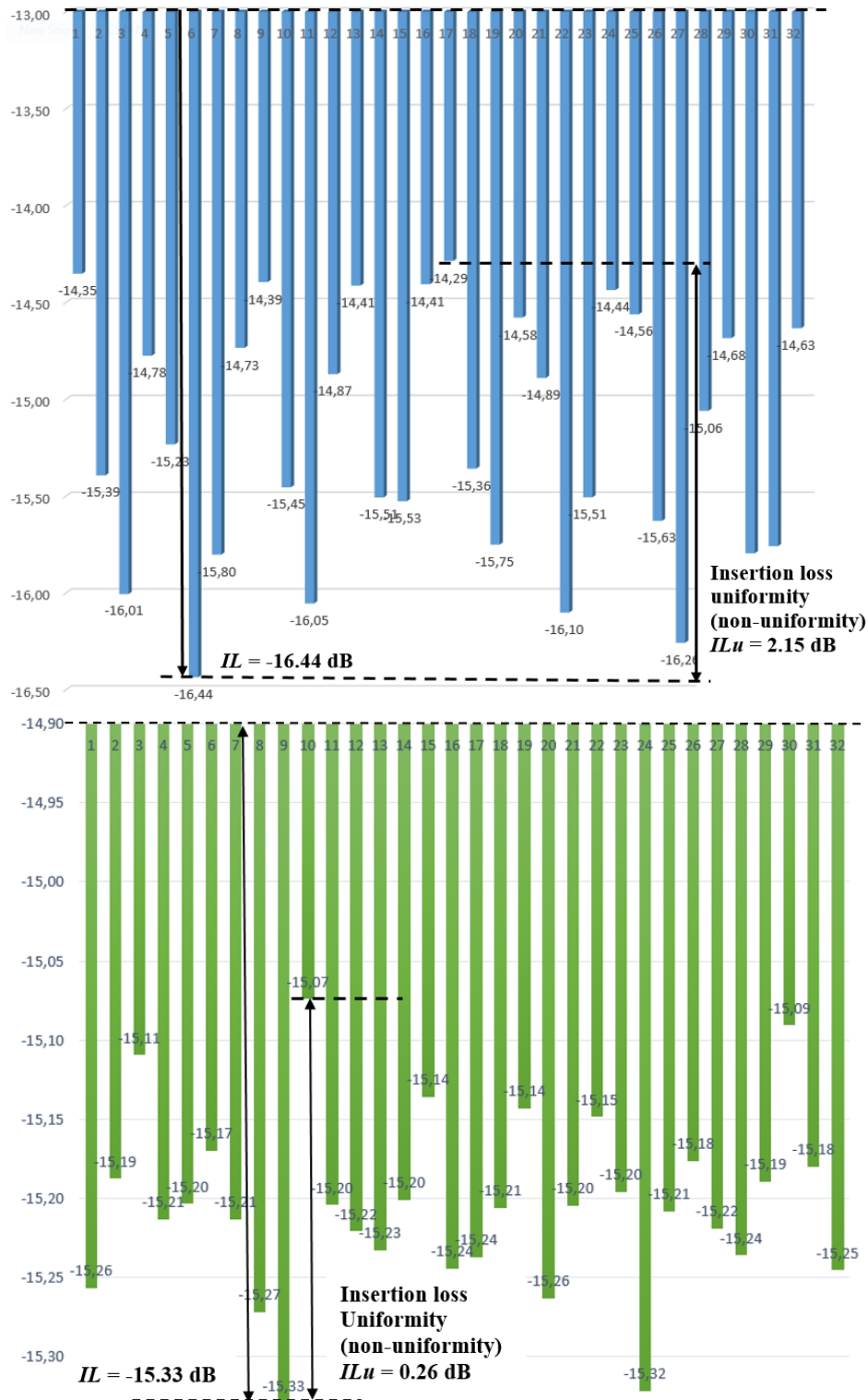


Figure 61: Simulation results of the “standard” 1x32 Y-branch splitter structure (6×6) μm^2 (top); “length optimized” 1x32 Y-branch splitter structure with the waveguide core size of (5.5×5.5) μm^2 (bottom).

Consequently, the “length-optimized” structure with the core size $(5.5 \times 5.5) \mu\text{m}^2$ was simulated and the results are shown in Figure 61-bottom. As can be seen, the non-uniformity, $ILu = 0.26$ dB and the insertion loss was $IL = -15.33$ dB.

From this follows that optimizing the waveguide core size led again to strong improvement of the splitting parameters of the Y-branch structure, namely the insertion loss, IL from -16.44 dB (“standard” structure) to -15.33 dB (“optimized” structure) and the non-uniformity, ILu from 2.15 dB (“standard” structure) to 0.26 dB (“optimized” structure).

Table 16 summarizes the results achieved from all designed and simulated 1x32 Y-branch splitters with both software tools, namely in 2D with OptiBPM photonics tool and in 3D with RSoft photonics tool from Synopsys Inc. As can be seen, the insertion loss was suppressed by $\Delta IL = 1.65$ dB (OptiBPM tool), and by $\Delta IL = 1.11$ dB (RSoft tool), $\Delta ILu = 3.09$ dB (OptiBPM), and $\Delta ILu = 1.89$ dB (RSoft).

Table 16: Comparison of splitting parameters achieved from the simulations of “standard” and “length optimized” 1x32 Y-branch splitters with waveguide core sizes of $(6 \times 6) \mu\text{m}^2$ and $(5.5 \times 5.5) \mu\text{m}^2$.

1x32 Y-BRANCH SPLITTER						
	OptiBPM			RSoft		
Waveguide core size	“standard” ($6 \times 6 \mu\text{m}^2$) (Fig. 54)	“Length-Optimized” ($5.5 \times 5.5 \mu\text{m}^2$) (Figure 59-right)	Δ	“standard” ($6 \times 6 \mu\text{m}^2$) (Fig. 61-top)	“Length-Optimized” ($5.5 \times 5.5 \mu\text{m}^2$) (Figure 61-bottom)	Δ
Non-uniformity, ILu	4.21 dB	1.12 dB	3.09 dB	2.15 dB	0.26 dB	1.89 dB
Insertion loss, IL	-18.54 dB	-16.7 dB	1.65 dB	-16.44 dB	-15.33 dB	1.11 dB
Chip size	158000 μm	86000 μm	72000 μm	158000 μm	86000 μm	72000 μm

Conclusion

From the simulations is evident that the reduction of the waveguide core size from $(6 \times 6) \mu\text{m}^2$ to $(5.5 \times 5.5) \mu\text{m}^2$ leads to significant improvement of optical properties of 1x32 Y-branch splitters. Namely, we reached symmetric splitting ratio, ensuring good uniformity over all the output signals. Particularly, for insertion loss uniformity ILu , one third of original non-uniformity of “standard” splitter was reached (for OptiBPM) and one tenth of the original value (for RSoft). Additionally, our proposed optimization led to the length reduction of the “standard” splitter almost to the half of the original value (“length-optimized” splitter). It is also important to point out that the further reduction of the waveguide core size to $(5 \times 5) \mu\text{m}^2$ did not bring any significant improvement of the parameters compared to “length-optimized” splitter having core size $(5.5 \times 5.5) \mu\text{m}^2$. From the results can also be concluded that more satisfying simulation results were obtained in 3D environment with RSoft software tool.

4.3 Simulation Results of “New Shape” High Splitting Ratio SoS Splitters

4.3.1 Simulation Results of “New Shape” 1x32 Y-Branch Splitter Using OptiBPM Tool

1x32 Y-branch splitter with a new shape and having waveguide core size of $(6 \times 6) \mu\text{m}^2$ (from Figure 34-right) was simulated in OptiBPM. Figure 62 shows the top view of the simulated structure. As can be seen 32 output signals are well separated, the light is guided well in the waveguides and comparing the top view of the “new-shape” 1x32 Y-branch splitter with the “standard” 1x32 Y-branch splitter (from Figure 53) it can be seen that the scattered light at the branching points in a new design is significantly reduced.

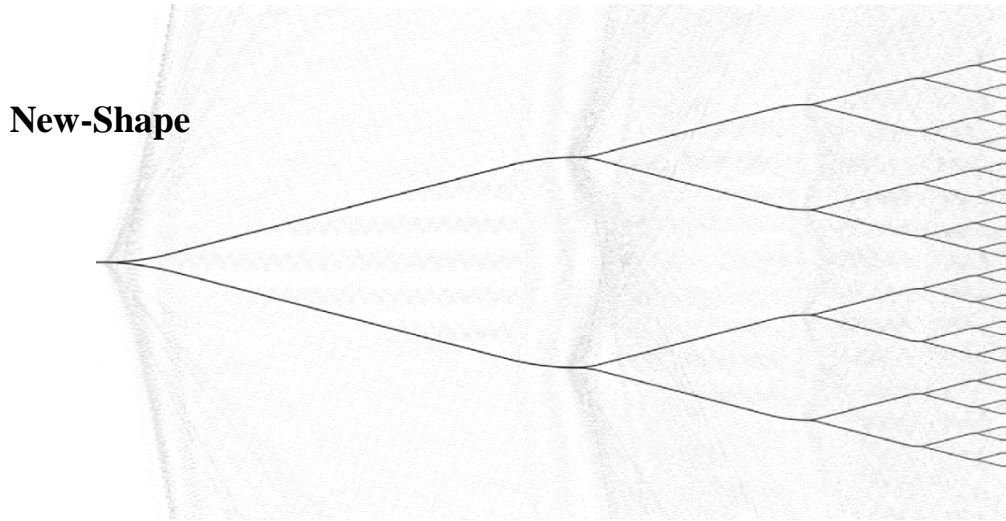


Figure 62: Detailed view of simulated “new shape” 1x32 Y-branch splitter.

This is also confirmed by the calculated splitting parameters. The background crosstalk of the “new-shape” 1x32 Y-branch splitter, $BX = -44.65$ dB (see Figure 63-left), the non-uniformity, $ILu = 2.3$ dB and the insertion loss, $IL = -17.15$ dB (see Figure 63-right).

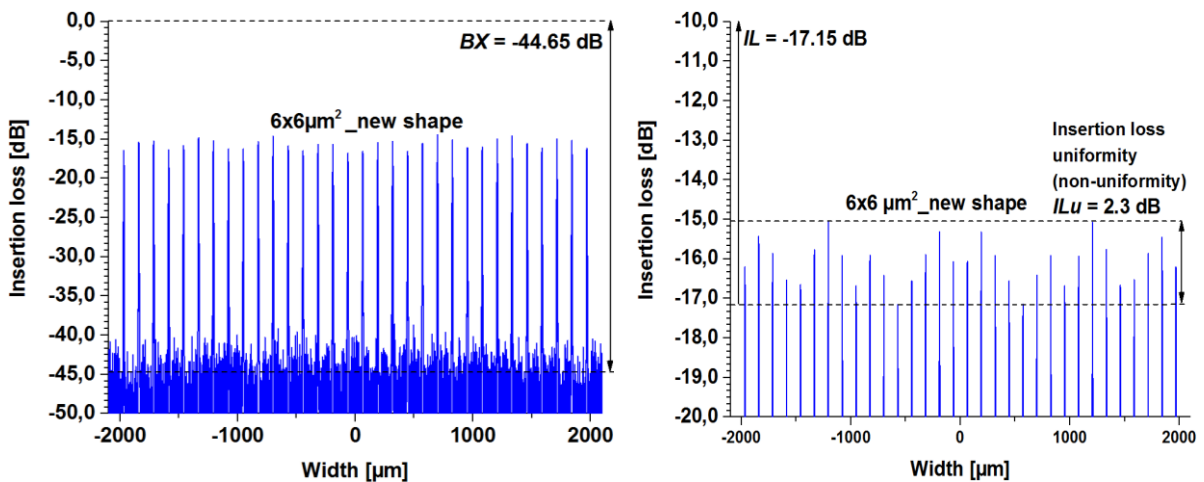


Figure 63: Simulation results of the “new shape” 1x32 Y-branch splitter structure with the core size of $(6 \times 6) \mu\text{m}^2$: Field distribution at the end of simulated structure together with background crosstalk, BX (left); Detailed view of the field distribution showing the non-uniformity, ILu and the insertion loss, IL (right).

4.3.2 Comparison of Optical Properties of “Standard” and “New Shape” 1x32 Y-Branch Splitter with OptiBPM Tool

Table 17 summaries the simulations results of booth, standard and new shape 1x32 Y-branch splitter.

Table 17: Comparison of splitting parameters of “standard” and “new shape” of 1x32 Y-branch splitters.

	“Standard” design (6x6) μm^2	“New-shape” design (6x6) μm^2	Improvement Δ
Non-uniformity, ILu	4.21 dB	2.3 dB	1.91 dB
Insertion loss, IL	-18.54 dB	-17.15 dB	1.39 dB
Background crosstalk, BX	-39.36 dB	-44.65 dB	5.29 dB

Conclusion

The 2D simulations in OptiBPM show that the splitting parameters of the “new-shape” 1x32 Y-branch splitter compared to the “standard” Y-branch splitter were significantly improved, i.e. particularly the background crosstalk, BX by more than one tenth, the non-uniformity, ILu to the half of the original value and the insertion loss IL was improved by more than 1 dB.

4.3.3 Waveguide Optimization of “New Shape” 1x32 Y-Branch Splitter

The “new-shape” 1x32 Y-branch splitter was simulated with waveguide structure (5.5x5.5) μm^2 keeping the same size of the structures. This confirmed better simulation results, namely for the “new-shape” 1x32 Y-branch splitter with the core size of (5.5x5.5) μm^2 is the maximum background crosstalk, $BX = -47.05$ dB (Figure 64-left), the non-uniformity, $ILu = 1.8$ dB, the insertion loss $IL = -16.26$ dB (Figure 64-rigth), having the same structure length 158000 μm .

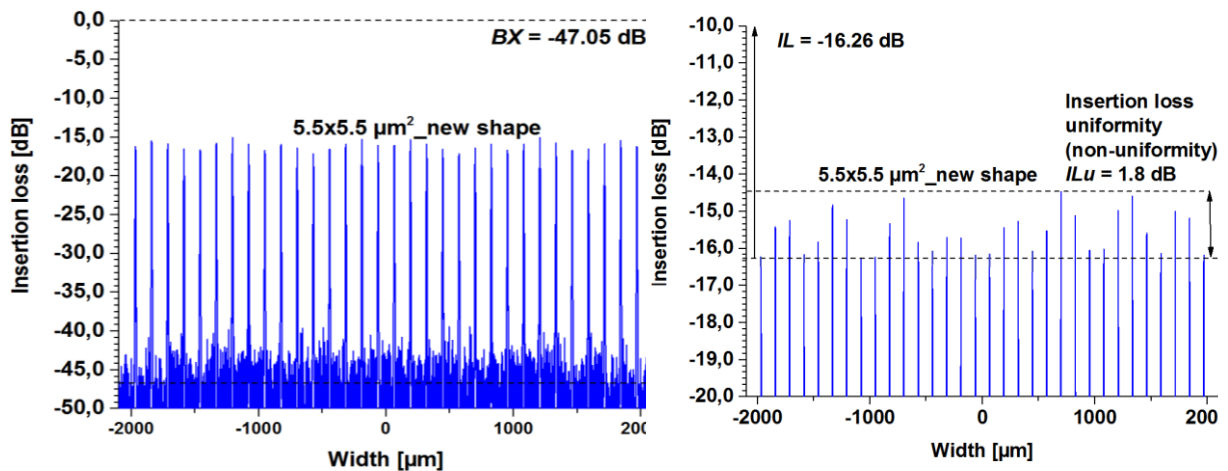


Figure 64: The maximum background noise, BX (left), the non-uniformity, ILu and the insertion loss, IL (right) of new shape 1x32 Y-branch splitter with the waveguide core size of (5.5x5.5) μm^2 .

4.3.4 Comparison of Optical Properties of “Standard” and “New Shape” Waveguide-Optimized 1x32 Y-Branch Splitter Applying OptiBPM Tool

Table 18 presents a comparison between the splitting parameters of the “standard” and “new-shape” waveguide-optimized 1x32 Y-branch splitter designs. As can be seen the non-uniformity, ILu was reduced from 4.21 dB (“standard” 1x32 Y-branch splitter) to 1.8 dB (“new-shape” waveguide-optimized structure); insertion loss, IL from -18.54 dB to -16.54 dB and background crosstalk, BX was improved from -39.36 dB to -47.05 dB. This design will be called “new-shape optimized” design. Thereby the splitting parameters were strongly improved, particularly the insertion loss, IL by $\Delta = 2.28$ dB and the non-uniformity, ILu by $\Delta = 2.41$ dB, i.e. the background noise, BX by 7.69 dB.

Table 18: Comparison of splitting parameters of “standard” and “new-shape” waveguide optimized 1x32 Y-branch splitters.

	“Standard” design (6x6) μm^2	“New-shape optimized” design (5.5x5.5) μm^2	Δ
Non-uniformity, ILu	4.21 dB	1.8 dB	2.41 dB
Insertion loss, IL	-18.54 dB	-16.26 dB	2.28 dB
Background crosstalk, BX	-39.36 dB	-47.05 dB	7.69 dB

Conclusion

Compared to the “standard” structure (reference structure) (see Table 15 or Figure 54), the optical parameters of the “new-shape” waveguide-optimized structure were strongly improved, namely the non-uniformity has been more than half reduced, as well as the theoretical insertion loss was reduced by 2 dB and the background crosstalk of the proposed structure was reduced by astonishing 8 dB.

In practice, such splitters could significantly improve the reach of passive optical networks by several kilometres, since the overall attenuation in PON, as per ITU recommendation, is around 30 dB [5]. It could also open door for new attenuation classes, where requirements (not only) for the attenuation are much more demanding, even for the same fiber reach.

4.4 Simulation Results of 1x64 Y-Branch Splitters

4.4.1 Simulation and Waveguide Optimization of “Standard” 1x 64 Y-Branch Splitters Using OptiBPM Tool

Design of the “standard” 1x64 Y-branch splitter having the length of 318 000 μm (from Figure 30-left) was simulated 2D in OptiBPM tool. Figure 65 shows the top view of simulated 1x64 Y-branch splitter for a waveguide core size of (6x6) μm^2 . As can be seen again the 64 output signals are well separated, the light is guided well in the waveguides but at the branching points is a lot of scattered light.

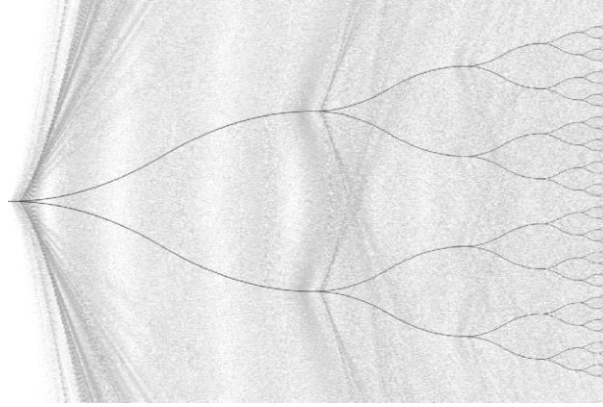


Figure 65: Detailed view of simulated standard 1x64 Y-branch splitter.

The background crosstalk of standard 1x64 Y-branch splitter, BX is better than -42 dB. The uniformity of the split power over all the output waveguides, $ILu = 2.67$ dB and the insertion loss (worst peak) $IL = -19.89$ dB as illustrated in Figure 66-top. The “standard” 1x64 Y-branch splitter was also optimized with regard to the waveguide core size. To this purpose the design of “standard” 1x64 Y-branch splitter with waveguide core size of $(5.5 \times 5.5) \mu\text{m}^2$ was simulated. The achieved simulated results are shown in Figure 66-bottom. Decreasing the waveguide core size the non-uniformity, ILu achieved 2.36 dB, the insertion loss, $IL = -22.98$ dB and the background crosstalk, $BX = -42.96$ dB.

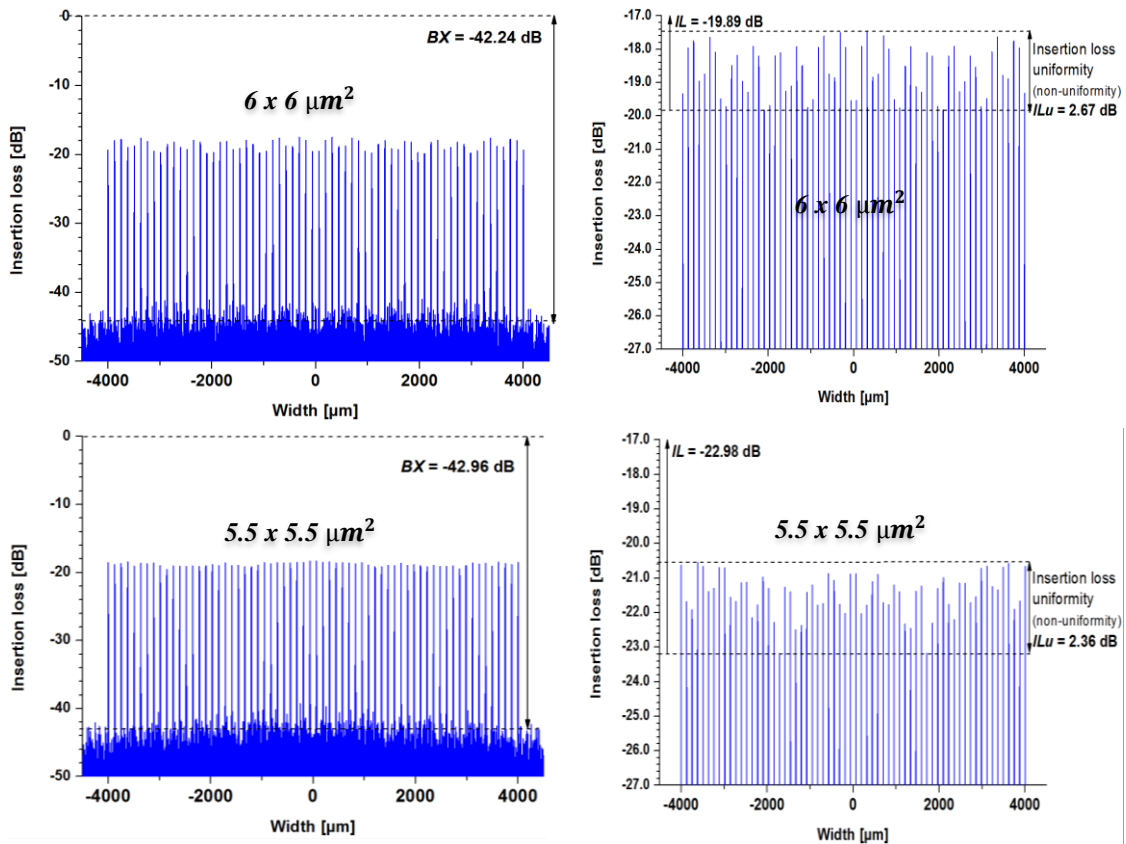


Figure 66: The background crosstalk, BX (left), the non-uniformity, ILu and the insertion loss, IL (right) of standard 1x32 Y-branch splitter with the waveguide core size of $(6 \times 6) \mu\text{m}^2$ (top), $(5.5 \times 5.5) \mu\text{m}^2$ (bottom).

4.4.2 Simulation of “Length-Optimized” 1x 64 Y-Branch Splitters Using OptiBPM Tool

The “length-optimized” 1x64 Y-branch splitter with three design variants (Variant 1, Variant 2 and Variant 3, see sub-section 3.4.3.2, Figure 30) were simulated and the top view of two simulated splitter structures are shown in the Figure 67.

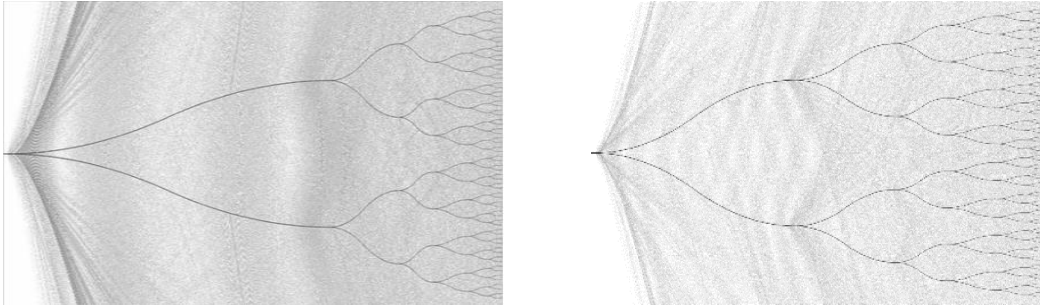


Figure 67: Detailed view of simulated “length-optimized” 1x64 Y-branch splitter: Variant 1 (left) and Variant 2 (right).

Variant 1: The simulation results of “length-optimized” 1x64 Y-branch splitter having the length $L = 246\,000\ \mu\text{m}$ and a waveguide core size of $(6 \times 6)\ \mu\text{m}^2$ are shown in Figure 68. The background crosstalk, BX reached $-41.19\ \text{dB}$, the non-uniformity, ILu is $3.98\ \text{dB}$ and the insertion loss, $IL = -22.29\ \text{dB}$ (see Figure 68-top). For the same length optimization of the Y-branch splitter structure but with the waveguide core size $(5.5 \times 5.5)\ \mu\text{m}^2$ is the background crosstalk, $BX = -41.12\ \text{dB}$, the non-uniformity, $ILu = 2.98\ \text{dB}$ and the insertion loss, $IL = -21.7\ \text{dB}$ (see Figure 68 bottom).

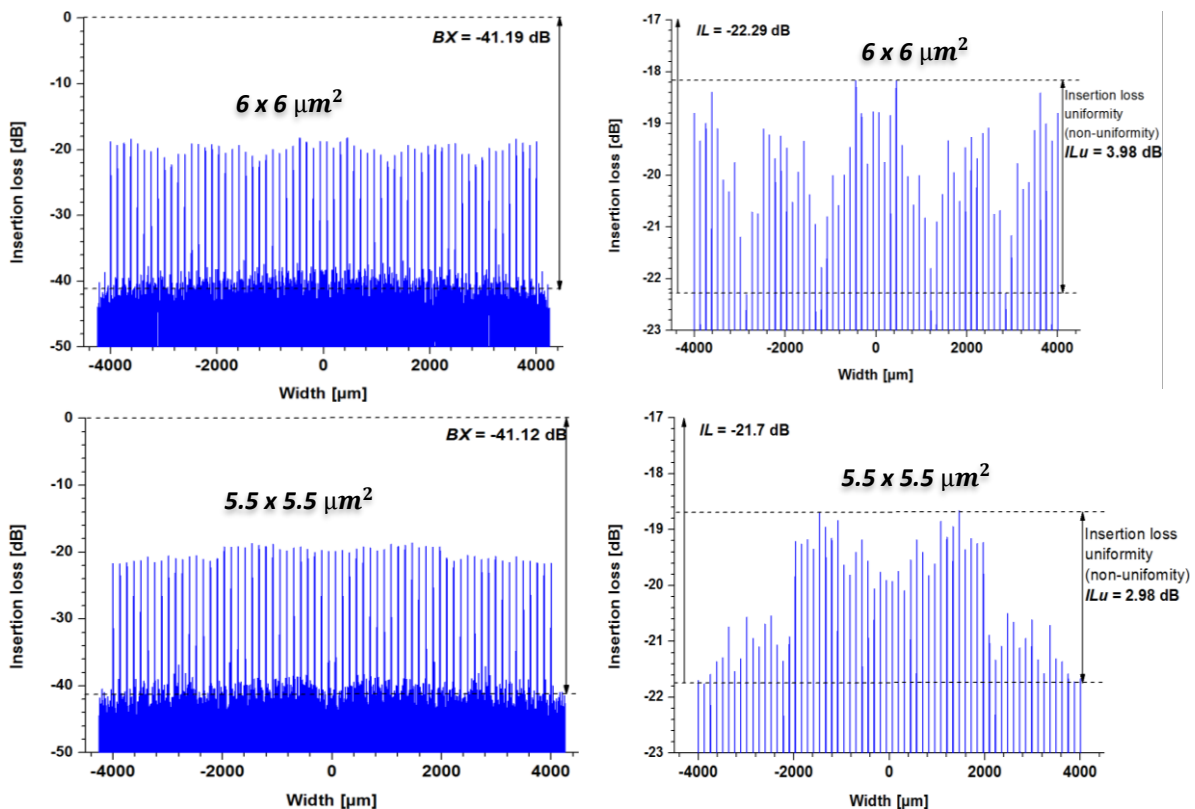


Figure 68: The achieved simulated results of “length optimized” 1x64 Y-branch splitter with a waveguide core size of $(6 \times 6)\ \mu\text{m}^2$ and $(5.5 \times 5.5)\ \mu\text{m}^2$ Variant 1.

Variant 2: The simulated results of the “length-optimized” 1x64 Y-branch structure using Variant 2 (length $L = 154\,000\ \mu\text{m}$) for a waveguide core size of $(6 \times 6)\ \mu\text{m}^2$ and $(5.5 \times 5.5)\ \mu\text{m}^2$ are illustrated in Figure 69.

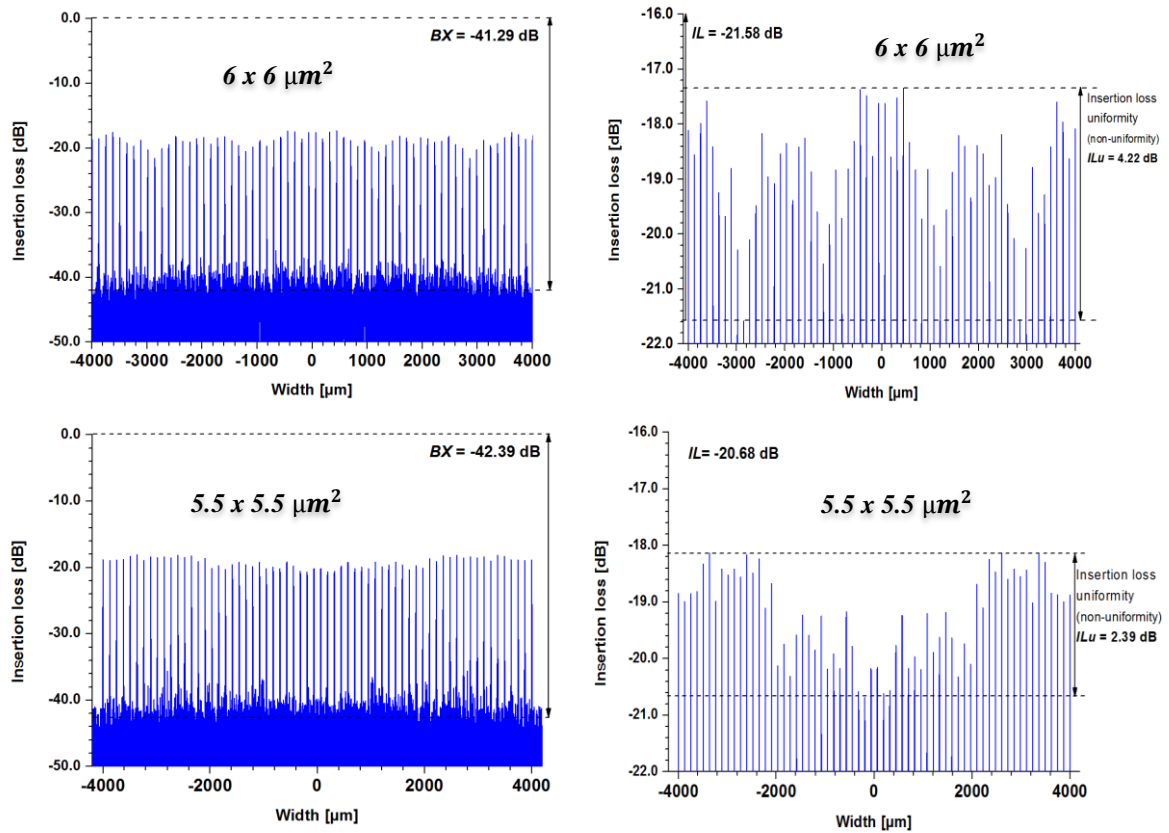


Figure 69: The achieved simulated results of “length-optimized” 1x64 Y-branch splitter with a waveguide core size of $(6 \times 6)\ \mu\text{m}^2$ and $(5.5 \times 5.5)\ \mu\text{m}^2$ Variant 2.

As shown for a waveguide core size of $(6 \times 6)\ \mu\text{m}^2$ the maximum background noise, $BX = -41.29\ \text{dB}$, the non-uniformity, $ILu = 4.22\ \text{dB}$ and the insertion loss, $IL = -21.58\ \text{dB}$ (see Figure 67-top). For a waveguide core size of $(5.5 \times 5.5)\ \mu\text{m}^2$ the background crosstalk, BX features $-42.39\ \text{dB}$, the non-uniformity, ILu reached $2.39\ \text{dB}$ and the insertion loss, $IL = -20.68\ \text{dB}$ (see Figure 67-bottom).

Variant 3: The top view of the simulated “length-optimized” 1x64 Y-branch structure using Variant 3 is illustrated in Fig. 70 and the Fig. 71 presents the simulation results. The achieved simulation results with a waveguide core size of $(6 \times 6)\ \mu\text{m}^2$ (see Figure 71-top) are: the background crosstalk, $BX = -40.82\ \text{dB}$, the insertion loss, $IL = -21.27\ \text{dB}$ and the non-uniformity, $ILu = 4.21\ \text{dB}$. The non-uniformity, $ILu = 1.98\ \text{dB}$, the insertion loss, $IL = -19.93\ \text{dB}$ and the background crosstalk, $BX = -41.85\ \text{dB}$ are reached with waveguide core size of $(5.5 \times 5.5)\ \mu\text{m}^2$ (see Figure 71-bottom).

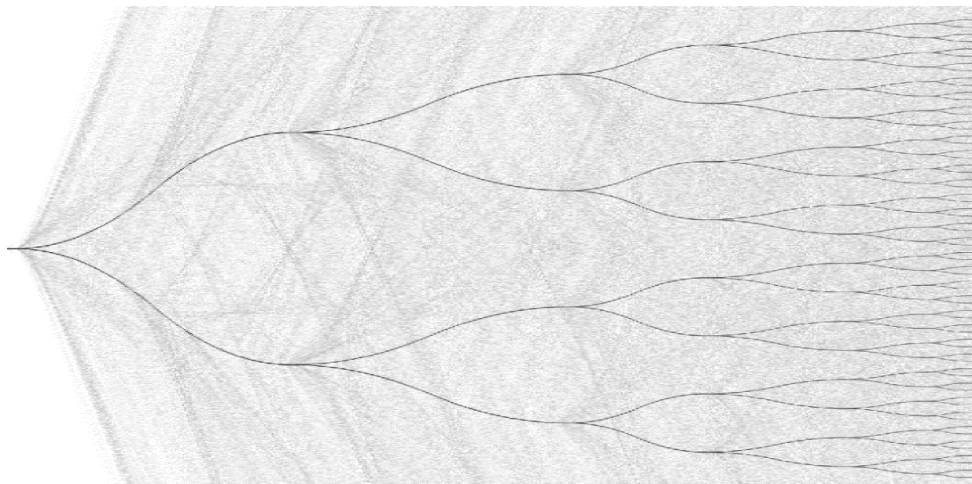


Figure 70: Detailed view of simulated “length optimized” 1x64 Y-branch splitter: Variant 3.

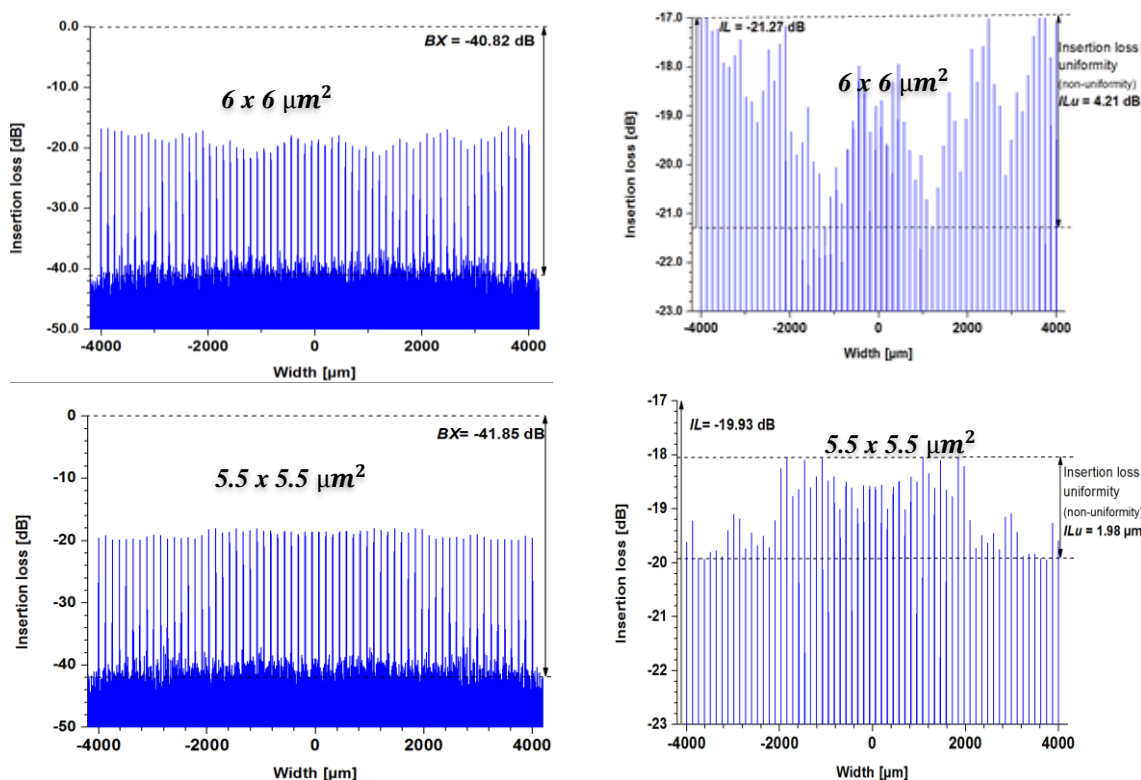


Figure 71: The achieved simulated results of “length-optimized” 1x64 Y-branch splitter with a waveguide core size of $(6 \times 6) \mu\text{m}^2$ and $(5.5 \times 5.5) \mu\text{m}^2$ Variant 3.

4.4.3 Comparison of Optical Properties of the “Length-Optimized” 1x 64 Y-Branch Splitters

Table 18 shows an overview of the splitting parameters achieved from all three optimization variants of 1x64 Y-branch splitter. As can be seen the splitting parameters insertion loss, IL and background noise, BX do not vary very much from each other. The best simulation results were achieved with a waveguide core size of $(5.5 \times 5.5) \mu\text{m}^2$, namely the background crosstalk, $BX =$

-41.85 dB, the insertion loss, $IL = -19.93$ dB and the non-uniformity, $ILu = 1.98$ dB. For the convenience, we will call this design “low-loss length-optimized” design.

Table 19: Comparison of splitting parameters achieved from the simulations of “Variant 1”, Variant 2”, Variant 3” for 1x64 Y-branch splitter having waveguide core sizes of $(6 \times 6) \mu\text{m}^2$, $(5.5 \times 5.5) \mu\text{m}^2$.

Variant/ core size	Non-uniformity, ILu	Insertion loss, IL	Background crosstalk, BX	Chip size
Variant 1 $(6 \times 6) \mu\text{m}^2$ $(5.5 \times 5.5) \mu\text{m}^2$	3.98 dB 2.98 dB	-22.29 dB -21.70 dB	-41.19 dB -41.12 dB	246000 μm
Variant 2 $(6 \times 6) \mu\text{m}^2$ $(5.5 \times 5.5) \mu\text{m}^2$	4.22 dB 2.39 dB	-21.58 dB -20.68 dB	-41.29 dB -42.39 dB	154000 μm
Variant 3 $(6 \times 6) \mu\text{m}^2$ $(5.5 \times 5.5) \mu\text{m}^2$	4.21 dB 1.98 dB	-21.27 dB -19.93 dB	-40.82 dB -41.85 dB	120000 μm

4.4.4 Comparison of Optical Properties of “Standard” and “Low-Loss Length-Optimized” 1x 64 Y-Branch Splitters

Table 19 shows an overview of the important splitting parameters achieved from the simulations of “standard” and “low-loss length-optimized” 1x64 Y-branch splitters with waveguide core size of $(5.5 \times 5.5) \mu\text{m}^2$ and $(6 \times 6) \mu\text{m}^2$ and the reached length of the splitter structure. Compared to a “standard” 1x64 Y-branch splitter with the waveguide core size $(6 \times 6) \mu\text{m}^2$ the “low-loss length-optimized” splitter with $(5.5 \times 5.5) \mu\text{m}^2$ waveguide core size reached better values of the non-uniformity (ILu was reduced from 2.67 dB to 1.98 dB), the insertion loss, IL and the background crosstalk, BX do not vary much.

Table 20: Comparison of splitting parameters of “standard” and “low-loss length-optimized” 1x64 Y-branch splitter having waveguide core sizes of $(6 \times 6) \mu\text{m}^2$ and $(5.5 \times 5.5) \mu\text{m}^2$.

1X64 Y-BRANCH SPLITTER			
Waveguide core size	Standard $(6 \times 6) \mu\text{m}^2$	Low-loss length-optimized $(5.5 \times 5.5) \mu\text{m}^2$	Δ
Non-uniformity, ILu	2.67dB	1.98 dB	0.69 dB
Insertion loss, IL	-19.89 dB	-19.93 dB	0.04 dB
Background crosstalk, BX	-42.24 dB	-41.85 dB	0.39 dB
Chip length	318 000 μm	120 000 μm	198 000 μm

Conclusion: Even though the length of “standard” 1x64 Y-branch splitter was reduced to nearly one third, applying the smaller waveguide core size, the “low-loss length-optimized”

1x64 Y-branch splitter features more satisfying optical properties. In this way, “standard” design of 1x64 Y-branch splitter was optimized for its properties and length (“low-loss length-optimized”). Particularly, the chip length was decreased by 198 000 μm and non-uniformity by 0.7 dB.

4.5 Simulation Results of Low-Loss Length-Optimized Y-Branch Splitter Implementation in PON/XG-PON

The achieved splitting parameters of optimized splitter structures were incorporated in the simulations of particular passive optical network scenarios. For this purpose “OptSim” environment using Time Domain Split Step method was employed. The main specifications of the “standard” $(6 \times 6) \mu\text{m}^2$ and “low-loss length-optimized” $(5.5 \times 5.5) \mu\text{m}^2$ 1x64 Y-branch splitters, such as non-uniformity ILu , insertion loss IL , background crosstalk BX and chip size were compared in Table 19 (column left and middle) (see section 4.4.4). Because the most significant changes in splitter design are related to the better value of parameter “non-uniformity” ILu , the individual values of the insertion losses per each output port have been calculated, and the results are illustrated in Figure 72. Here the scale of y axis has been adjusted to better distinguish between particular deviations from the mean attenuation value and to compare both optical splitter designs. Figure 72 clearly proves that the non-uniformity has been significantly improved when we used the low-loss length-optimized 1x64 optical splitter with $(5.5 \times 5.5) \mu\text{m}^2$ waveguide core size. This is very beneficial especially for PONs with triple-play services as the provider can offer similar signal quality and therefore it can maintain more efficiently the same Service Level Agreement (SLA) for each of the customers.

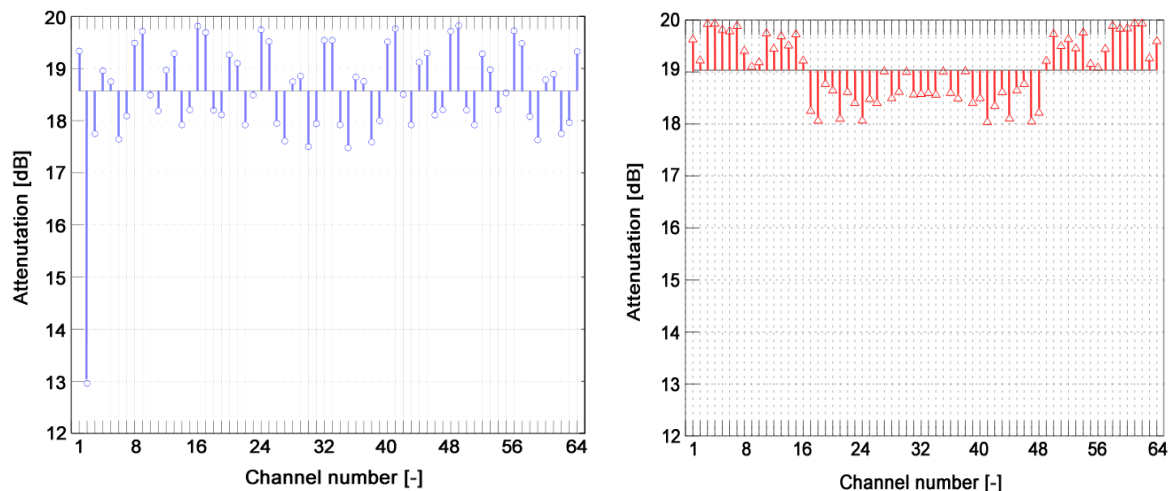


Figure 72: Attenuation and deviation from the mean value for each of the output ports for both: conventional (blue circle-left) and low-loss length-optimized (red triangle-right) 1x64 Y-branch splitters.

Figure 73 and 74 show the results on data/voice components when deploying both splitters in GPON and XG-PON scenarios. As the changes didn't concern the video signal, the video service delivery remained the same under acceptable thresholds in both cases, hence it is not taken into account for comparison. The minimum and maximum reached values of Q -factor and BER are displayed with the blue and red dashed lines. GPON traffic runs at 2.5 Gbps

data/voice stream and the splitting non-uniformity enhancement was just slightly improved, as all the BER values were too low (respectively Q -factor too high) at the receivers.

As a result, small changes in attenuation of splitter's output ports were not noticeably influencing the overall service quality to end users. The minimum and maximum achieved BER values were differing by a factor of 10^6 when the standard splitter was used, and by a factor of 10^5 in case of the optimized splitter. For the higher speed rates as those in XG-PON and above 10 Gbps, the optical signal quality significantly decreases if the other network parameters are not properly tuned.

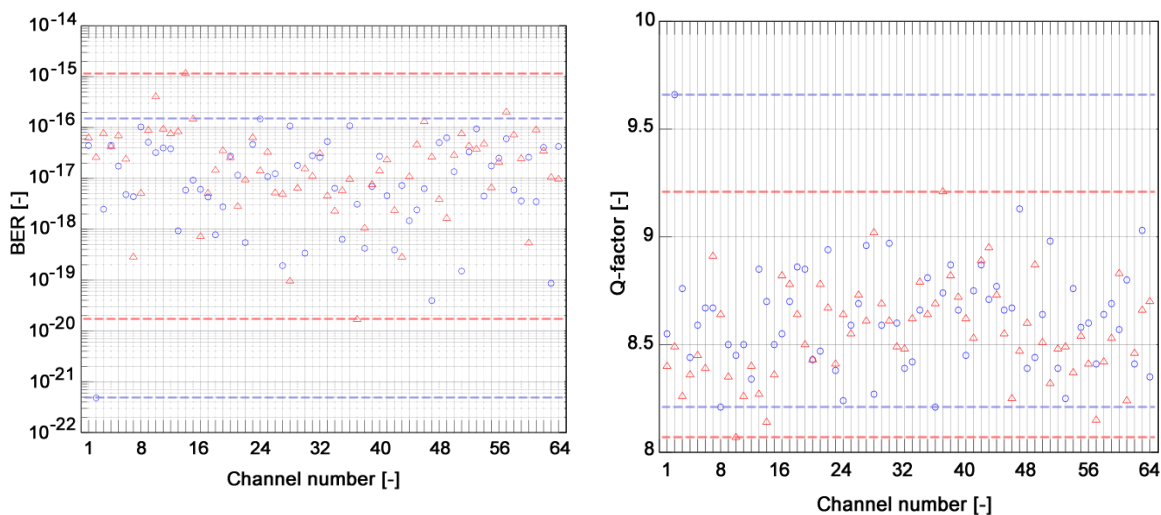


Figure 73: BER (left) and Q-factor (right) values for GPON with triple-play services (blue circles-standard splitter; red triangles-optimized splitter).

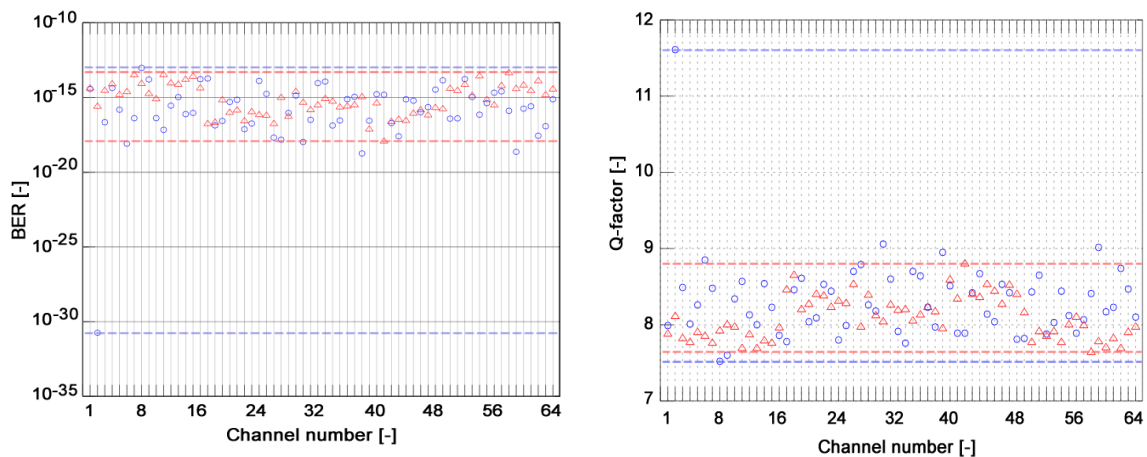


Figure 74: BER (left) and Q-factor (right) values for XG-GPON with triple-play services (blue circles-standard splitter; red triangles-optimized splitter).

From Figure 74 it can be seen that the minimum and maximum obtained BER values in XG-PON scenario differ by a factor of 10^{17} in case of the standard splitter deployment and by only 10^4 when the optimized optical splitter is deployed in the network. Therefore, the power split over all output ports becomes a more crucial parameter to maintain similar customer SLAs.

Conclusion: With the proposed “low-loss length-optimized” 1x64 Y-branch optical splitter with a $(5.5 \times 5.5) \mu\text{m}^2$ waveguide core size, which suppressed the presence of the first mode and in this way it is reduced the non-uniformity of the power split compared to standard (6 x 6)

μm^2 waveguide core size splitter. In this way it is possible to optimize the signal distribution in access network using WDM technique. For comparison purposes, we selected GPON and XG—PON with triple-play services. I showed that the length-optimized splitter with $(5.5 \times 5.5) \mu\text{m}^2$ waveguide core achieved better rates like 10 Gbit/s (XG_PON), and they could eventually provide with the improvement of the overall system performance, whereas maintaining the same implementation and operational costs.

4.6 Simulation Results of Silicon Nitride Based 1x8 Y-Branch Splitter

The simulations of silicon nitride based 1x8 Y-branch splitter were performed by BeamPROP™ tool from RSoft, applying BPM. The splitter was simulated at $\lambda = 850 \text{ nm}$ for both polarizations. Figure 73 depicts the top view of the simulation of the optical beam propagation in the designed structure. Figure 74-left presents the optical power simulated in each output waveguide for TE polarization and Figure 75-left for TM polarization.

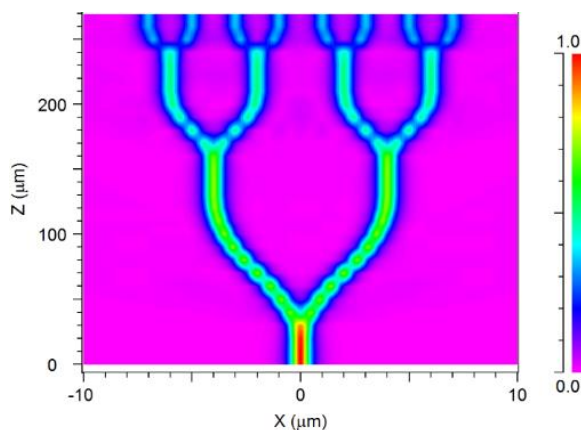


Figure 75: The simulation of the optical beam propagation in the silicon nitride based 1x8 Y-branch splitter.

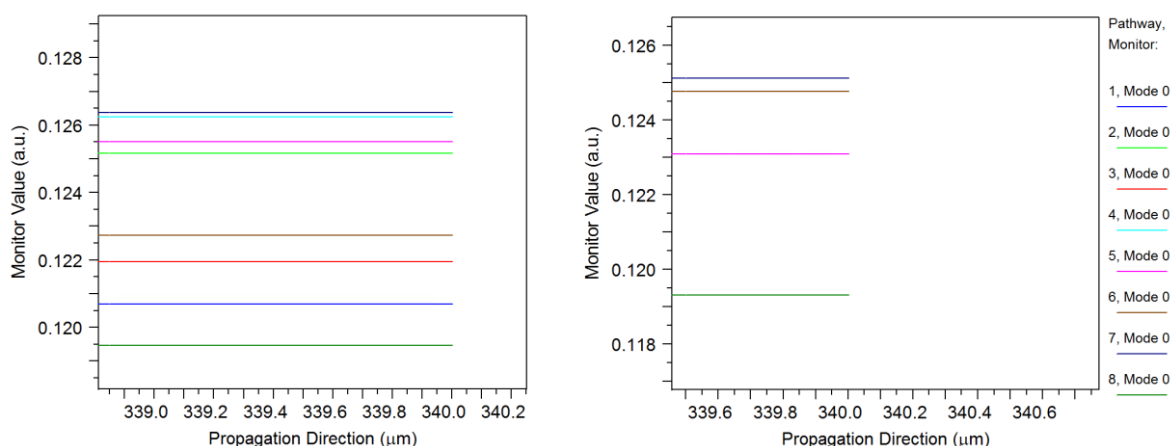


Figure 76: The optical power in each output waveguide simulated for TE (left) and TM (right) polarization.

Table 20 summarizes the optical power from each output waveguide taken from Figure 74 and calculated insertion losses (IL) for both polarizations, namely $IL = 9.143 \text{ dB}$ (the worst case

considering both polarizations). Finally, the insertion loss uniformity, ILu is calculated. Insertion loss uniformity reached $ILu = 0.19$ dB. Simulations also show that the TE polarization features lower losses and more uniform splitting compared to the TM polarization.

Table 21: Output power from Figure 74 together with calculated insertion loss, IL and non-uniformity, ILu for both polarizations.

Output waveguide	Output power [a.u.]	IL [dB]	Output power [a.u.]	IL [dB]
1	0.124	9.059	0.121	9.143
2	0.126	8.965	0.127	8.952
3	0.128	8.906	0.126	8.965
4	0.125	9.010	0.121	9.141
5	0.125	9.010	0.121	9.141
6	0.128	8.906	0.126	8.965
7	0.126	8.965	0.127	8.952
8	0.124	9.059	0.121	9.143
Min IL		8.906		8.952
Max IL		9.059		9.143
Non-uniformity, ILu		0.153		0.190

5 Conclusions

The main goal of this thesis was the modelling and optimization of photonic structures with focus on the design and simulation of high splitting ratio Y-branch splitters used in telecommunication for optical transmission systems. To reach this, the design, simulation and optimization of SoS based high splitting ratio $1 \times N$ Y-branch passive optical splitters ($N \geq 16$) was performed.

In the first step, the SoS based waveguide structure was designed and consequently used to design a “standard” low splitting ratio 1×4 and 1×8 Y-branch and MMI splitters. All these splitters were simulated by commercially available software tools as OptiBPM and Apollo Photonics.

Based on the simulation results, the optical properties of designed “standard” 1×8 splitters were analysed. As expected, the Y-branch splitters feature much higher non-uniformity, higher insertion loss and a large size compared to MMI splitters.

Deep analysis of the achieved results shown that the optical properties of “standard” Y-branch optical splitters depend strongly on the used waveguide structure and that the main reason for such a high non-uniformity is the presence of the first mode (besides the zero mode) propagating in the standard $(6 \times 6) \mu\text{m}^2$ waveguide. To suppress this influence the waveguide core size was reduced to $(5.5 \times 5.5) \mu\text{m}^2$ and to $(5 \times 5) \mu\text{m}^2$. From the simulations is evident that keeping the same layout and decreasing the waveguide core size from $(6 \times 6) \mu\text{m}^2$ to $(5.5 \times 5.5) \mu\text{m}^2$, the non-uniformity of 1×8 Y-branch splitter was reduced from 1.41 dB (for the waveguide core size of $(6 \times 6) \mu\text{m}^2$) to 0.73 dB (for the waveguide core size of $(5.5 \times 5.5) \mu\text{m}^2$), i.e. nearly to the half of its original value. The optical properties of 1×8 MMI splitter were also slightly improved (objective 1).

The knowledge gained from the design and simulation of SoS based low splitting ratio 1×8 optical splitters provided the required theoretical background to realize the “standard” high splitting ratio Y-branch splitter designs, simulations and optimizations. As a first, 1×16 Y-branch and MMI splitters were designed, simulated and optimized. The results again confirm the positive influence of the waveguide core size $(5.5 \times 5.5) \mu\text{m}^2$ on the optical properties of particularly Y-branch splitters, i.e. the non-uniformity was strongly reduced from $ILu = 1.77$ dB for $(6 \times 6) \mu\text{m}^2$ to $ILu = 0.89$ dB, that is less than one half of its original value (objective 1).

To design these optical components a standard commercially available optical software tools, OptiBPM (2D) and RSoft (3D) were used. From the simulations of standard high splitting ratio 1×32 Y-branch splitters is clear that increasing the number of output waveguides leads to a strong degradation of splitting parameters as well as to a huge increase in the length of the structure. Therefore, these splitters were optimized according to waveguide structure and the size. With this optimization, I was able to reach symmetric splitting ratio, ensuring good uniformity over all the output signals. As example, optimizing the waveguide core size led again to strong improvement of the splitting parameters of the 1×32 Y-branch structure, namely the insertion loss, IL from -16.44 dB (“standard” structure) to -15.33 dB (“optimized” structure) and the non-uniformity, ILu from 2.15 dB (“standard” structure) to 0.26 dB (“optimized” struc-

ture), which is nearly one tenth of the original value. Additionally, the proposed length optimization led to the length reduction of the “standard” splitter (150000 μm) almost to the half of the original value (“further length-optimized” splitter, 86000 μm). It is also important to point out that the further reduction of the waveguide core size to (5 x 5) μm^2 did not bring any significant improvement of the parameters compared to “length-optimized” splitter having core size (5.5 x 5.5) μm^2 . From the results can also be concluded that better simulation results were obtained in 3D environment with RSoft software tool (objective 2).

Based on the know-how gained from the design and simulation of “standard” 1x32 Y-branch splitter together with its optimization, the “low-loss high-uniformity” 1x64 Y-branch splitter was designed. The length of this 1x64 Y-branch splitter was reduced from 320000 μm to 120000 μm , i.e. to nearly one third of its original value. In spite of that, this low-loss length-optimized” splitter with (5.5x5.5) μm^2 waveguide core size reached better values of the non-uniformity (ILu was reduced from 2.67 dB to 1.98 dB) compared to a “standard” 1x64 Y-branch splitter with the waveguide core size (6x6) μm^2 (objective 2).

The design of “low-loss length-optimized” 1x64 Y-branch splitter together with “standard” 1x64 Y-branch splitter were used in access network as for example GPON and XG-PON by ITU-T with triple-play services and the achieved splitting parameters were incorporated in the simulations of particular passive optical network scenarios. The simulations results with “OptiSim” environment using Time Domain Split Step Method in case of “low-loss length-optimized” splitter achieved better results in terms of BER, Q-factor, especially for high speed rates like 10 Gbps for XG-PON compared to “standard” 1x64 splitter. In this case, they could eventually provide with the improvement of overall system performance, whereas maintaining the same implementation and operational costs (objective 3).

For the further improvement of optical properties of high splitting ratio Y-branch splitters also the shape of used waveguides was optimized. To this purpose, a new shape of the Y-branch splitter was designed to suppress the scattering of the light in the waveguide structure. This has led to the great improvement of the optical properties, particularly the non-uniformity was additionally improved by 2 dB and the background crosstalk was also additionally reduced by astonishing more than 5 dB.

The waveguide core of the “new shape” Y-branch splitter was optimized and in this way the non-uniformity, ILu and insertion loss, IL were improved by 2.41 dB and 2.28 dB and background crosstalk, BX was improved by astonishing 8 dB (objective 4, objective 5 and objective 6). To our best knowledge, such as low background crosstalk was not yet presented.

The high index contrast silicon nitride based 1x8 Y-branch splitter with shallow rib waveguide structure was designed, simulated and optimized using RSoft, for both polarizations. Here the calculated insertion loss uniformity showed that the TE polarization features lower losses and more uniform splitting compared to the TM polarization (objective 7).

Bibliography

- [1] X. Yu, G. Xiao, T-H. Cheng, "Influence of link cost and routing methods on dynamic multicasting in overlay IP/MPLS over WDM networks", 14th International Conference on Optical Communications and Networks (ICO CN), August 2015, **DOI:** [10.1109/ICO CN.2015.7203687](https://doi.org/10.1109/ICO CN.2015.7203687).
- [2] S. Tao, B. Yang, H. Xia, H. Wang, G. Q. Lo, "An Optical Power Splitter With Variable Power Splitting Ratio", IEEE Photonics Technology Letters, vol. 23, Issue 14, Mai 2011, **DOI:** [10.1109/LPT.2011.2150209](https://doi.org/10.1109/LPT.2011.2150209).
- [3] K. Voigt, L. Zimmermann, G. Winzer, K. Petermann, C. M. Weinert, "Silicon-on-insulator 90° optical hybrid using 4x4 waveguide couplers with C-band operation", Proc. ECOC'08, TU3C5, 2008.
- [4] M. Bachmann, M. K. Smith, P. A. Besse, E. Gini, H. Melchior and L. B. Soldano, "Polarization-insensitive low-voltage optical waveguide switch using InGaAsP/InP four-port Mach-Zender interferometer", in Tech. Dig. OFC/IOOC'93, San Jose, CA, pp. 32-33, 1993.
- [5] T. Rasmussen, J. K. Rasmussen, and J. H. Povlsen, "Design and performance evaluation of 1-by-64 multimode interference power splitter for optical communications", Journal of Lightwave Technology, vol. 13, Issue 10, pp. 2069-2074, 1995.
- [6] S. Romero-Garcia, F. Merget, F. Zhong, H. Finkelstein, J. Witzens, "Silicon nitride CMOS-compatible platform for integrated photonics applications at visible wavelengths", Optics Express, vol.21, Issue 12, pp. 14036-14046, 2013, **DOI:** <https://doi.org/10.1364/OE.21.014036>.
- [7] O. Bryngdahl, "Image formation using self-imaging techniques", Journal of Optical Society of America, 63 (4), April 1973, **DOI:** [10.1364/JOSA.63.000416](https://doi.org/10.1364/JOSA.63.000416).
- [8] Optiwave Systems Inc., <https://optiwave.com/> [accessed November 2018].
- [9] Apollo Photonics, Inc., [http:// www.apollophoton.com](http://www.apollophoton.com) [accessed December 2018].
- [10] Synopsys, <https://www.synopsys.com/> [accessed November 2018].
- [11] A. Katara, A. Bapat, A. Selokar, R. Chalse, "Hybrid Optical Wireless Access Networks", 5th International Conference and Computational Intelligence and Communication Networks, November 2013, **DOI:** [10.1109/CICN.2013.41](https://doi.org/10.1109/CICN.2013.41).
- [12] R. Agalliu, M. Lucki, "Transmission Transparency and Potential Convergence of Optical Network Solutions at the Physical Layer for Bit Rates from 2.5 Gbps to 256 Gbps", Advances in Electrical and Electronic Engineering, 2017, **DOI:** 10.15598/aeec.v15i5.2502.
- [13] ITU-T Recommendation G.982, "Optical access networks to support services up to the ISDN primary rate or equivalent bit rates", available from <http://www.itu.int/rec/T-REC-G.982-199611-I/en> , November 1996.
- [14] E. Bonsma, N. Karunatilake, R. Shipman, M. Shackleton, and D. Mortimore, "Evolving Greenfield Passive Optical Networks", BT Technology Journal, vol. 21, no. 4, 2003.

- [15] J. Li and G. Shen, "Cost Minimization Planning for Greenfield Passive Optical Networks", *Journal of Optical Communications and Networking*, vol. 1, no. 1, pp. 17-29, 2009.
- [16] S. Pato, J. Santos, J. Pedro, P. Monteiro and H. Silva, "On supporting radio over fiber and passive optical network systems with a common fiber plant: Compatibility aspects", *IEEE Conference*, January 2011, **DOI:** [10.1109/ICTON.2008.4598633](https://doi.org/10.1109/ICTON.2008.4598633).
- [17] K. Grobe and J.P. Elbers, "PON Evolution from TDMA to WDM-PON", *Optical Fiber communication/National Fiber Optic Engineers Conference*, San Diego: IEEE, 2008 pp. 1-7. ISBN 978-1-55752-856-8. **DOI:** [10.1109/OFC.2008.4528293](https://doi.org/10.1109/OFC.2008.4528293).
- [18] S. Chatzi and I. Tomkos, "Techno-economic study of high-splitting ratio PONs and comparison with conventional FTTH-PONs/FTTH-P2P/FTTB and FTTC deployments", *IEEE 2011 Optical Fiber Communication Conference and Exposition and the National Fiber Optic Engineers Conference*, June 2011.
- [19] R. P. Davey, P. Healey, I. Hope, P. Watkinson, D. B. Payne, O. Marmur, J. Ruhmann and Y. Zuiderveld, "DWDM reach extension of a GPON to 135 km", *Journal of Lightwave Technology*, vol. 24, Issue 1, pp. 29-31, January 2006.
- [20] K. Sumanpreet and S. Dewra, "A review on Gigabit Passive Optical Network (GPON)", *International Journal of Advanced Research in Computer and Communication Engineering*, vol. 3, Issue 3, March 2014.
- [21] "10-Gigabit-capable Passive Optical Networks (XG-PON): Physical Media Dependent (PDM) Layer Specification", ITU-T G.987.2, 2010.
- [22] X. Yu, T. Braidwood Gibbon, R. Rodes, T.T. Pham and I. T. Monroy, "System Wide Implementation of Photonically Generated Impulse Radio Ultra-Wideband for Gigabit Fiber-Wireless Access" *Journal of Lightwave Technology*, vol. 31, Issue 2 pp. 264-274, 15 January 2013.
- [23] ITU-T Recommendation G.984.1. "Gigabit-capable passive optical networks (GPON): General characteristics", Geneva: ITU-T, 2008.
- [24] N. Kumar, "Improved performance analysis of Gigabit passive optical networks" *Journal of Optic*, pp. 1-4, September 2013.
- [25] C. Lam, "Passive Optical Network Principles and Practice" Academic press, 2011.
- [26] M. P. McGarry, M. Maier, M. Reisslein, "A survey of dynamic bandwidth allocation (DBA) algorithms", *IEEE Communications Magazine*, vol. 42, September 2013.
- [27] M. P. McGarry, M. Reisslein, M. Maier, "Ethernet passive optical network architectures and dynamic bandwidth allocation algorithms", *IEEE Communications Surveys & Tutorials*, vol. 10, Issue 3, 16 September 2008, **DOI:** [10.1109/COMST.2008.4625804](https://doi.org/10.1109/COMST.2008.4625804).
- [28] K. M. Sivalingam and S. Subramanian, "Emerging Optical Network Technology; Architecture, Protocols, and Performance", Springer Science+Business Media, Inc., New York, 2005.

- [29] ITU-T Recommendation G.987.1. "10-Gigabit-capable passive optical networks (XG-PON): General characteristics", Geneva: ITU-T, 2010.
- [30] D. Müllerova, D. Korček, M. Dado, "On wavelength blocking for XG-PON coexistence with GPON and WDM-PON networks", 14th International Conference on Transparent Optical Networks (ICTON), July 2012, **DOI:** [10.1109/ICTON.2012.6253748](https://doi.org/10.1109/ICTON.2012.6253748).
- [31] J. Latal, P. Koudelka, P. Siska, J. Vitasek and V. Vasinek, "WDM_PON network simulation with different implementation of optical amplifier in the line." In: Novel Optical Systems Design and Optimization XVII. San Diego: SPIE, 2014, pp. 1-16. ISBN 978-1-62841-220-8.
- [32] ITU-T Recommendation G.984.7. "Gigabit-capable passive optical networks (G-PON): Long reach", Geneva: ITU-T, 2010.
- [33] S. A. Huda and M. Gregory, "The next generation of passive optical networks: A review." Journal of Network and Computer Applications, vol.67, pp.53-74, **DOI:** [10.1016/j.jnca.2016.02.015](https://doi.org/10.1016/j.jnca.2016.02.015).
- [34] E. Harstead, D. V. Veen and P. Vetter, "Technologies for NGPON2: Why I think 40G TDM PON (XLG-PON) is the clear winner", in Proc. Opt. Fiber Comm. Conf/Nat. Fiber Opt Eng. Conf. Workshop, 2012.
- [35] C. Ling, S. Dahlfort and D. Hood, "Evolution of PON: 10 GPON and WDM PON", Communications and Photonics Conf., pp.709, Shanghai, 2010.
- [36] C.C. Chi, C.W. Tarn, H.M. Lin and H.L. Lin G., "Cost-effective and monitoring-active technique for TDM-passive optical networks," in Optical Fiber Technology, vol. 20, Issue 4, pp. 434-441, August 2014.
- [37] P. J. Urban and S. Dahlfort, "Cost-effective remote PON monitoring based on OTDR measurement and OTM functionality" 13th International Conference on Transparent Optical Networks, Stockholm, Sweden, 01 August 2011, **DOI:** [10.1109/ICTON.2011.5970975](https://doi.org/10.1109/ICTON.2011.5970975).
- [38] K. Satyanarayana and B. Abhinov, "Recent trends in future proof fiber access passive networks: GPON and WDM PON", International Conference on Recent Trends in Information Technology, December 2012, **DOI:** [10.1109/ICRTIT.2014.6996129](https://doi.org/10.1109/ICRTIT.2014.6996129).
- [39] A. Valenti, F. Matera, D. Del Buono, G.M. Tosi Beleffi, "Energy impact of the future fibre optics access networks: Economic perspectives", Fotonica AEIT Italian Conference on Photonics Technologies, November 2015, **DOI:** [10.1049/cp.2015.0115](https://doi.org/10.1049/cp.2015.0115).
- [40] A. Ouali, K. F. Poon, B. S. Lee, K. A. Romaihi, "Towards achieving practical GPON FTTH designs", IEEE 20th International Workshop on Computer Aided Modelling and Design of Communication Links and Networks (CAMAD), January 2016.
- [41] FTTH Handbook, Fibre to the Home, February 2014.
- [42] A. Bley, I. Ljubic and O. Maurer, "Lagrangian decomposition for the two-level FTTx network design problem", EURO Journal on Computational Optimization, vol. 1(3-4), pp. 221-252, 2013.

- [43] M. Zotkiewicz, M. Mycek, "Impact of demand uncertainty models on FTTH network design", 18th International Conference on Transparent Optical Networks (ICTON), August 2016, **DOI:** [10.1109/ICTON.2016.7550445](https://doi.org/10.1109/ICTON.2016.7550445).
- [44] FTTH Conference 2018: Europe sees 20% growth in fibre subscribers <https://www.fibre-systems.com/news/ftth-conference-2018-europe-sees-20-growth-fibre-subscribers>.
- [45] H. Kanamori, "Passive Optical Components and Their Applications to FTTH Networks", SEI Tech. Rev. 73, 2011, pp. 14-21.
- [46] E. Harstead, "Future bandwidth demand favours TDM PON, not WDM PON", Optical Fiber Communication Conference/National Fiber Optic Engineers Conference, 2011, **DOI:** <https://doi.org/10.1364/NFOEC.2011.NTuB7>.
- [47] FTTH Council Europe, https://www.ftthcouncil.eu/.../FTTH_introduction_whatisit_2016.
- [48] L. Chinlon, "Broadband Optical Access Networks and Fiber-to-the-Home", Wiley, 2006.
- [49] R. Jirachariyakool, N. Sraium, S. Lerkvaranyu, "Design and implement of GPON-FTTH network for residential condominium", 14th International Joint Conference on Computer Science and Software Engineering (JCSSE), September 2017, **DOI:** [10.1109/JCSSE.2017.8025942](https://doi.org/10.1109/JCSSE.2017.8025942).
- [50] K. Hadjadj, A. Djouama, F. Y. Ettoumi, "Point-to-point FTTH supervision using geographic information system tool", 8th International Conference on Modelling, Identification and Control (ICMIC), November 2016, **DOI:** [10.1109/ICMIC.2016.7804290](https://doi.org/10.1109/ICMIC.2016.7804290).
- [51] A. Z. G. Zahid, F. N Hasoon, H. Bakarman, S. Shaari, "Implementing EDW in Point to multipoint optical access network for FTTH applications", IEEE 9th Malaysia International Conference on Communication (MICC), March 2010, **DOI:** [10.1109/MICC.2009.5431533](https://doi.org/10.1109/MICC.2009.5431533).
- [52] K. Wang, C. Masmachuca, L. Wosinska, P. J Urban, A. Gavler, K. Brunnstrom, J. Chen, "Techno-economic analysis of active optical network migration toward next-generation optical access", IEEE/OSA Journal of Optical Communications and Networking, vol. 9, Issue 44, April 2017, **DOI:** [10.1364/JOCN.9.000327](https://doi.org/10.1364/JOCN.9.000327).
- [53] T. Rokkas, I. Neokosmidis, D. Katsianis, D. Varoutas, "Cost Analysis of WDM and TDM Fiber-to-the-Home (FTTH) Networks: A System-of-Systems Approach", IEEE Transactions on Systems, Man, and Cybernetics, Part C (Applications and Reviews), vol. 42, Issue: 6, December 2012, **DOI:** [10.1109/TSMCC.2012.2227999](https://doi.org/10.1109/TSMCC.2012.2227999).
- [54] M. Chardy, M-C. Costa, A. Faye and M. Trampont, "Optimizing splitter and fiber location in a multilevel optical FTTH network", European Journal of Operational Research, vol. 222, pp. 430-440, 2012.
- [55] C. Hervet and M. Chardy, "Passive optical network design under operation administration and maintenance consideration", Journal of Applied Operational Research, vol. 222(3), pp. 152-172, 2012.

- [56] J. Li and G. Shen, "Cost minimization planning for greenfield passive optical networks", *Journal of Optical Communication and Networking*, vol. 1(1), pp. 17-29, 2009.
- [57] A. Mitsenkov, G. Paksy and T. Cinkler, "Geography- and infrastructure aware topology design methodology for broadband access networks (FTTx)", *Photonic Network Communications*, vol. 9(21), pp. 253-266, 2011.
- [58] M. Van der Wee, C. K. Bauters, S. Verbrugge, D. Colle, M. Pickavet, "A modular and hierarchically structured techno-economic model for FTTH deployments", 16th international conference on Optical networking Design and Modelling, Proceedings 2012, New York, NY, USA, 17-20 April 2012.
- [59] H. S. Felix, A. M. O. Duarte, "FTTH-GPON access networks: Dimensioning and optimization", 21st Telecommunications Forum Telfor (TELFOR), November 2014,
DOI: [10.1109/TELFOR.2013.6716198](https://doi.org/10.1109/TELFOR.2013.6716198)
- [60] M. Zotkiewicz, M. Mycek and A. Tomaszewski, "Profitable areas in large-scale FTTH network optimization", *Telecommunication Systems*, vol. 61(3), pp. 591-608, 2016.
- [61] A. Eira, J. Pedro and J. Pires, "Optimized Design of Multistage Passive Optical Networks", *IEEE/OSA Journal of Optical Communications and Networking*, vol. 4, no. 5, pp. 402-411, May 2012.
- [62] O. Kipouridis, C. Machuca, A. Autenrieth and K. Grobe, "Streetaware infrastructure planning tool for the next generation optical access networks", in *Optical Network Design and Modelling (ONDM)*, 16th International Conference on, pp. 1-6, April 2012.
- [63] M. Chardy, M. C. Costa, A. Faye and M. Trampont, "Optimizing splitter and fiber location in a multilevel optical FTTH network", *European Journal of Operational Research*, vol. 222, no.3, pp. 430-440, 2012.
- [64] S. P. V. Loggerenberg, M. J. Grobler and S. E. Terblanche, "Optimizing of PON planning for FTTH deployment with fiber duct sharing", in *International Network Optimization Conference (INOC)*, 2013.
- [65] OpenStreetMap, 2015. Available: <https://www.openstreetmap.org/#map=7/47.714/13.349>
- [66] T. Ivaniga, J. Ruzbarsky, L. Ovsenik and J. Turan, "Optical Networks FTTH and Reduced Attenuation Balance with Passive Optical Splitter", *Carpathian Journal of Electronic & Computer Engineering*, vol. 7 Issue 1, pp. 30-35, 2014.
- [67] P. Lafata, "Optimization of asymmetric passive optical splitters", *International Conference on Applied Electronics*, Pilsen, Czech Republic, 5-7 September 2012.
- [68] E. Radius, "Fiber to the home technology", OS3 Fiber Day, May 22, 2013, The Netherlands, Available on internet: https://www.os3.nl/_media/2012-2013/courses/an/sne_lecture_2013_erikradius.pdf
- [69] L. Wang, Y. Wu, J. Zhang, J. Wang, J. Li, H. Wang, X. Zhang, P. Pan, F. Zhong, Q. Zha, X. Hu and D. Zhao, "Design and Fabrication of Novel Symmetric Low-Loss 1x24 Optical

- Power Splitter”, *Journal of Lightwave Technology*, vol. 32, no. 18, pp. 3112-3118, July 2014, DOI: [10.1109/JLT.2014.2337301](https://doi.org/10.1109/JLT.2014.2337301).
- [70] K. Y-Lee, “An Interesting Characteristic of Designing n-fold SOI-MMI Splitter”, 2010 Symposium on Photonics and Optoelectronics, July 2010, DOI: [10.1109/SOPO.2010.5504402](https://doi.org/10.1109/SOPO.2010.5504402).
- [71] H. Hirota, Y. Kawano, M. Shimpo, K. Noto, N. Honda, T. Manabe, “Novel test light injection tool for fiber identification below an optical splitter in a PON”, 18th OptoElectronics and Communications Conference held jointly with 2013 International Conference on Photonics in Switching (OECC/PS), Kyoto, Japan, September 2013.
- [72] N. Araki, T. Yamane and H. Fujimoto, “A new optical fiber line testing function for service construction work that checks for optical filters below an optical splitter in a PON”, Conference on Optical Fiber Communication (OFC/NFOEC), collocated National Fiber Optic Engineers Conference, May 2010, DOI: <https://doi.org/10.1364/NFOEC.2010.NMC5>.
- [73] K. Grobe, J. P. Elbers, “PON Evolution from TDMA to WDM-PON”, Conference on Optical Fiber communication/National Fiber Optic Engineers (OFC/NFOEC), pp. 1-7, February 2008, DOI: [10.1109/OFC.2008.4528293](https://doi.org/10.1109/OFC.2008.4528293).
- [74] E. Wong, “Next-Generation Broadband Access Networks and Technologies”, in *Journal of Lightwave Technology*, vol. 30, Issue 4, pp. 597-608, 2012, DOI: [10.1109/JLT.2011.2177960](https://doi.org/10.1109/JLT.2011.2177960).
- [75] J. Segarra, V. Sales, V. Polo, J. Prat, “Dimensioning OLT Architectures for UDWDM-PONs Employing Coherent Transceivers”, 17th International Conference on Transparent Optical Networks (ICTON), pp. 1-6, August 2015, DOI: [10.1109/ICTON.2015.7193367](https://doi.org/10.1109/ICTON.2015.7193367).
- [76] J. Prat, I. Cano, M. Presi, I. Tomkos, D. Klondis, G. Vallosera, R. Brenot, R. Pous, G. Papastergiou, A. Rafel, E. Ciaramella, “Technologies for Cost-Effective WDM-PONs”, *Journal of Lightwave Technology*, vol. 34, no. 2, pp. 783-791, January 2016, DOI: [10.1109/JLT.2015.2499381](https://doi.org/10.1109/JLT.2015.2499381).
- [77] S. Varghese, “Fabrication and Characterization of All-Fiber Components for Optical Access Networks”, International School of Photonics Cochin University of Science and Technology, Cochin, 682022, Kerla, India, December 2008.
- [78] S. Tao, Q. Fang, J. F. Song, M. B. Yu, G. Q. Lo and D.L. Kwong, “Cascade wide-angle Y-junction 1x16 optical power splitter based on silicon wire waveguides on silicon-on-insulator”, In *Optics express*, 2008.
- [79] V. A. Amorim, J. M. Maia, D. Alexandre, P. V. S. Marques, “Optimization of Broadband Y-Junction Splitters in Fused Silica by Femtosecond Laser Writing”, *IEEE Photonics Technology Letters*, vol. 29, Issue 7, March 2017, DOI: [10.1109/LPT.2017.2675858](https://doi.org/10.1109/LPT.2017.2675858).
- [80] G. Fan, Y. Li and B. Han, “A Wide Wavelength Range of 1x8 Optical Power splitter With an Imbalance of Less Than ± 1.0 dB on Silicon-on-Insulator Technology”, In *IEEE Photonics Journal*, October 2017, DOI: [10.1109/JPHOT.2017.2762353](https://doi.org/10.1109/JPHOT.2017.2762353).

- [81] T. M. Morgado, C. Pinho, B. Neto, F. Rodrigues and A. Teixeira, "Software Tool to Design MMI Splitters/Couplers for Photonic Integrated Circuits", In 2018 20th International Conference on Optical Networks (ICTON), July 2018, **DOI:** [10.1109/ICTON.2018.8473958](https://doi.org/10.1109/ICTON.2018.8473958).
- [82] K. P. Yap, A. Delage, J. Lapointe, B. Lamontagne, J. H. Schmid and P. Waldron, "Correlation of Scattering Loss, Sidewall Roughness and Waveguide Width in Silicon-On-Insulator (SOI) Ridge Waveguides", Journal of Lightwave Technology, vol. 27, Issue 18, September 2009, **DOI:** [10.1109/JLT.2009.2021562](https://doi.org/10.1109/JLT.2009.2021562).
- [83] D. Seyringer, "Arrayed Waveguide Gratings", SPIE. Digital Library, 2016, vol. SL16, **DOI:** <https://doi.org/10.1117/3.2242852>.
- [84] D. Seyringer, C. Burtscher, S. Partel, J. Etlinger, A. Maese-Novo, P. Muellner, R. Hainberger, J. Kraft, G. Koppitsch, G. Meinhardt, "Design and simulation of Si₃N₄ based arrayed waveguide ratings applying AWG-Parameters tool", 18th International Conference on Transparent Optical Networks (ICTON), August 2016, **DOI:** [10.1109/ICTON.2016.7550586](https://doi.org/10.1109/ICTON.2016.7550586).
- [85] R. Baharom, A. Idris, N. R. Hamzah, M. K. Hamzak, "Computer simulation of single-phase control rectifier using single-phase matrix convertor with reduced switch count", IEEE Applied Power Electronics Colloquium (IAPEC), May 2011, **DOI:** [10.1109/IAPEC.2011.5779848](https://doi.org/10.1109/IAPEC.2011.5779848).
- [86] T. Tanemura, A. Al Amin, Y. Nakano, "Development and field demonstration of an optical burst switching testbed with PLZT optical matrix switch", International Conference on Photonics in Switching, November 2009, **DOI:** [10.1109/PS.2009.5307847](https://doi.org/10.1109/PS.2009.5307847).
- [87] R. Honnugar, S. Talabatulla, "Design and Simulation of an Optical Integrated Passive S-Bend Waveguide Delay Line Phase Shifter", Fourth International Conference on Computational Intelligence, Communication Systems and Networks, July 2012, **DOI:** [10.1109/CICSSyN.2012.32](https://doi.org/10.1109/CICSSyN.2012.32).
- [88] M. Itoh, T. Kominato, M. Abe, M. Itoh, T. Hashimoto, "Low-loss Silica-Based SiO₂-Ta₂O₅ Waveguides With Extremely High Δ Fabricated Using Sputtered Thin Films", Journal of Lightwave Technology, vol.33, Issue 2, January 2015, **DOI:** [10.1109/JLT.2014.2381644](https://doi.org/10.1109/JLT.2014.2381644).
- [89] Y. Wang, J. Wang, C. Sun, B. Xiong, Y. Luo, Z. Hao, Y. Han, L. Wang, H. Li, "A simple fabrication process for SiN_x/SiO₂ waveguide based on sidewall oxidation of patterned silicon substrate", Opto-Electronics and Communications Conference (OECC), December 2015, **DOI:** [10.1109/OECC.2015.7340155](https://doi.org/10.1109/OECC.2015.7340155).
- [90] R. K. Nalakhe, N. Dasgupta, B. K. Das, "Design of Low-Loss Compact 90° Bend Optical Waveguide for Photonic Circuit Applications in SOI Platform", IEEE Region 10 and the Third international Conference on Industrial and Information Systems, March 2009, **DOI:** [10.1109/ICIINFS.2008.4798423](https://doi.org/10.1109/ICIINFS.2008.4798423).

- [91] D. Shimura, T. Horikawa, H. Okayama, S. H. Jeong, M. Tokushima, H. Sasaki, T. Mogami, "High precision Si waveguide devices designed for 1.31 μm and 1.55 μm wavelengths on 300mm-SOI", 11th International Conference on Group IV Photonics (GFP), November 2014, **DOI:** [10.1109/Group4.2014.6962013](https://doi.org/10.1109/Group4.2014.6962013).
- [92] F. Bontempi, S. Faralli, N. Andriolli, G. Contestabile, "An InP Monolithically Integrated Unicast and Multicast Wavelength Converter", IEEE Photonics Technology Letters, vol. 25, Issue 22, September 2013, **DOI:** [10.1109/LPT.2013.2281509](https://doi.org/10.1109/LPT.2013.2281509).
- [93] D. Dai "Silicon Nanophotonic Integrated Devices for On-Chip Multiplexing and Switching", Journal of Lightwave Technology, vol.35, Issue 4, 2016, **DOI:** [10.1109/JLT.2016.2587727](https://doi.org/10.1109/JLT.2016.2587727).
- [94] J. Beals, O. Hadeler, S. M. Morris, T. D. Wilkinson, R. V. Penty, I. H. White, "Electro-optic integration of liquid crystal cladding switch with multimode passive polymer waveguide on PCB", Conference on Lasers and Electro-Optics and 2009 Conference on Quantum electronics and Laser Science Conference, August 2009, **DOI:** [10.1364/CLEO.2009.CFV6](https://doi.org/10.1364/CLEO.2009.CFV6).
- [95] H. Numata, Y. Taira, T. Barwicz, "Low loss polymer waveguide components for silicon packaging", IEEE CPMT Symposium Japan (ICSJ), 2015, **DOI:** [10.1109/ICSJ.2015.7357377](https://doi.org/10.1109/ICSJ.2015.7357377).
- [96] A. Shahpari, S. Ziaie, J. D. Reis, Z. Vujicic, M. Lima, A. Teixeira, "Impact of splitter configuration strategies on power consumption in PON", OptoElectronics and Communications Conference held jointly with International Conference on Photonics in Switching (OECC/PS), pp.1-2, July 2013.
- [97] G. Rentao, L. Xiaoxu, L. Hui, B. Lin, "Evolutional algorithm based cascade long reach passive optical networks planning", China Communications, vol. 10, Issue 4, pp. 59-69, April 2013, **DOI:** [10.1109/CC.2013.6506931](https://doi.org/10.1109/CC.2013.6506931).
- [98] C. Zukowski, D. B. Payne, M. Ruffini, "Optical splitters configuration for long-reach passive optical network deployment", 18th European Conference on Network and Optical Communications (NOC) and 8th Conference on Optical Cabling and Infrastructure (OC&I), pp.185-190, July 2013, **DOI:** [10.1109/NOC-OCI.2013.6582888](https://doi.org/10.1109/NOC-OCI.2013.6582888).
- [99] S. Pal, C. Zukowsky, A. Nagg, D. B. Payne, M. Ruffini, "Cable length minimization in long-reach-PON planning for sparsely populated areas", International Conference on Optical Network Design and Modelling, pp.234-239, May 2014.
- [100] D. Piehler, "Long-reach and High Split Ratio Passive Optical Networks", Asia Optical Fiber Communication and Optoelectronic Exposition and Conference, **DOI:** [10.1364/AOE.2008.FF3](https://doi.org/10.1364/AOE.2008.FF3), November 2008.
- [101] R. Agalliu, C. Burtscher, M. Lucki, D. Seyringer, "Optical splitter design for telecommunication access networks with triple-play services", Journal of Electrical Engineering, vol. 69, No.1, pp. 32-38, 2018.
- [102] P. J. Chiang, C. L. Wu, C. H. Teng, C. S. Yang, H. C. Chang, "Full-Vectorial Optical Waveguide Mode Solvers Using Multidomain Pseudospectral Frequency-Domain

- (PSFD) Formulations”, IEEE Journal of Quantum Electronics, vol. 44, Issue 1, December 2007, DOI: [10.1109/JQE.2007.910454](https://doi.org/10.1109/JQE.2007.910454).
- [103] J. Cordoba-Ramirez, F. Amaya-Fernandez, H. E. Hernandez-Figueroa, H. L. Fragnito, “Beam Propagation Method (BPM) for bend loss analysis in waveguide”, IEEE Colombian Communications Conference (COLCOM), July 2012, DOI: [10.1109/ColComCon.2012.6233667](https://doi.org/10.1109/ColComCon.2012.6233667).
- [104] A. Iguchi, Y. Tsuji, T. Yasui, K. Hirayama, “Topology optimal design of optical waveguides in Consideration of polarization dependence using BPM and AVM”, 2016 Progress in Electromagnetic Research Symposium (PIERS), November 2016, DOI: [10.1109/PIERS.2016.7734788](https://doi.org/10.1109/PIERS.2016.7734788).
- [105] L. R. D. Suresh, S. Sundaravadivelu, R. Prema Latha, “Design of Novel Photonic Antennas for Optical Wireless Communications Using Beam Propagation Method”, First International Conference on Emerging Trends in Engineering and Technology, July 2008, DOI: [10.1109/ICETET.2008.215](https://doi.org/10.1109/ICETET.2008.215).
- [106] H. Nihei, C. P. Chen, T. Anada, Z. Ma, “Time Domain FD-BPM for Calculating Pulse Propagation Properties of MMI Device with Photonic Crystal Structure”, China-Japan Joint Microwave Conference, February 2009, DOI: [10.1109/CJMW.2008.4772364](https://doi.org/10.1109/CJMW.2008.4772364).
- [107] M. Hongthong, T. Angkaew, “The transverse vectorial finite element beam propagation method with rectangular nodal element for optical waveguide analysis”, 12th International Conference on Electrical Engineering/Electronics, Computer, Telecommunications and Information Technology (ECTI-CON), August 2015, DOI: [10.1109/ECTICon.2015.7207003](https://doi.org/10.1109/ECTICon.2015.7207003).
- [108] J. Sharma, R. Sharma, L. K. Dusad, “Review and analysis of photonic crystal beam splitters for optical communication applications”, 2015 International Conference on Green Computing and Internet of Things (ICGClOT), January 2016, DOI: [10.1109/ICGClOT.2015.7380449](https://doi.org/10.1109/ICGClOT.2015.7380449).
- [109] K. Taira, S. Fujino, “An FETD Method for Wave guide Problems”, China-Japan Joint Microwave Conference, February 2009, DOI: [10.1109/CJMW.2008.4772370](https://doi.org/10.1109/CJMW.2008.4772370).
- [110] S. Gedney, “Introduction to the Finite-Difference Time-Domain (FDTD) Method for Electromagnetics”, Publisher: Morgan and Claypool, 2011, Electronic ISBN: 9781608455232, DOI: [10.2200/S00316ED1V01Y201012CEM027](https://doi.org/10.2200/S00316ED1V01Y201012CEM027).
- [111] S. Hada, A. B. M. Rahman, “Rigorous analysis of numerical methods: a comparative study”, Optical and Quantum Electronics, vol. 48, Issue 2, 2016, DOI: [10.1007/s11082-016-0579-x](https://doi.org/10.1007/s11082-016-0579-x).
- [112] W. J. Westerveld, S. M. Leinders, K. W. A. van Dongen, H. P. Urbach, M. You, “Extension of Marcatili’s Analytical Approach for Rectangular Silicon Optical Waveguides”, Journal of Lightwave Technology, vol. 30, Issue 14, July 2012, DOI: [10.1109/JLT.2012.2199464](https://doi.org/10.1109/JLT.2012.2199464).

- [113] S. L. Hada, B .M. A. Rahman, "Rigorous analysis of numerical methods: a comparative study", Optical and Quantum Electronics, June 2016.
- [114] C. Scheiber, A. Schultschik, O. Biro, R. Dyczij-Edlinger, "A model order reduction method for efficient band structure calculations of photonic crystals", Digests of the 14th Biennial IEEE Conference on Electromagnetic Field Computation, 2010, DOI: [10.1109/CEFC.2010.5481828](https://doi.org/10.1109/CEFC.2010.5481828).
- [115] B. M. A. Rahman, A. Agraval, "Finite Element Modelling Methods for Photonics", Artech House, Boston, 2013.
- [116] J. Reitterer, "Numerical Analysis of Optical Multi-Core Waveguides", Master thesis, Wien, June 2010.
- [117] K. Q. Le, P. Bienstman, "Wide-angle beam propagation method without using slowly varying envelope approximation", Journal of the Optical Society of America B, vol.26, Issue 2, February 2009, DOI: [10.1364/JOSAB.26.000353](https://doi.org/10.1364/JOSAB.26.000353).
- [118] L. Du, R. S. Chen, Z. B. Ye, Y. Yang, "A Further Study on the Use of the Alternating-Direction Implicit Scheme for the Finite-Element Time-Domain Method", IEEE Antennas and Wireless Propagation Letters, vol. 8, July 2009, DOI: [10.1109/LAWP.2009.2027342](https://doi.org/10.1109/LAWP.2009.2027342).
- [119] K. Yee, "Hybrid Technique Combining the FDTD Method and Its Convolution Formulation Based on the Discrete Green's Funktion", IEEE Antennas and Wireless Propagation Letters, vol. 12, pp. 1448-1451, November 2013, DOI: [10.1109/LAWP.2013.2288412](https://doi.org/10.1109/LAWP.2013.2288412).
- [120] T. P. Stefanski, "Hybrid Technique Combining the FDTD Method and Its Convolution Formulation Based on the Discrete Green's Function", IEEE Antennas and Wireless Propagation Letters, vol. 12, pp. 1448-1451, November 2013, DOI: [10.1109/LAWP.2013.2288412](https://doi.org/10.1109/LAWP.2013.2288412).
- [121] C. S. Paidimarry, B. P. Kumar, B. P. Kumar, T. A. Reddy, "Study of a parallel plate waveguide using computationally efficient explicit FDTD algorithm", 9th International Symposium on Communication Systems, Networks & Digital Sign (CSNDSP), October 2014, DOI: [10.1109/CSNDSP.2014.6923876](https://doi.org/10.1109/CSNDSP.2014.6923876).
- [122] A. N. Papadimopoulos, N. V. Kantartzis, "High-order stochastic-FDTD schemes for electromagnetic field statistical uncertainties", 18th International Symposium on Electromagnetic Fields in Mechatronics, Electrical and Electronic Engineering (ISEF) Book of Abstracts, November 2017, DOI: [10.1109/ISEF.2017.8090677](https://doi.org/10.1109/ISEF.2017.8090677).
- [123] W. Wei, L. Pei-Guo, Q. Yu-Jian, "A novel unconditional stable FDTD method for the transient analysis of high-speed interconnects within a circuit simulator", ISAPE2012, January 2013, DOI: [10.1109/ISAPE.2012.6408915](https://doi.org/10.1109/ISAPE.2012.6408915).
- [124] A. K. Saxena, K. V. Srivastava, "A Three-Dimensional Unconditionally Stable Five-Step LOD-FDTD Method", IEEE Transactions on Antennas and Propagation, vol. 62, Issue 3, December 2013, DOI: [10.1109/TAP.2013.2293790](https://doi.org/10.1109/TAP.2013.2293790).

- [125] T. Ohtani, Y. Kanai, J. B. Cole, "A Stability Improvement Technique Using PML Condition for the Three-Dimensional Nonuniform Mesh Nonstandard FDTD Method", IEEE Transactions on Magnetics, vol. 49, Issue 5, May 2013, DOI: [10.1109/TMAG.2013.2238613](https://doi.org/10.1109/TMAG.2013.2238613).
- [126] M. Fuji, P. Russer, "A nonlinear and dispersive APML ABC for the FDTD methods", IEEE Microwave and Wireless Components Letters, vol. 12, Issue 11, December 2012, DOI: [10.1109/LMWC.2002.805539](https://doi.org/10.1109/LMWC.2002.805539).
- [127] J. A. Pereda, A. Serroukh, A. Grande, A. Vegas, "Implementation of Absorbing Boundary Conditions Based on the Second-Order One-Way Wave Equation in the LOD-and the ADI-FDTD Methods", IEEE Antennas and Wireless Propagation Letters, vol. 11, pp. 981-983, August 2012, DOI: [10.1109/LAWP.2012.2212411](https://doi.org/10.1109/LAWP.2012.2212411).
- [128] S. Kirkup, I. Mulla, G. Ndou, J. Yazdani, "Electromagnetic simulation by the FDTD method in Java", MAMECTIS'08 Proceeding of the 10th WSEAS international conference on Mathematical methods, computational techniques and intelligent systems, pp. 370-375, October 2008.
- [129] K. S. Yee, "Numerical solution of initial boundary value problems involving Maxwell's equation in isotropic media", IEEE Trans. Antennas Propagat., vol. AP-14, pp. 302-307, 1966.
- [130] K. Niu, Z. Huang, M. Li, X. Wu, "Optimizing of the Artificially Anisotropic Parameters in WCS-FDTD Method for Reducing Numerical Dispersion", IEEE Transactions on Antennas and Propagation, vol. 65, Issue 12, October 2017, DOI: [10.1109/TAP.2017.2758844](https://doi.org/10.1109/TAP.2017.2758844).
- [131] X. Kuang, Z. Huang, M. Chen, X. Wu, "High-Order Symplectic Compact Finite-Different Time-Domain Algorithm for Guide-Wave Structures", IEEE Microwave and Wireless components Letters, vol. 29, Issue 2, February 2019, DOI: [10.1109/LMWC.2019.2891109](https://doi.org/10.1109/LMWC.2019.2891109).
- [132] S. Yaocheng, "Design Simulation and Characterization of Some Planar Lightwave Circuits", Doctoral Thesis, Stockholm 2008.
- [133] Photeon Technologies, <http://www.photeon.com/>.
- [134] International Laser Centre, Bratislava 81219, Slovak Republic <http://www.istc.int/en/institute/14085>.
- [135] D. Seyringer, "Low loss and high uniformity multimode interference splitter operating in a wide wavelength band", 9th International Conference on Optical Communications and Networks (ICOCN 2010), May 2011, DOI: [10.1049/cp.2010.1231](https://doi.org/10.1049/cp.2010.1231).
- [136] D. Benedikovic, J. Litvik, M. Kuba, M. Dado, J. Dubovan, "Influence of nonlinear effects in WDM system with non-equidistant channel spacing using different types of high-order PSK and QAM modulation formats", Proc. SPIE 8429, Optical Modelling and Design II, June 2012, DOI: [10.1117/12.921836](https://doi.org/10.1117/12.921836).

- [137] J. Latal, P. Koudelka, P. Siska, J. Vitasek, V. Vasinek, "WDM-PON network simulation with different implementation of optical amplifier in the line", Proc. SPIE 9193, Novel Optical Systems Design and Optimization XVII, September 2014, <https://doi.org/10.1117/12.2060112>.
- [138] F. Perecar, O. Marcinka, L. Bednarek, M. Lucki, A. Liner, L. Hajek, M. Papes, J. Jaros, V. Vasinek, "The impact of ageing effects due to radiation burden on optical fiber couplers", Proc. SPIE 9586, Photonic Fiber and Crystal Devices: Advances in Materials and Innovations in Device Applications IX, August 2015, <https://doi.org/10.1117/12.2187517>.
- [139] Telcordia, "Generic Requirements for Passive Optical Components", TR-NWT-001209, Issue 04, September 2010, <https://telecom-info.telcordia.com/site/cgi/ido/docs.cgi?ID=SEARCH&DOCUMENT=GR-1209&>
- [140] I. Yulianti, A. Sahmah, M. Supaat, S. M. Idrus, M. Ridwanto, A. M. Al-hetar, "Low loss 1x2 optical coupler based on cosine S-bend with segmented", International Conference on Enabling Science and Nanotechnology (ESciNano), 2011, DOI: [10.1109/ESCINANO.2010.5701032](https://doi.org/10.1109/ESCINANO.2010.5701032).
- [141] R. W. Purnamaningsih, N. R. Poespawati, T. Abuzairi, S. Rahardjo, M. Hamidah, E. Dogheche, "The effect of waveguide parameters on gan based S-bend Y-junction optical power divider", 15th International Conference on Quality in Research (QiR): International Symposium on Electrical and Computer Engineering, 2017, DOI: [10.1109/QIR.2017.8168510](https://doi.org/10.1109/QIR.2017.8168510).
- [142] P. P. Sahu, "A Double S-Bend Geometry With Lateral Offset for Compact Two Mode Interference Coupler", Journal of Lightwave Technology, vol. 29, Issue 13, 2011, DOI: [10.1109/JLT.2011.2153178](https://doi.org/10.1109/JLT.2011.2153178).
- [143] I. J. Devayani, A. Syahriar, D. Astharini, "Characteristics of S-bend optical waveguides based on back-to-back and sinusoidal structures", International Conference on Electrical Engineering and Computer Science (ICEECS), 2015, DOI: [10.1109/ICEECS.2014.7045221](https://doi.org/10.1109/ICEECS.2014.7045221).
- [144] K. Okamoto, "Progress and technical challenge for planar waveguide devices: silica and silicon waveguides", Laser Photonics, Rev.6, 14-23, 2012.
- [145] S. T., S. Cheung, B. Guan, S. S. Djordjevic, K. Okamoto, S. J. B. Yoo, "Low-loss and high contrast silicon-on-insulator (SOI) arrayed waveguide grating", in Proc. Conf. Lasers Electro-Optics (CLEO), pp. 1-2, 2012, DOI: [10.1364/CLEO_SI.2012.CM4A.5](https://doi.org/10.1364/CLEO_SI.2012.CM4A.5).
- [146] W. Bogaerts, S. K. Selvaraja, P. Dumon, J. Brouckaert, K. De Vos, D. Van Thourhout, R. Baets, "Silicon-on-insulator spectral filters fabricated with CMOS technology" IEEE Journal of Selected Topics in Quantum Electronics, vol. 16, Issue 1, 2010, DOI: [10.1109/JSTQE.2009.2039680](https://doi.org/10.1109/JSTQE.2009.2039680).
- [147] R. W. Chuang, G.S. Wang, M. T. Hsu, "High contrast long-period waveguide gratings on silicon-on-insulator (SOI) substrates", Photonics Global Conference (PGC), 2012, DOI: [10.1109/PGC.2012.6458124](https://doi.org/10.1109/PGC.2012.6458124).

- [148] D. Dai, X. Fu, Y. Shi, S. He, "Experimental demonstration of an ultracompact Si-nanowire-based reflective arrayed-waveguide grating (de)multiplexer with photonic crystal reflectors", *Opt. Lett.*, vol 35, Issue 15, pp. 2594-2596, 2010, <https://doi.org/10.1364/OL.35.002594>.
- [149] F. M. Soares, N. K. Fontaine, R. P. Scott, J. H. Baek, X. Zhou, T. Su, S. Cheung, Y. Wang, C. Junesand, S. Lourudoss, K. Y. Liou, R. A. Hamm, W. Wang, B. Patel, L.A. Gruezke, W. T. Tsang, J. P. Heritage, S. J. B. Yoo, "Monolithically integrated InP wafer-scale 100-channel times 10-GHz AWG and Michelson interferometers for 1-THz-bandwidth optical arbitrary waveform generation", in *Proc. Conf. Optical Fiber Communication, Collocated National Fiber Optic Engineers Conf.*, pp. 1-3, 2010.
- [150] J. Missinne, L. Misseeuw, X. Liu, P. S. Salter, G. V. Steenberge, K. Adesanya, S. V. Vlierberghe, M. J. Booth, P. Dubruel, "Planar polymer waveguides with a graded-index profile resulting from intermixing of methacrylates in closed microchannels", *Optical Materials*, vol. 76, pp. 210-215, 2018, **DOI:** <https://doi.org/10.1016/j.optmat.2017.12.039>.
- [151] Y. Shi, "Design, Simulation and Characterization of Some Planar Lightwave Circuits", Doctoral Thesis in Microelectronics and Applied Physics, Sweden, 2008.
- [152] K. K. Nan, M. M. Shahimin, F. R. M. Adikan, "Optimization of Silicon Nitride Y-Branch Optical Waveguide for Evanescent Field Biosensor", *Advanced Materials Research*, vol. 875-877, pp. 1183-1188, 2014, **DOI:** <https://doi.org/10.4028/www.scientific.net/AMR.875-877.1183>.
- [153] R. Baets, A. Z. Subramanian, S. Clemmen, B. Kuyken, P. Bienstman, N. L. Thomas, G. Roelkens, D. V. Thourhot, P. Helin, S. Severi, "Silicon Photonics:silicon nitride versus silicon on-insulator", *Optical Fiber Communication Conference, In Proceedings of OFC 2016, CA, Th3J.1* (2016).
- [154] P. J. French, P. M. Sarro, R. Mallee, E. J. M. Fakkeldij, R. F. Wolffenbuttel, "Optimization of a low-stress silicon nitride process for surface-miscomachining applications", *Sensors and Actuators*, vol. 58, Issue 2, pp. 149-157, February 1997.
- [155] L. Kohler, Study of the optical properties of passive optical splitters based on MMI and Y-branch approach", Master Thesis, Research center for Microtechnology, Vorarlberg University of Applied Science Austria, Sep. 2012.
- [156] C. Burtscher, M. Lucki, D. Seyringer, "Comparison of optical properties of 1x8 splitters based on Y-branch and MMI approaches", *Romanian Reports in Physics*, vol. 67, Issue 4, pp. 1578-1585, January 2015.
- [157] C. Burtscher and D. Seyringer, "Influence of waveguide structure on Y-branch splitting ratio", *SPIE Photonics Europe 2014, Silicon Photonics and Photonic Integrated Circuits conference IV*, in *Proc. SPIE 9133, Brussels 2014*, **DOI:** [10.1117/12.2050846](https://doi.org/10.1117/12.2050846).
- [158] ITU-T Recommendation G.983.1, "Broadband optical access systems based on Passive Optical Networks (PON)," available from: <<http://www.itu.int/rec/T-REC-G.983.1/en>>, January 2005.

- [159] G. Z. Markovic, "Wavelength Converters Placement in Optical Networks Using Bee Colony Optimization", *Advances in Electrical and Computer Engineering*, vol.16, no.1, pp.3-10, 2016 **DOI:** [10.4316/AECE.2016.01001](https://doi.org/10.4316/AECE.2016.01001).
- [160] F. Perecar, O. Marcinka, L. Bednarek, M. Lucki, A. Liner, L. Hajek, M. Papes, J. Jaros, V. Vasinek, "The impacts of ageing effects due to radiation burden on optical fiber couplers", *Proc. SPIE 9586, Photonic Fiber and Crystal Devices: Advances in Materials and Innovations in Device Applications IX*, 2015. <https://doi.org/10.1117/12.2187517>.
- [161] Gigabit-capable passive optical networks (GPON): General characteristics: The impacts of ageing effects due to radiation burden on optical fiber couplers, in ITU-T Recommendation G.984.1, 2008. [Online]. Available: <https://www.itu.int/rec/T-REC-G.984.1/en>.
- [162] IEEE Standard for Information technology; Telecommunications and information exchange between system; Local and metropolitan area networks; Specific requirements. Part 3: "Carrier Sense Multiple Access with Collision Detection (CSMA/CD) Access Method and Physical Layer Specifications. Amendment: Media Access Control Parameters, Physical Layers, and Management Parameters for Subscriber Access Networks", in IEEE Standard 802.3ah, 2004.
- [163] ITU-T Recommendation G.987.1."10-Gigabit-capable passive optical networks (XG-PON): General requirements", 2010. [Online]. Available: <http://www.itu.int/rec/T-REC-G.987.1/en>.
- [164] RSOFT Design Group, software manuals: OptSim Application Notes and Examples OptSim models reference, 2010.
- [165] L. Wang et al., "Design and Fabrication of Novel Symmetric Low-Loss 1×24 Optical Power Splitter", in *Journal of Lightwave Technology*, vol. 32, no. 18, pp. 3112-3118, 2014, **DOI:** [10.1109/JLT.2014.2337301](https://doi.org/10.1109/JLT.2014.2337301).
- [166] W. Freude, R. Schmogrow, B. Nebendahl, M. Winter, A. Josten, D. Hillerkuss, S. Koenig, J. Meyer, M. Dreschmann, M. Huebner, C. Koos, J. Becker, J. Leuthold, "Quality metrics for optical signals: Eye diagram, Q-factor, OSNR, EVM and BER", in *14th International Conference on Transparent Optical Networks (ICTON)*, pp.1-4, 2012, **DOI:** [10.1109/ICTON.2012.6254380](https://doi.org/10.1109/ICTON.2012.6254380).
- [167] B. Nebendahl, R. Schmogrow, T. Dennis, A. Josten, D. Hillerkuss, S. Koenig, J. Meyer, M. Dreschmann, M. Winter, M. Huebner, W. Freude, C. KOOS, J. Leuthold, "Quality Metrics in optical modulation analysis" *Communications and Photonics Conference (ACP)*, 2012 Asia, Guangzhou, pp. 1-3, 2012. [Online] Available: <http://ieeexplore.ieee.org/stamp/stamp.jsp?tp=&arnumber=6510607&isnumber=6510568>.
- [168] Y. Zhu, D. V. Plant, "Optimal Design of Dispersion Filter for Time-Domain Split-Step Simulation of Pulse Propagation in Optical Fiber", *Journal of Lightwave Technology*, vol. 30, no. 10, pp. 1405-1421, 2012, **DOI:** [10.1109/JLT.2012.2187172](https://doi.org/10.1109/JLT.2012.2187172).
- [169] T. Yipsirimetee, P. Kaewplung, "Optimal dispersion compensation and polarization-mode dispersion compensation in all-optical 40 Gbps-per-channel-based WDM wave-

- length-routed optical fiber networks”, 21st Annual Wireless and Optical Communications Conference (WOCC), Kaohsiung, pp. 158-162, 2012. DOI: [10.1109/WOCC.2012.6198174](https://doi.org/10.1109/WOCC.2012.6198174).
- [170] C. Burtscher, M. Lucki and D. Seyringer, “Comparison of Optical Properties of 1x8 Splitters Based on Y-Branch and MMI Approaches”, Micro- to Nano-Photonics IV- ROMOPTO 2015, September, 2015, Bucharest, Romania (published in Romanian Reports in Physics, Vol. 67, No. 4, P. 1578-1585. ISSN 1221-1451, 2015).
- [171] C. Burtscher, D. Seyringer, M. Lucki, A. Kuzma, “Design and simulation of 1x32 Y-branch splitter applying different photonics tools”, APCOM 2017, 12-14 June 2017, High Tatras, Transka Lomnica, Slovakia.
- [172] C. Burtscher, M. Lucki, D. Seyringer, and A. Kuzma, “Comparison of splitting properties of various 1x16 splitters”, Advanced in Electrical and Electronic Engineering, vol. 15, Issue 1, pp. 107-113, <http://dx.doi.org/10.15598/aeec.v15i1.2014>.
- [173] B. Fischer, B. Hopf, M. Lindner, A. W. Koch, J. Roths, “Verification of three dimensional FEM model for FBGs in PANDA fibers by transversal load experiments”, 25th Optical fiber Sensors Conference (OFS), June 2017, DOI: [10.1117/12.2263262](https://doi.org/10.1117/12.2263262).
- [174] H. J. Lee, F. Abdullah, S. D. Emami, A. Ismail, “Fiber modelling and simulation of effective refractive index for tapered fiber with finite element method”, IEEE 6th International Conference on Photonics (ICP), July 2016, DOI: [10.1109/ICP.2016.7509998](https://doi.org/10.1109/ICP.2016.7509998).
- [175] K. Kato, N. Umemura, K. Miyata, ”High-accuracy Sellmeier equations for LiInS₂ and its applications to the nonlinear optics in LiIn(S_xSe_{1-x})₂”, 2014 International Conference Laser Optics, August 2014, DOI: [10.1109/LO.2014.6886417](https://doi.org/10.1109/LO.2014.6886417).
- [176] B. Joshi, P. Saxena, N. Khara, ”Optical properties of Zinc oxide (ZnO) thin films for applications in optical devices: Matlab simulation”, 3rd International Conference on Computing for Sustainable Global Development (INDIACom), October 2016.
- [177] H. Li, X. Dong, E. Li, Z. Liu, Y. Bai, ”Highly compact 2x2 multimode interference coupler in silicon photonic nanowires for array waveguide grating demodulation integration microsystem”, Optics & Laser Technology, vol. 47, Pages 336-371, April 2013, DOI: [10.1016/j.optlastec.2012.09.032](https://doi.org/10.1016/j.optlastec.2012.09.032).
- [178] K. Chandrashekar, G.V. Attimarad, N. Nagaraja, J. Sangamesh, “Comparative analysis of scattering matrix calculation of dielectric waveguide discontinuity models by using FEM solution of two dimensional Helmholtz equations”, 2016 International Conference on Electrical, Electronics and Optimization Techniques (ICEEOT), November 2016, DOI: [10.1109/ICEEOT.2016.7755532](https://doi.org/10.1109/ICEEOT.2016.7755532).
- [179] V. Chtcherbakov, “An Accurate electromagnetic Model of a Circular Aperture With Analytical Solution for On-Axis Near Field”, IEEE Transactions on Electromagnetic Compatibility, vol. 59, Issue 2, December 2016, DOI: [10.1109/TEMC.2016.2629459](https://doi.org/10.1109/TEMC.2016.2629459).
- [180] A. T. Tran, D. C. Truong, H. T. Nguyen, Y. V. Vu, “A new simulation design of three-mode division (de)multiplexer based on a trident coupler and two cascaded 3x3 MMI

silicon waveguides”, *Optical and Quantum Electronics*, vol. 49, Issue 12, December 2017, **DOI:** <https://doi.org/10.1007/s11082-017-1248-4>.

Publications of the Author

Unless the percentage of authorship (as in v3s.cvut.cz) is displayed, it is the same for all the authors.

Impact factor journal articles:

1. C. Burtscher (49%), M. Lucki (49%) and D. Seyringer (2%), “Comparison of Optical Properties of 1x8 Splitters Based on Y-Branch and MMI Approaches”, Micro- to Nano-Photonics IV- ROMOPTO 2015, 1 to 4 September, 2015, Bucharest, Romania (published in Romanian Reports in Physics, Vol. 67, No. 4, P. 1578-1585. ISSN 1221-1451, 2015).
2. C. Burtscher (45%), D. Seyringer (9%), M. Lucki (45%), A. Kuzma (1%), “Modelling and optimization of 1x32 y-branch splitter for optical transmission system”, Optical and Quantum Electronics, Vol.49(12),pp.1-12, Springer, October 2017, ISSN 0306-8919. DOI: [10.1007/s11082-017-1228-8](https://doi.org/10.1007/s11082-017-1228-8).
3. R. Agalliu (30%), C. Burtscher (30%), M. Lucki (30%), D. Seyringer (10%), “Optical splitter design for telecommunication access networks with triple-play services”, Journal of Electrical Engineering, vol. 69, No.1, pp. 32-38, 2018. ISSN 1335-3632. DOI: [10.1515/jee-2018-0004](https://doi.org/10.1515/jee-2018-0004).

The paper has been cited in:

- J. Latal, Z. Wilcek, J. Kolar, J. Vojtech, “Measurement of IPTV Services on a Hybrid Access Network”, 2018 20th International Conference of Transparent Optic Networks (ICTON), September 2018, Bucharest, Romania, DOI: [10.1109/ICTON.2018.8473724](https://doi.org/10.1109/ICTON.2018.8473724)
- J. Dubovan, M. Frniak, J. Litvik, M. Markovic, M. Dado, “Optical Sensors Utilization as a Part of Intelligent Transport Systems”, 2019 Conference on Microwave Techniques (COMITE), June 2019. DOI: [10.1109/COMITE.2019.8733538](https://doi.org/10.1109/COMITE.2019.8733538)
- J. Litvik, I. Dolnak, M.Dado, “ High-Capacity Wavelength Division Multiplexing Optical Transmission Systems”, 2018 16th International conference on Emerging eLearning Technologies and Applications (ICETA), December 2018. DOI: [10.1109/ICETA.2018.8572287](https://doi.org/10.1109/ICETA.2018.8572287)

Peer-reviewed Journal:

4. C. Burtscher (45%), M. Lucki (45%), D. Seyringer (10%), “Comparison of splitting properties of various 1x16 splitters”, Advances in Electrical and Electronic Engineering, Vol. 15, No. 1, P. 107-113), March, 2017, ISSN 1336-1376. DOI: [10.15598/aeee.v15i1.2014](https://doi.org/10.15598/aeee.v15i1.2014).

The paper has been cited in:

- J. Latal, Z. Wilcek, J. Kolar, J. Vojtech, “Measurement of IPTV Services on a Hybrid Access Network”, 2018 20th International Conference of Transparent Optic Networks (ICTON), September 2018, Bucharest, Romania, DOI: [10.1109/ICTON.2018.8473724](https://doi.org/10.1109/ICTON.2018.8473724)

- J. Latal, Z. Wilcek, J. Kolar, J. Vojtech, “Measurement of IPTV Qualitative Parameters on EPON/VDSL2 Topology”, 2018 International Conference on Broadband Communications for Next Generation Networks and Multimedia Applications (CoBCom). August 2018, Graz, Austria. DOI: [10.1109/COBCOM.2018.8443981](https://doi.org/10.1109/COBCOM.2018.8443981)

Papers in indexed conference proceedings (WoS and SCOPUS):

5. C. Burtscher, D. Seyringer, “Design of low loss 1x64 Y-Branch splitter having symmetric splitting ratio”, ASDAM 2014, 20-22 October, 2014, Smolenice, Slovakia, DOI: [10.1109/ASDAM.2014.6998686](https://doi.org/10.1109/ASDAM.2014.6998686).

The paper has been cited in:

- S. Soltani, “Fabrication and Characterization of Toroidal Resonators for Optical Process Improvement”, PhD Dissertation, Faculty of the USC Graduate School, The University of Southern California, May 2018, ProQuest Number 11017208.
6. C. Burtscher, D. Seyringer, “Influence of waveguide structure on Y-branch splitting ratio”, SPIE Photonics Europe 2014, Silicon Photonics and Photonic Integrated Circuits conference IV, Brussels 2014, Brussels, in Proc. SPIE 9133, DOI: [10.1117/12.2050846](https://doi.org/10.1117/12.2050846).

The paper has been cited in:

- X. Han, Y. Yu, “Optimization of a thermally tuned silicon-based reconfigurable optical power splitter with thermal isolations”, Optical Engineering, 56(1), 017106, January 2017, <https://doi.org/10.1117/1.OE.56.1.017106>.
7. C. Burtscher (49%), D. Seyringer (2%), M. Lucki (49%), “Study of Optical Properties of 1x16 Splitter Based on Y-Branch and MMI Approaches”, International Conference of Transparent Optical Network (ICTON) 2016, 10-14 July, Trento, Italy.

The paper has been cited in:

- R. W. Pumamaningsih, M. Hamidah, D. Fithriaty, M. R. Gumelar, “III nitride based waveguide parameters optimisation of 1x2 optical power divider for telecommunication links”, Third International Seminar on Photonics, Optics and Its Applications (ISPhOA 2018), 2018, Surabaya, Indonesia. <https://doi.org/10.1117/12.2504903>
8. C. Seyringer, C. Burtscher, S. Partel, J. Edlinger, A. Maese-Novo, P. Muellner, R. Hainberger, J. Kraft, G. Koppitsch, G. Meinhardt, “Design and Simulation of Si₃N₄ Based Arrayed Waveguide Gratings Applying AWG-Parameters Tool”, ICTON 2016 (18th International Conference on Transparent Networks), 10-14 July 2016, Trento, Italy.

The paper has been cited in:

- P. Mahmoudi, H. Veladi, F. G. Pakdel, J. Frounchi, “Optimization of a thermally tuned silicon-based reconfigurable optical power splitter with thermal isolations”, Journal of

Micro/Nanolithography, MEMS and MOEMS, vol.18. No. 1, January 2019, 015502 (2019). <https://doi.org/10.1117/1.JMM.18.1.015502>

9. C. Burtscher (45%), D. Seyringer (9%), M. Lucki (45%), L. Kohler (1%): “New waveguide shape for low-loss and high-uniformity Y-branch splitter”, SPIE Photonics West, 27.1. – 2.2.2017, San Francisco, Paper 101061M, Proc. SPIE 10106, Integrated Optics: Devices, Materials, and Technologies XXI, 101061M (February 16, 2017), DOI: [10.1117/12.2249758](https://doi.org/10.1117/12.2249758).
10. D. Seyringer, C. Burtscher, S. Partel, J. Etlinger, A. Maese-Novo, P. Muellner, R. Hainberger, J. Kraft, G. Koppitsch, G. Meinhardt: “Design and simulation of 20-channel, 50-GHz Si₃N₄ based arrayed waveguide grating applying AWG-Parameters tool”, SPIE Photonics West, 27.1. – 2.2.2017, San Francisco, Paper 101061M, Proc. SPIE 10106, Integrated Optics: Devices, Materials, and Technologies XXI, 101061M (February 16, 2017), DOI: [10.1117/12.2249675](https://doi.org/10.1117/12.2249675)
11. C. Burtscher, M. Lucki, D. Seyringer “Waveguide Shape Modelling and Optimization for High Channel Y-Branch Splitter in Optical Transmission Systems”, 20th International Conference of Transparent Optical Network (ICTON) 2018, 01-05 July, Bucharest, Romania.
12. D. Seyringer, C. Burtscher, J. Etlinger, W. Drexler, E. Rank, P. Muellner, R. Hainberger, A. Maese-Novo, M. Vlaskovic, H. Zimmermann, J. Kraft, G. Koppitsch, M. Sagmeister, G. Meinhardt, “Size reduction of high-channel Si₃N₄ based AWG-spectrometer for medical applications”, SPIE Nanoscience+Engineering, August 2018, San Diego, California, United States, Proceedings Volume 10730, Nanoengineering: Fabrication, Properties, Optics and Devices XV; <https://doi.org/10.1117/12.2319670>.

Other conference articles:

1. C. Burtscher (40%), M. Lucki (40%) and D. Seyringer (20%), “Design, Simulation and Optimization of High Channel Optical Splitters”, Advances in Electronic and Photonic Technologies (ADEPT) 2015, 1 to 4 June, 2015, High Tatras, Strbske Pleso, Slovakia.
2. C. Burtscher, D. Seyringer and M. Lucki, “Study of Splitting Properties of 1x16 MMI Splitter based on Different Widths of the Multimode Interference Section”, Advanced in Electronic and Photonic (ADEPT) 2016, 20-22 June, High Tatras, Tatranska Lomnica, Slovakia. ISBN 978-80-554-1226-9.
3. D. Seyringer, C. Burtscher, G. Piressa, A. Prasad and J. Zehetner, “The Night of Science: Optics and Photonics for All“, The European Conference on Technology in the Classroom 2016 (ECTC 2016), Iafor (The International Academic Forum), Brighton, UK, June 29-July 3, 2016.
4. D. Seyringer, L. Gajdosová, C. Burtscher, “Arrayed Waveguide Gratings, “Design and Simulation”, 19th school of vacuum technology: Vacuum and new materials”, 9-12 November 2016, Hohe Tatra, Slovakia.
5. C. Burtscher (45%), D. Seyringer (9%), M. Lucki (45%), A. Kuzma (1%): “Design and simulation of 1x32 Y-branch splitter applying different photonics tools”, APCOM 2017, 12-14 June 2017, High Tatras, Transka Lomnica, Slovakia.

6. D. Seyringer, C. Burtscher, L. Gajdosova: “Si₃N₄ based 40-ch, 50-GHz AWG for medical applications”, APCOM 2017, 12-14 June 2017, High Tatras, Transka Lomnica, Slovakia.
7. D. Pudiš, P. Gašo, M. Goraus, D. Seyringer, L. Gajdosova, C. Burtscher: POLYMER BASED Y-BRANCH AND MMI SPLITTER WITH PLANAR AND 3D GEOMETRY, In: 20. Skola Vakuovej Techniky. Nanoelektronika a Vakuum. Nanoelectronics and vacuum. Zbornik príspevkov. 23. - 26. Oktober 2018. Strbske Pleso. Bratislava: Slovenska vakuova spolocnost, S. 70–73.
8. D. Seyringer, J. Chovan, C. Burtscher, L. Gajdosova, D. Figura, F. Uherek, “Design and Optimization of Silicon Nitride Based 1x8 Y-Branch Splitter”, ASDAM 2018, 21. - 24. Oktober 2018, Smolenice Slovakia.
9. D. Seyringer, L. Gajdosova, C. Burtscher, P. Gašo, D. Pudiš, “Design of Polymer Waveguides for Photonic Component”, ADEPT 2018, 18. - 21. June 2018, High Tatras, Tatranska Lomnica, Slovakia.
10. D. Seyringer, L. Gajdosova, C. Burtscher, A. Kuzma, J. Chovan, F. Uherek, “Design of low loss silicon nitride 8-channel AWG”, APCOM 2018, 20. - 22. June 2018, High Tatras, Tatranska Lomnica, Slovakia. (Citation: AIP Conference Proceedings 1996, 020042 (2018); <https://doi.org/10.1063/1.5048894>).
11. L. Gajdosova, D. Seyringer, C. Burtscher, J. Chovan, A. Kuzma, F. Uherek, “Simulation of Silicon Nitride based Arrayed Waveguide Gratings applying three different photonics tools”, APCOM 2018, 20. - 22. June 2018, High Tatras, Tatranska Lomnica, Slovakia.

Appendix A

A.1 Refractive, Effective and Refractive Contrast (Difference) Index of a Material

For a material, the *refractive index* is the ratio of speed of the light in vacuum and the speed of the light in a given media for given frequency [174].

$$\text{Refractive index} \quad n(\omega, \mu_r, \epsilon_r) = \frac{c}{v} = \frac{\sqrt{\epsilon(\omega)\mu(\omega)}}{\sqrt{\epsilon_0\mu_0}} = \sqrt{\epsilon_r(\omega)\mu_r(\omega)} \quad (\text{A.1})$$

with relative permeability, μ_r and relative permittivity, ϵ_r . It should be pointed out that all of these indices are statements of a ratio of the velocity, wavelength, or wavenumber of the light in vacuum to that of light in the material, namely $c = \lambda_0 v$ and $v = \lambda v$

$$n(\omega, \mu_r, \epsilon_r) = n = \frac{\lambda_0 v}{\lambda v} = \frac{\frac{2\pi}{k_0}}{\frac{2\pi}{k}} = \frac{k}{k_0} \quad (\text{A.2})$$

The refractive index can be calculated in an analytical form by Sellmaier dispersion formula [175] or by another approximating formula for example by Cauchy formula [176].

$$n(\lambda) = \sqrt{1 + \sum \frac{A_j \lambda^2}{\lambda^2 - B_j}} \quad (\text{A.3})$$

where A_j [-] and B_j [μm^2] are Sellmeier coefficients for wavelength and are obtained by a least-square fitting procedure, applied to the refractive indices measured in a wide wavelength range.

The *effective index* is defined as a ratio of the velocity in vacuum to the velocity of a mode for a given polarization in the direction of propagation in a guiding structure, for example along the waveguide in the z direction. The effective index is defined as

$$n_{eff_{pm}} = \frac{c}{v_{z_{pm}}} = \frac{\lambda_0 v}{\lambda_{z_{pm}} v} = \frac{\lambda_0}{\lambda_{z_{pm}}} = \frac{\frac{2\pi}{k_0}}{\frac{2\pi}{k_{z_{pm}}}} = \frac{k_{z_{pm}}}{k_0} = \frac{\beta_{pm}}{k_0} \quad (\text{A.4})$$

with $k_{z_{pm}} \equiv \beta_{pm}$, p is the polarization (TE or TM), m is the m^{th} mode of the polarization, k_0 is the waveguide number in free space for a given frequency of the light, λ_0 is the wavelength in free space and v is the frequency in all media. A key point to note about the frequency is that it is constant in all media, but the wavelength changes depending on the media. The parameter β_{pm} is termed the propagation constant. This is the component of the wavenumber in guiding structure which is in the direction of propagation of the light, for a given mode and polarization.

For TE mode,

$$n_{eff}^2 = \frac{\int n(x)^2 E_y(x) dx}{\int E_y(x) dx} \quad (A.5)$$

For TM mode,

$$n_{eff}^2 = \frac{\int H_y(x) dx}{\int \frac{H_y(x)}{n(x)^2} dx} \quad (A.6)$$

where E_y and H_y are the mode profiles in the background for TE respectively, TM and $n(x)$ is the index profile for the etched low index area of the wedge. The effective index is defined as the propagation constant divided by the free space wavenumber, therefore modes will not exist when there is total internal reflection, and then the effective index is always between the highest refractive index value of the other materials and the guiding/core/film material.

$$n_{\max(n_s, n_c)} < n_{eff_{pm}} < n_f \quad (A.7)$$

where n_f is the refractive index of the guiding material, n_s is the refractive index of the substrate and n_c is the refractive index of the core.

A condition for extremely small devices [177] is the ultrahigh *refractive-index (difference) contrast* between Si and SiO₂, which are expressed as

$$\Delta = \frac{n_{core} - n_{cladding}}{n_{core}} \times 100\% \quad (A.8)$$

B.1 Wave equation

The modal analysis of optical waveguide [113] is the procedure to find the propagation characteristics and the field profiles of all the supported modes of a waveguide. The propagation constants are solutions of the Maxwell's equations, which describe the fundamental theory behind most of the phenomenon in photonic components:

$$\vec{\nabla} \times \vec{E} + \frac{\partial \vec{B}}{\partial t} = 0 \quad (B.1)$$

$$\vec{\nabla} \times \vec{H} - \frac{\partial \vec{D}}{\partial t} = \vec{j} \quad (B.2)$$

$$\vec{\nabla} \cdot \vec{D} = \rho \quad (B.3)$$

$$\vec{\nabla} \cdot \vec{\mathbf{B}} = 0 \quad (\text{B.4})$$

where \mathbf{E} is the electric field, \mathbf{H} is the magnetic field, \mathbf{D} is the electric flux density, \mathbf{B} is the magnetic flux density, \mathbf{J} is the current density and ρ is the density of volume charge. For a linear and isotropic lossless medium-but not necessarily homogeneous- these electromagnetic fields can be written as:

$$\vec{\mathbf{D}} = \varepsilon \vec{\mathbf{E}} \quad (\text{B.5})$$

$$\vec{\mathbf{B}} = \mu \vec{\mathbf{H}} \quad (\text{B.6})$$

where the permittivity ε and the permeability μ are defined as:

$$\varepsilon = \varepsilon_0 \varepsilon_r \quad (\text{B.7})$$

$$\mu = \mu_0 \mu_r \quad (\text{B.8})$$

Here, $\varepsilon_0 = (\mu_0 c^2)^{-1}$ and $\mu_0 = 4\pi \cdot 10^{-7} \text{Vs}/(\text{Am})$ are the permittivity and permeability of a vacuum, and ε_r and μ_r are the permittivity and permeability of a material.

Equations (3.1.9) and (3.1.10) are called Helmholtz wave equations [178] for homogenous media and can be obtained by eliminating the magnetic flux density in and the electric flux density components for Maxwell's Eqs. (3.1.1) and (3.1.2):

$$\nabla^2 \mathbf{E} + k^2 \mathbf{E} = 0 \quad (\text{B.9})$$

$$\nabla^2 \mathbf{H} + k^2 \mathbf{H} = 0 \quad (\text{B.10})$$

Where k (rad/m) is the wavenumber, is $k = \omega \sqrt{\varepsilon \mu_0}$ (see Appendix A.1) and ∇^2 is the Laplacian operator:

$$\nabla^2 = \frac{\partial^2}{\partial x^2} + \frac{\partial^2}{\partial y^2} + \frac{\partial^2}{\partial z^2} \quad (\text{B.11})$$

The paraxial form of the Helmholtz equation, known as the Fresnel equation [179] is valid for paraxial propagation in slowly varying optical structure and it is starting point to develop BPM algorithms [180]. The basic formulas and their description of the TE and TM Mode and the Finite-Difference Mode Solver are describe in Appendix B.1.

A general vector field \vec{F} oscillating at the single angular frequency ω can be expressed as:

$$\vec{F}(\vec{r}, t) = \{\vec{\epsilon}(\vec{r})\exp(j\omega t)\} \quad (\text{B.12})$$

If we plug this form of representation in Equations (3.1) to (3.4), with the mention that from now on $\vec{F}(\vec{r}, t)$ is a function only of \vec{r} , the electromagnetic fields can be written as:

$$\vec{\nabla} \times \vec{E} = -j\omega\vec{B} = -j\omega\mu_0\vec{H} \quad (\text{B.13})$$

$$\vec{\nabla} \times \vec{H} = -j\omega\vec{D} = j\omega\epsilon_0\epsilon_r\vec{E} \quad (\text{B.14})$$

$$\vec{\nabla} \cdot \vec{H} = 0 \quad (\text{B.15})$$

$$\vec{\nabla} \cdot (\epsilon_r\vec{E}) = 0 \quad (\text{B.16})$$

where $\rho = 0$, $\mu_r = 1$ and \vec{j} is assumed. The two-dimensional semivectorial analysis assume that the structure of the waveguide to be uniform in the y direction and the derivatives with respect to y can be set to zero, i.e.

$$-\partial_z E_y = -j\omega\mu_0 H_x \quad (\text{B.17})$$

$$\partial_z E_x - \partial_x E_z = -j\omega\mu_0 H_y \quad (\text{B.18})$$

$$\partial_x E_y = -j\omega\mu_0 H_z \quad (\text{B.19})$$

$$-\partial_z H_y = j\omega\epsilon_0\epsilon_r E_x \quad (\text{B.20})$$

$$\partial_z H_x - \partial_x H_z = j\omega\epsilon_0\epsilon_r E_y \quad (\text{B.21})$$

$$\partial_x H_y = j\omega\epsilon_0\epsilon_r E_z \quad (\text{B.22})$$

The Equations for electric field component in the TE and TM Mode Analysis are expressions in Appendix B.1.

C.1 Electric field components in TE and TM mode

TE Mode: The electric field component in the longitudinal direction in TE mode is zero, i.e. $E_z = 0$, then we assume $\partial_y = 0$ and $\partial_x H_y = 0$, $H_y = 0$, $E_z = H_y = 0$. The wave equation for the principal electric field component E_y is:

$$\partial_z^2 E_y + \partial_x^2 E_y + k_0^2 \epsilon_r E_y = 0 \quad (\text{C.1})$$

where $k_0^2 = \omega^2 \epsilon_0 \mu_0$.

With the follow approximation, and implicitly the used approximation in BPM $\partial_z \epsilon_r \approx 0$,

$$\partial_z (\epsilon_r E_y) = E_y \partial_z \epsilon_r + \epsilon_r \partial_z E_y \approx \epsilon_r \partial_z E_y \quad (\text{C.2})$$

Similarly, the wave equation for the x -directed magnetic field component can obtained:

$$\partial_z^2 H_x + \partial_x^2 H_x + k_0^2 \epsilon_r H_x = 0 \quad (\text{C.3})$$

TM Mode: The magnetic field component in the longitudinal direction in TM mode is zero, i.e. $H_x = 0$. Similarly to the TE mode we now get $\partial_x E_y = 0$, $\partial_y = 0$, $H_z = E_y = 0$.

The wave equation for the x -directed electric field component E_x is:

$$\partial_z^2 E_x + \partial_x \left[\frac{1}{\epsilon_r} \partial_x (\epsilon_r E_x) \right] + k_0^2 \epsilon_r E_x = 0 \quad (\text{C.4})$$

And the wave equation for H_z

$$\partial_z^2 H_y + \epsilon_r \partial_x \left[\frac{1}{\epsilon_r} \partial_x H_y \right] + k_0^2 \epsilon_r H_y = 0 \quad (\text{C.5})$$

All these four wave equations can be solved numerically using finite-difference expressions.

D.1 Finite-Difference Mode Solver

Finite-difference mode solver, an eigenmode solver, is a very important solver in analysis and design of the waveguide structures.

From the wave equation, after some mathematical manipulations we obtain following equation:

$$P_{xx}E_x = \frac{\partial}{\partial x} \left[\frac{1}{n^2} \frac{\partial(n^2 E_x)}{\partial x} \right] + \frac{\partial^2 E_x}{\partial y^2} + n^2 k_0^2 E_x \quad (\text{D.1})$$

$$P_{xy}E_y = \frac{\partial}{\partial x} \left(\frac{1}{n^2} \frac{\partial(n^2 E_x)}{\partial y} \right) - \frac{\partial^2 E_y}{\partial x \partial y} \quad (\text{D.2})$$

$$P_{yy}E_y = \frac{\partial}{\partial y} \left[\frac{1}{n^2} \frac{\partial(n^2 E_y)}{\partial y} \right] + \frac{\partial}{\partial x} \frac{\partial^2 E_x}{\partial y^2} + n^2 k_0^2 E_x \quad (\text{D.3})$$

The electromagnetic field, assuming that light is propagating along the z axis, could be expressed as:

$$\vec{E} = \vec{E}(x, y) \exp(-j\beta z) \quad (\text{D.4})$$

where β is the propagation constant and noting that $\frac{\partial}{\partial z} = -j\beta$ and $\frac{\partial^2}{\partial z^2} = -\beta^2$, than:

$$\begin{pmatrix} P_{xx} & P_{xy} \\ P_{yx} & P_{yy} \end{pmatrix} \begin{pmatrix} E_x \\ E_y \end{pmatrix} = \left(-\beta^2 + 2j\beta \frac{\partial}{\partial z} + \frac{\partial^2}{\partial z^2} \right) \begin{pmatrix} E_x \\ E_y \end{pmatrix} \quad (\text{D.5})$$

For the finite-difference method, the eigenmode is considered for a z -invariant waveguide, so we have $\frac{\partial}{\partial z} = 0$ and $\frac{\partial^2}{\partial z^2} = 0$, in this case resulting a linear eigenvalue problem of the form:

$$\begin{pmatrix} P_{xx} & P_{xy} \\ P_{yx} & P_{yy} \end{pmatrix} \begin{pmatrix} E_x \\ E_y \end{pmatrix} = \beta^2 \begin{pmatrix} E_x \\ E_y \end{pmatrix} \quad (\text{D.6})$$